# Max-Planck-Institut für Meteorologie

## EXAMENSARBEIT Nr. 83

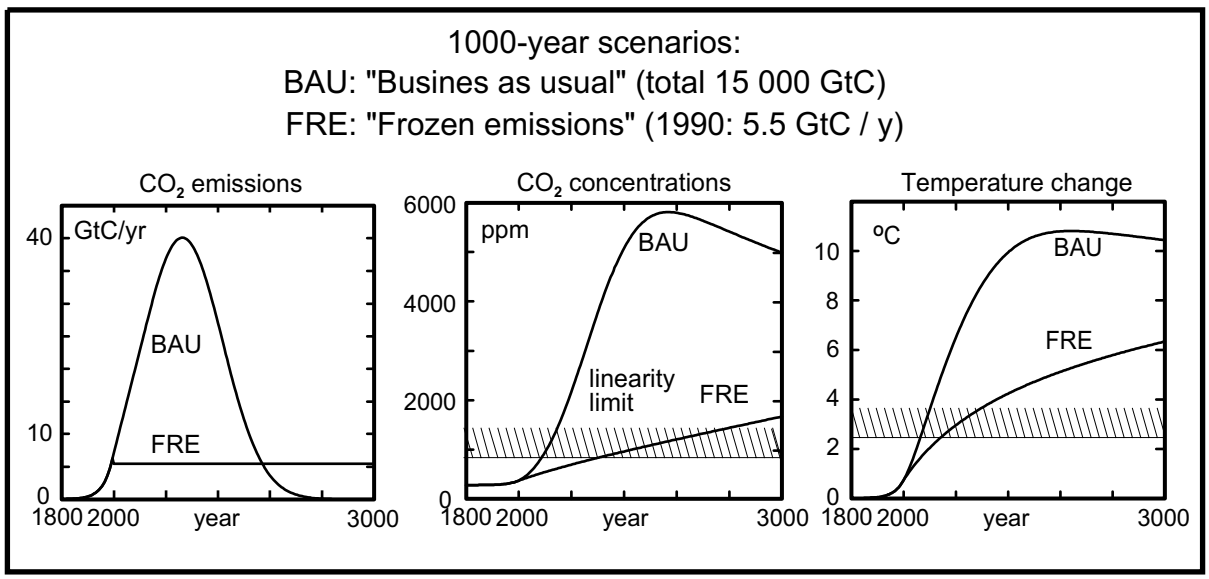


# AGGREGATE MODELS OF CLIMATE CHANGE. DEVELOPMENT AND APPLICATIONS

by

Kurt Georg Hooss

HAMBURG, July 2001

Dissertation zur Erlangung des Doktorgrades

Autor:

Kurt Georg Hooss

Max-Planck-Institut
für Meteorologie

MAX-PLANCK-INSTITUT
FÜR METEOROLOGIE
BUNDESSTRASSE 55
D - 20146 HAMBURG
GERMANY

Tel.: +49-(0)40-4 11 73-0
Telefax: +49-(0)40-4 11 73-298
E-Mail: <name> @ dkrz.de

# Aggregate models of climate change: development and applications

Dissertation
zur Erlangung des Doktorgrades
der Naturwissenschaften
im Fachbereich Geowissenschaften
der Universität Hamburg

vorgelegt von
**Kurt Georg Hooss**
geboren in
Marburg an der Lahn

Hamburg
2001

ISSN 0938-5177

**Als Dissertation angenommen**

**vom Fachbereich Geowissenschaften**

**der Universität Hamburg**

aufgrund der Gutachten von Herrn Prof. Dr. Klaus Hasselmann
und Herrn Prof. Dr. Jürgen Sündermann

Hamburg, den 26.Juli 2001

Prof. Dr. U. Bismayer
Dekan des Fachbereichs Geowissenschaften

**Abstract**

Impulse-response-function (IRF) models are designed for applications requiring a large number of climate simulations, such as multi-scenario climate change impact studies or cost-benefit integrated-assessment studies. The models apply linear response theory to reproduce the characteristics of the climate response to external forcing computed with sophisticated state-of-the-art climate models like general circulation models of the physical ocean-atmosphere system and three-dimensional oceanic-plus-terrestrial carbon cycle models. Although highly computer efficient, IRF models are nonetheless capable of reproducing the full set of climate-change information generated by the complex models against which they are calibrated.

While limited in principle to the linear response regime (less than about $3^oC$ temperature change), the applicability of the IRF model presented in this paper has been extended into the nonlinear domain through explicit treatment of the climate system's dominant nonlinearities: $CO_2$ chemistry in ocean water, $CO_2$ fertilization of land biota, and sublinear radiative forcing. The resultant Nonlinear Impulse-response model of the coupled Carbon cycle-Climate System (NICCS) computes the temporal evolution of spatial patterns of climate change in four climate variables of particular relevance for climate impact studies: near-surface temperature, cloud cover, precipitation, and sea level. The space-time response characteristics of the model are derived from an EOF analysis of a transient 850-year greenhouse warming simulation with the Hamburg atmosphere-ocean general circulation model ECHAM3-LSG and a similar response experiment with the Hamburg ocean carbon cycle model HAMOCC.

Emission scenarios studied with the model cover time horizons ranging from 30 years (the Kiel-Volkswagen model) over projections for the $21^{st}$ century (IIASA) to two idealized 1000-year scenarios which demonstrate that the use of all currently estimated fossil fuel resources would carry the Earth's climate far beyond the range of climate change for which reliable quantitative predictions are possible today, and that even a freezing of emissions to present-day levels would not be sufficient to prevent a major global warming in the long term.

Further applications of the model include its combination with, and incorporation into, other models: integrated assessment studies, investigations of

climate change feedbacks onto the terrestrial carbon cycle, and an educational tool developed for the EXPO2000 World Exhibition.

# Contents

SIC ERGO CLAMAT NATURA
VAE MISER MEUM CORPUS

# Chapter 1

# Introduction

## 1.1 Context: Climate and Life, Man and Machine

Global-scale man-made (or rather, machine-made) climate change, known as the *anthropogenic greenhouse effect*, predicted and observed in recent years and decades with a high degree of scientific confidence, is new in the history of man.

We note that man-made climate change is not new on *local to regional scales*. Examples cover urban heat and smog in and around many of today's megacities, as well as changes on subcontinental scale, like the partial deforestation of the mediterranean region for more than 2000 years ago and of Europe and North America during the two millenia since then.

The examples illustrate that human interferences have long and repeatedly been resulting in moderate to severe changes in the energy, water, and other physical, chemical, and biological cycles, as reflected in many variables like temperature, precipitation, surface albedo, and the abundance, concentrations, and densities of chemical and biological species. As these changes also affect slowly varying natural systems like vegetation, soil, and ground water, they must be considered, at least in part, as irreversible at least on century time scales. Species extinctions and historical eradication of whole ecosystem types are not reversible on the even longer time scales of genetic ecological evolution: millions of years.

Certainly, the examples also illustrate that the complex, self-regulating system of nature on Earth has tolerated and, at least partly, compensated anthropogenic disturbances for millennia. However, we must state that to-

day's anthropogenic greenhouse effect is of a new quality in two aspects. First, it is new in its *planetary pervasiveness*, with all major subsystems of the Earth's climate affected: the world ocean, the atmosphere, the soil, and the ice, and the totality of life in these four spheres. Second, it is new in its combination of *amplitude, speed*, and yet unmitigated *acceleration*, which is unprecedented at least during the period that has been reconstructed from ice core measurements: during the past 400 000 years, considerably longer than the biological species of Homo sapiens has existed, and 100 times longer than the age of civilization.

*Integrated assessment* of global change includes consideration of the impacts of future climate change and of the necessities and costs of avoiding it. As the tools of our time, simulation models of the interacting spheres of climate, life, and civilization are made communicable and brought together. The climate change model presented in this thesis, together with its application to plausible scenarios of our unpredictable future, and its combination with models of ecology and economy into multi-aggregate world models, is understood as a climatological contribution to interdisciplinary attempts at global change.

## 1.2 Model hierarchy and aggregation

A *complex model* (of e.g. a physical or economic system) is an aggregate of (sometimes many) functionally related detail models (e.g. of dynamical, thermodynamical, radiation and surface interaction processes; detail models can again be complex models). The aggregate properties of complex models, i.e. some specific choice of input-output relations accomplished by the model as a whole (its grand-total sensitivities, so to speak), can be parameterized by mathematically simpler relations that are less computationally demanding. Such simple models of the aggregate behaviour of complex models are referred to as *aggregate models*.

Models can be structurally simplified by the replacement of complex submodels by aggregate models. Models thus simplified are said to be *aggregated*. *Aggregation* (or *disaggregation*) of macro-economic models, for example, is performed by combination (or separation) of economic sectors or regions into larger (or smaller) sectors or regions.

Examples of highest-level aggregation of models of natural physical systmes are elaborated in this thesis. These aggregate models parameterize, in a very small number of variables, the response of the entire Earth's carbon cycle and climate system to one single time-dependent perturbation through

man: namely humanity's total combustion of fossil fuels: coal, oil, and gas. The models thus represent the utmost extreme of aggregation in the field of climate science. Further aggregation, namely to the unique response in one scalar output variable to a given change in one scalar input variable, (e.g. the response in global-mean temperature in the year 2100 to the total accumulated fossil-fuel $CO_2$ emissions by then), is found infeasible, as the response always depends not only on the integral perturbation but also on its time history.

## 1.3 Impulse-response climate models

For comprehensive integrated assessment and other climate impact studies, computations of climate change are often required for a large number of greenhouse gas emission scenarios. The most reliable instruments currently available for the estimation of anthropogenic climate change are coupled atmosphere-ocean general circulation models (AOGCMs) in combination with three-dimensional models of the carbon cycle and other, non-$CO_2$ greenhouse gases. However, for multi-scenario investigations, these models are prohibitively expensive in computation time. Ideally, a climate model designed for application in integrated assessment and climate impact studies should provide the desired climate-change information without excessive computational cost, while nevertheless approaching the reliability and detail of sophisticated, top-of-the-line climate models.

While AOGCMs process a huge amount of information on the three-dimensional ocean-atmosphere system, only a small subset of the data is normally required as output to characterize the resulting climate change. One is interested typically only in some vector $x(t)$ representing, for example, the change in a set of two-dimensional fields such as near-surface temperature, cloud cover, precipitation or sea level. As input characterizing the external anthropogenic forcing $f(t)$ one is similarly concerned only with low-dimensional fields, or even a scalar, like the globally integrated input of fossil-fuel carbon dioxide into the atmosphere.

Provided the change relative to a reference climate state is small, the response of $x(t)$ to an arbitrary (but sufficiently small) forcing $f(t)$ is given generally by a convolution with the climate system's linear impulse response function (IRF) $R$:

$$x(t) = \int_{-\infty}^{t} R(t-t')f(t')dt' \quad . \tag{1.1}$$

The function $R(t)$ represents the response to a $\delta$-function forcing at time

$t = 0$. Once the IRF has been determined, for example by fitting to a single climate change simulation with a sophisticated climate model (or, in practice, to separate response experiments for the individual physical climate and greenhouse-gas modules from which the full climate model is constructed), the simple convolution (IRF) model can be applied to any time-dependent forcing scenario without further reference to the sophisticated climate model against which it was calibrated. As long as one remains within the linear regime, the IRF model then serves as an exact substitute for the full model.

In principle, IRF models can be designed to reproduce, without loss of information, any output from a sophisticated model, including annual cycles and derived quantities like extreme value statistics. They provide a highly efficient method of computing credible time-dependent climate-change scenarios. For a single input variable, the CPU times are of the order of a second on a workstation. For a multidimensional input with $n_f$ independent degrees of freedom (as would be required, for example, to describe spatially variable aerosol emissions), the CPU time increases linearly with $n_f$, and one requires $n_f + 1$ AOGCM reference experiments (including a control run) to calibrate the model. In our applications, however, we shall consider only $CO_2$ emissions as input. Since $CO_2$ is well mixed in the atmosphere on the time scales relevant for climate change, the input can be characterized in this case by a single scalar variable representing the global integral of the $CO_2$ emissions.

## 1.4 Extended applicability

According to the linear-response-fitting exercises for oceanic $CO_2$ uptake by Maier-Reimer and Hasselmann [1987], the linear response range for the carbon cycle is constrained to $CO_2$ concentrations less than about twice the preindustrial value of $pCO_{2,p} = 280$ ppm, corresponding to an equilibrium warming of less than about 3 $^o$C. This is consistent with the linear-response limits found by Hasselmann et al. [1993] in their analysis of the cold-start errors of global warming simulations with AOGCMs.

The goals of this study are twofold: to extend this range of applicability by including the main limiting nonlinear physical processes into an IRF-based model, and to generalize an earlier IRF model for global mean temperature, used by Hasselmann et al. [1997] in a coupled climate-socioeconomic model for the cost-benefit analysis of optimal $CO_2$ emission paths, to spatially dependent fields and other climate variables (cloudiness, precipitation, and sea level). The following nonlinearities are considered:

1. The solubility of additional $CO_2$ in ocean surface water decreases with rising concentrations. This reduces the uptake of the mixed surface layer and thereby the downward transport from the mixed layer into the large deep-ocean reservoir.

2. The net primary production of land vegetation, which is believed to act as a sink for anthropogenic carbon, is assumed to respond logarithmically to increasing atmospheric $CO_2$ (Bacastow and Keeling [1973], Enting et al. [1994]). This has been incorporated previously in a terrestrial biosphere model by Joos et al. [1996]).

3. The radiative greenhouse forcing increases only logarithmically with increasing $CO_2$ concentrations, as the infrared absorption is already close to saturation in the principal $CO_2$ absorption bands.

Caldeira and Kasting [1993] have pointed out that the higher $CO_2$ concentrations resulting from the decrease in solubility tend to be compensated by the weaker logarithmic radiative forcing in the nonlinear system. Thus IRF models of the combined carbon-cycle and physical ocean-atmosphere system give a better linear approximation of the net response of the system than the IRF models of each of the subsystems separately. However, we find that the cancellation of nonlinearities is only partial. Furthermore, since the climate policy debate often focusses on $CO_2$ concentrations rather than global warming scenarios, it is desirable to model each of the subsystems as accurately as possible.

In summary, the Nonlinear Impulse-response model of the coupled Carbon cycle-Climate System (NICCS) presented in the following is an extended version of the impulse response function (IRF) climate model used in the Structural Integrated Assessment Model (SIAM) by Hasselmann et al. [1997], augmented by nonlinear ocean carbon chemistry, a simple IRF representation of the terrestrial biosphere adapted from Joos et al. [1996], a logarithmic formulation of the radiative greenhouse forcing, and spatial patterns of change in four impact-relevant climate variables.

Comprehensive climate models used to compute the climate response to anthropogenic $CO_2$ emissions normally consist of two modules: a carbon cycle module to compute the atmospheric concentration of $CO_2$ for given $CO_2$ emissions, and a coupled atmosphere-ocean general circulation model (AOGCM) to compute the climate change resulting from the change in atmospheric $CO_2$ concentration. Our IRF model similarly consists of two IRF modules: a carbon-cycle (CARC) IRF module calibrated against a three-dimensional ocean carbon cycle model and augmented by a terrestrial biosphere model, and a physical-climate change (CLIC) IRF module calibrated

against an AOGCM. The net NICCS (Nonlinear Impulse-response model of the coupled Carbon cycle-Climate System), comprising the CARC and CLIC IRF modules, can be run in a coupled or sequential mode. In the experiments discussed later we have run the two IRF modules sequentially, as we found the temperature feedback to be relatively small (see also Maier-Reimer et al. [1996]). For greater transparency in illustrating other more important features of the model, we have therefore preferred to neglect this effect.

A more complete representation of the climate feedback on the carbon cycle would need to include also the impact of a change in the ocean circulation on the physical carbon pump (the downwelling of $CO_2$ enriched surface waters in the North Atlantic and Antarctica into the deeper ocean) and the biological pump (the downward transport of $CO_2$ through the rain of decaying plankton), see Maier-Reimer et al. [1996] and Sarmiento et al. [1998]. These feedbacks were found to partially cancel (Maier-Reimer and Hasselmann [1987]) and were not included in the carbon cycle model against which our CARC IRF module was calibrated. Also not activated in the computed response of the parent ocean carbon cycle model to anthropogenic emissions (although included in the model) were marine biological processes, as the biological pump is limited by nutrients rather than $CO_2$ and is thus insensitive to anthropogenic $CO_2$ emissions. Other feedbacks which we have neglected, largely because of lack of reliable information, concern the impact of changes in temperature, water availability and other climatic factors on the terrestrial biosphere.

The thesis is organized as follows: the next two Chapters 2 and 3 describe the carbon-cycle IRF module, consisting of the ocean and terrestrial components. The atmosphere-ocean climate IRF module is presented in Chapters 4, while applications of the coupled IRF model NICCS are discussed in the following Chapters 5 through 7. The final Chapter 8 summarizes the principal conclusions. Lists of variables and parameters and an overview of the technical implementation are given in the Appendices.

# Chapter 2

# The carbon cycle (CARC) module: principles

The carbon-cycle IRF module consists of two components: the ocean carbon cycle and a land vegetation module.

## 2.1 The oceanic carbon cycle submodule

A number of 3D ocean carbon cycle models have been developed to compute the oceanic uptake of $CO_2$, for example the Hamburg Model (HAMOCC1, Maier-Reimer and Hasselmann [1987]) or the Princeton Model [Sarmiento et al., 1992, Sarmiento and Sundquist, 1992, Siegenthaler and Sarmiento, 1993]. For changes in the atmospheric $CO_2$ concentration less than a factor of about 2, most 3D ocean carbon cycle models can be characterized by their linear IRFs $\hat{R}_c(t)$ [Maier-Reimer and Hasselmann, 1987].

Linear IRF models of the oceanic carbon uptake have been developed and applied e.g. by Siegenthaler and Oeschger [1978], Oeschger and Heimann [1983] and Siegenthaler [1983]. We base our nonlinear IRF model on a linear impulse response representation of HAMOCC by Maier-Reimer and Hasselmann [1987]. Their linear IRF model has previously been used for estimating future atmospheric $CO_2$ e.g. by Harvey [1989] and for incorporation in a coupled climate-socioeconomic model (SIAM: Structural Integrated Assessment Model) by Hasselmann et al. [1997].

Since the advective and diffusive transport within the ocean is essentially linear (unless the circulation is significantly changed through feedback from

the climate change), the accuracy of the linear approximation is limited only by the nonlinear uptake of $CO_2$ through the ocean surface, which is governed by the chemical dissociation equilibrium relating the $CO_2$ partial pressure $pCO_2$ to the concentration of dissolved inorganic carbon (DIC) in the near-surface water. At higher concentrations, additional carbon becomes less soluble, and thus a smaller amount of surface-water carbon for a given increase of $pCO_2$ is available for mixing down into the deep ocean by thermohaline overturning [Maier-Reimer and Hasselmann, 1987, Joos et al., 1996].

A successful attempt to circumvent the limitation of ocean carbon cycle IRF models to small perturbations was made by Joos et al. [1996]. An IRF representation was used to describe the linear mixing and transport processes within the ocean, while the nonlinear air-sea exchange was modelled by a differential equation. The explicit formulation of the gas exchange not only extended the range of applicability to greater concentrations, but enabled also the model to be applied to all conservative tracers with sources and sinks in the atmosphere, like bomb radiocarbon or even (for small temperature changes) the oceanic heat uptake. Although requiring only modest CPU resources, the IRF substitute model reproduced the response of spatially resolving models to within a few percent, both for a wide range of carbon emission scenarios and for the uptake of bomb radiocarbon. However, the computational efficiency of the model was compromised by two factors: the need for two nested time-step loops (due to the differential treatment of the nonlinear air-sea exchange and the separate integral treatment of transport and diffusion), and, for very high anthropogenic $CO_2$-emission scenarios ($pCO_2 > 2000$ ppm), by the inelasticity of the air-sea exchange, which required very short time steps for the diffential mixed-layer computations.

## 2.2 The composite atmosphere-plus-mixed-layer system

In principle, the limitation to small time steps can be overcome by using an implicit integration method. But for a nonlinear system, this requires time-consuming iterations. Alternatively, the problem can be circumvented by regarding the mixed-layer-plus-atmosphere subsystem as equilibrated with respect to $CO_2$ exchange. This is permissible if the relevant time scales of climate change are long compared with the equilibration time of the mixed layer-plus-atmosphere subsystem (termed in the following simply the *composite layer*). The transport of $CO_2$ through the surface needs then no longer to be modelled by a dynamical equation, so that the shortest timescale is

suppressed and the model can be integrated with significantly longer time steps.

The composite-layer IRF can be obtained by supression of the shortest-time-scale component of the atmospheric IRF of the parent model (cf. Maier-Reimer and Hasselmann [1987]), which describes the atmosphere-mixed layer equilibration process, with subsequent renormalization of the reduced model. However, in its standard convolution-integral form the composite-layer IRF model is not suitable for the incorporation of the nonlinear chemistry governing the oceanic $CO_2$ uptake. For this purpose, the model needs to be translated into an equivalent differential representation that is physically interpretable in terms of the carbon capacities of the two subsystems of the composite-layer, the atmosphere and mixed layer. This can be achieved by constructing a box-model analogue of the IRF model in the form of a cascade of layers which are coupled through carbon fluxes proportional to the differences in the layer concentrations. Anthropogenic $CO_2$ emissions are introduced into the uppermost or zero$^{th}$ layer, which represents the composite atmosphere-plus-mixed-layer system. The $CO_2$ input into the composite layer is distributed quasi-instantaneously between the atmosphere and the mixed layer, and the composite layer is then coupled to the rest of the ocean via its mixed-layer subsystem, which is in contact with the next-deeper layer.

The cascade's parameters (layer thicknesses and Newtonian relaxation coefficients) are chosen such that the uppermost (composite) layer's IRF matches the composite-layer IRF derived from the parent 3D model's atmospheric response (see Appendix for the model equations and tuning conditions). The decomposition of the uppermost (composite) layer into its atmospheric and mixed-layer subsystems is chosen such that the ratio of carbon uptake into the sublayers is in accord with the preindustrial mixed-layer buffer factor [Revelle and Suess, 1957] for small perturbations. Once the linear cascade has been tuned in this way, the atmospheric and mixed-layer fractions for a larger change in the composite-layer carbon content $c_0$ are computed as nonlinear functions of $c_0$ from the nonlinear chemical equilibrium governing the relation between partial pressure and total inorganic carbon concentration in sea water, following Maier-Reimer and Hasselmann [1987].

## 2.3 Calibration

Our ocean carbon-cycle IRF is a recent least-squares fit to the HAMOCC3i (inorganic) response to a sudden increase of the atmospheric $CO_2$ concentration by 1% (2.78 ppm). The model was run without a biological pump and without $CaCO_3$ sediment interaction. The asymptotic airborne fraction

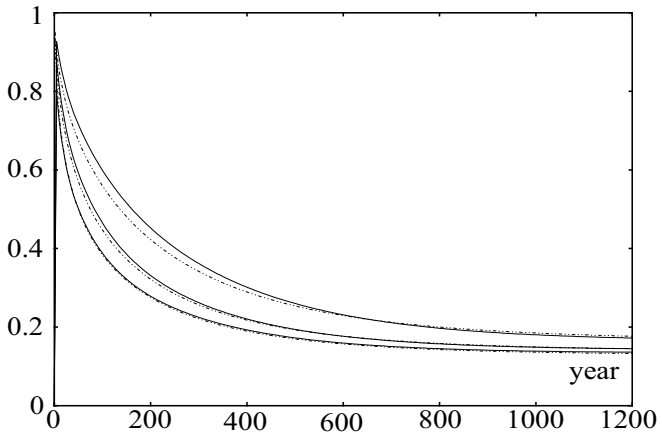


Figure 2.1: Nonlinear impulse-response of the nonlinear ocean carbon cycle IRF model (NO, *full lines*) compared with its parent 3D model HAMOCC3i (*dot-dot-dashed*) to impulses increasing the preindustrial atmospheric $CO_2$ content by 1% *(lowest)*, 100% *(medium)*, and 300% *(highest curve)*, respectively. Only the perturbations are shown, normalized to the impulse size.

(13%) is close to the value found for the 1987 HAMOCC1 IRF (14%; the small difference can be attributed to the onset of a nonlinear effect due to the different impulse sizes used for the two calibrations).

The nonlinear IRF model was checked, using values for the chemical equilibrium constants corresponding to the present-day global-mean temperature, against the full HAMOCC3i's response for impulses in which the preindustrial atmospheric $CO_2$ was increased by 1%, 25%, 100%, and 300% (Fig. 2.1, lower left panel).

For the largest impulse, the $CO_2$ uptake of the nonlinear IRF module is a few percent slower than in HAMOCC3i: the nonlinear retardation of the carbon uptake is slightly overestimated. However, small errors in this range are to be expected, as the nonlinear air-sea exchange in the 3D model is spatially dependent and cannot be accurately simulated by a one-dimensional model using only a single set of global-mean chemistry and mixed-layer parameters.

To assess the temperature effect on the oceanic carbon uptake, we repeated the impulse experiments using a different set of chemical parameters corresponding to temperatures near 0°C instead of the global-mean temperature. Near-zero temperatures correspond to conditions typical for deep water formation in the northern North Atlantic in winter, where most of the $CO_2$ uptake is transferred into the deeper ocean. The uptake in the cold exper-

iment (not shown) was found to be slightly retarded. Although the $CO_2$ solubility is higher at lower temperatures, the reference preindustrial atmospheric $pCO_2$ is also in equilibrium with higher DIC concentrations at lower temperatures (the buffer factor is larger). This more than counterbalances the temperature effect at higher concentrations.

A feedback of climatic temperature change, which would affect only the increased $CO_2$ concentration and not the pre-industrial reference state, would presumably have a stronger impact. The direct reduction in oceanic carbon uptake by sea surface warming through temperature-related chemistry changes only is consistently estimated by different global warming-marine carbon cycle studies (e.g. Sarmiento et al. [1998], Matear and Hirst [1999], Joos et al. [1999], Plattner et al. [2001]).

However the total reduction of oceanic carbon uptake through all climate feedbacks combined, (including modifications of the thermohaline overturning circulation) is hard to predict even with respect to the sign. There is almost no agreement between different climate models. Predictions of the THC range from a complete switch-off, especially of the Atlantic THC, up to a slight enhancement. The majority of models predict a moderate reduction. Clearly, such a reduction - if not compensated by Antarctic deep water - would cause a weakening of the downward transport of $CO_2$; it would, however, also reduce the upwelling of nutrient- and DIC-rich water to the surface. In high latitudes, the reduction of deep mixing would make the conditions for biological production more favourable (as the production takes place in the euphotic zone) and thus enhance the regional downward transport through the biological pump. Globally, changes in the biological cycle could lead to a transient increase or also decrease of the oceanic carbon uptake. Acting in opposite directions, the combined climate-induced changes in circulation, chemistry and biology were found in various studies to induce rather marginal modifications of the oceanic $CO_2$ uptake in the range between -7% and +7% [Maier-Reimer et al., 1996, Joos et al., 1999, Matear and Hirst, 1999, Plattner et al., 2001]. A strong decrease of the cumulated uptake, -10% at 2x$CO_2$ and -20% at 4x$CO_2$, was simulated by Friedlingstein et al. [2001]. Thus, our uncertainties in the oceanic $CO_2$ uptake are comparable to uncertainties in the present understanding of the surface-to-deep transport rates.

## 2.4 The terrestrial carbon cycle submodule

A $CO_2$ sink of roughly 2 GtC/yr in the global terrestrial biosphere is believed to approximately compensate carbon losses from deforestation and

other land use changes, mainly in the tropics. The allocation is ascribed to accelerated plant growth due to the rising $CO_2$ concentrations ($CO_2$ fertilization) and nitrate fertilization. The efficiency of the terrestrial carbon sink and the question whether it will counteract fossil-fuel emissions in the future is hotly debated. Despite numerous papers on this topic in recent years (see e.g. the review of Schlesinger [1993] and IPCC [1990], Tans et al. [1990], Keeling and Shertz [1992], IPCC [1995], Friedlingstein et al. [1995], Keeling et al. [1996], Sellers et al. [1996], Knorr [1997], Gayler and Claussen [1997], Joos and Bruno [1998], Claussen et al. [1999], Ganopolski et al. [1998] and many others), the issue is still far from resolved.

Terrestrial biosphere models of different complexity and spatial resolution have been mapped onto $CO_2$ uptake impulse response function models or equivalent box-type analogues [Meyer et al., 1999, Thompson and Randerson, 1999]. We augmented our ocean carbon cycle module by a simple four-box representation of the terrestrial biosphere [Siegenthaler and Oeschger, 1987], to account to first order for changes in the terrestrial carbon storage under rising $CO_2$. The global terrestrial net primary production (NPP) is assumed to be proportional to the logarithm of the atmospheric $CO_2$ concentration, and the respiratory $CO_2$ flux back into the atmosphere is linear in the four reservoir contents [Joos et al., 1996, Kicklighter et al., 1999]. Like other current terrestrial carbon cycle models, our terrestrial biosphere model neglects the effects of land-use changes and other interference and corresponding losses of biological diversity and productivity. It neglects furthermore complete NPP saturation even at high $CO_2$ levels, and it neglects an accelerated respirative return of carbon to the atmosphere as is expected in a warmer climate. It is possible that these additional feedbacks would reduce the terrestrial $CO_2$ uptake.

The aggregate model of the terrestrial carbon cycle is tuned to match estimates of the terrestrial carbon sink during the 1980's [Schimel et al., 1997]. When driven by emission scenarios, its response in terrestrial $CO_2$ uptake was well within the range obtained with current, spatially resolved models [Kicklighter et al., 1999].

# Chapter 3

# The CARC module: technique

## 3.1 Three impulse response functions from HAMOCC

The oceanic carbon cycle impulse response function used as baseline model in the NICCS CARC module is a recent fit to the inorganic version HAMOCC3i, while the two other IRFs shown in Fig.3.1 are obtained from the original HAMOCC1 by Maier-Reimer and Hasselmann [1987] and from an organic version containing an additional sediment pool [Maier-Reimer, 1993] whose $CO_2$ uptake reduces the asymptotic airborne fraction to 7%. The differences between the two inorganic versions arise through the onset of the nonlinear chemisry effect, as the older IRF is a fit to a larger impulse, increasing the preindustrial $CO_2$ by 25 % (compare also Fig.2.1). Parameters of these three ocean-CARC IRFs are listed in table 3.1.

## 3.2 The linear impulse response function of the composite-layer

A good fit to the linear atmospheric response $\hat{R}_c(t)$ of the 3D ocean carbon cycle model of Maier-Reimer and Hasselmann [1987] to atmospheric $CO_2$ input can be obtained by a sum of four decaying exponentials plus a constant defining the asymptotic equilibrium state:

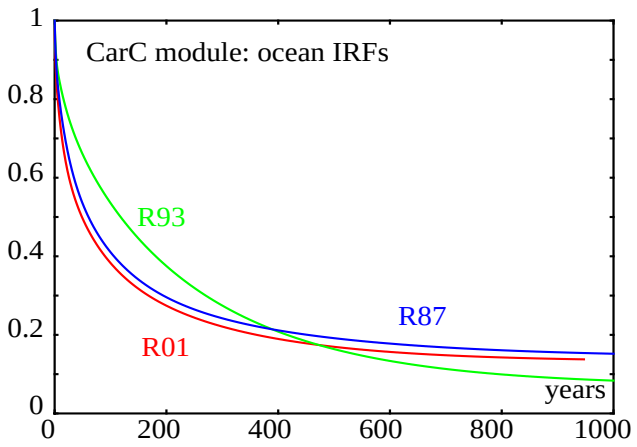


Figure 3.1: Three impulse response functions from HAMOCC

| | $A_0$ | $A_1$ | $\tau_1$ [y] | $A_2$ | $\tau_2$ [y] | $A_3$ | $\tau_3$ [y] | $A_4$ | $\tau_4$ [y] |
|---|---|---|---|---|---|---|---|---|---|
| $R01$ | 0.132 | 0.311 | 236.5 | 0.253 | 59.52 | 0.209 | 12.17 | 0.095 | 1.271 |
| $R93$ | 0.07 | 0.648 | 258.5 | 0.101 | 71.9 | 0.097 | 17.6 | 0.084 | 1.6 |
| $R87$ | 0.142 | 0.241 | 313.8 | 0.323 | 79.8 | 0.206 | 18.8 | 0.088 | 1.7 |

Table 3.1: Amplitudes and time constants for the oceanic $CO_2$ uptake IRF shown in Fig.3.1. The most recent one, R01, is a least-squares fit to the HAMOCC3i response to a sudden 1% increase of its preindustrial atmospheric $CO_2$ (cf. Fig. 2.1). R87 and R93 are fits to the response to 25% impulses, obtained by Maier-Reimer and Hasselmann [1987] and Maier-Reimer [1993] from other HAMOCC versions.

$$\hat{R}_c(t) = \sum_{i=0}^{4} A_i \exp(\frac{-t}{\tau_i}) \tag{3.1}$$

$$\text{with} \quad \tau_0 = \infty \tag{3.2}$$

$$\text{and} \quad \sum_i A_i = 1 \quad . \tag{3.3}$$

The shortest decay time $\tau_4$ can be interpreted as the composite-layer equilibration time, the associated amplitude $A_4$ representing the fraction of a given $\delta$-impulse carbon input into the atmosphere at time $t = 0$ which becomes dissolved in the ocean surface layer within the time scale $\tau_4$. The ratio of the impulse-added $CO_2$ content of the composite layer to the change

of the atmospheric $CO_2$ content shortly after equilibration is accordingly $1/(1-A_4)$. The linearized impulse response of the composite layer can thus be obtained from the IRF representation of the atmospheric response of the complete model of Maier-Reimer and Hasselmann [1987] by dropping the short-time-scale term and subsequently renormalizing:

$$R_c(t) = \sum_{i=0}^{3} a_i \exp(\frac{-t}{\tau_i}) \tag{3.4}$$

$$\text{with} \quad \tau_0 = \infty \tag{3.5}$$

$$\text{and} \quad a_i = \frac{A_i}{1-A_4} \tag{3.6}$$

## 3.3 The equivalent differential analogue

The IRF model (3.4) - (3.6) is replaced in NICCS by a numerically equivalent differential model representing a cascade of layers $i$ of carbon content $c_i$ which are coupled through Newtonian fluxes between neighboring layers proportional to the concentration differences. The flux into the uppermost (composite) layer $i = 0$ is given by the (prescribed) anthropogenic emissions: $q_0 = e(t)$. Thus the differential system has the form

$$\dot{\mathbf{c}} + \mathbf{D}\mathbf{c} = \mathbf{e} \tag{3.7}$$

where $\mathbf{c}(t) = (c_0, \ldots, c_{n-1})$, $\mathbf{e}(t) = (e(t), 0, \ldots, 0)$ and $\mathbf{D}$ represents the Newtonian transfer matrix. For the case of $n = 4$ relaxation times $\tau_i$, as in eq. (3.4), the transfer matrix is given by

$$\mathbf{D} = \begin{pmatrix} \frac{\eta_1}{h_0} & -\frac{\eta_1}{h_1} & 0 & 0 \\ -\frac{\eta_1}{h_0} & \frac{\eta_1+\eta_2}{h_1} & -\frac{\eta_2}{h_2} & 0 \\ 0 & -\frac{\eta_2}{h_1} & \frac{\eta_2+\eta_3}{h_2} & -\frac{\eta_3}{h_3} \\ 0 & 0 & -\frac{\eta_3}{h_2} & \frac{\eta_3}{h_3} \end{pmatrix} \quad . \tag{3.8}$$

The Newtonian transfer coefficients $\eta_i$ $(i = 1, \ldots, n-1)$ and the layer thicknesses $h_i$ $(i = 0, \ldots, n-1)$ are tunable constants. Unfortunatly, the relations between the parameters $h_i, \eta_i$ of the differential analogue and the the parameters $a_k, \tau_k$ of the of the composite-layer IRF $R_c$ are nonlinear and cannot be derived in closed form. They must be determined by satisfying a set of tuning conditions derived from the analytical Green function solution of the linear model equations.

## 3.4 Calibration of the diffential analogue

To find those values of its parameters at which the differential analague model matches a given linear IRF, we first diagonalize $\mathbf{D}$ by expressing both the solution $c_i(t)$ and the forcing $e_i(t)$ in terms of the eigenvectors of $\mathbf{D}$:

$$c_i(t) = \sum_k x_k(t)\, C_{ik} \quad , \tag{3.9}$$

$$e_i(t) = \sum_k r_k(t)\, C_{ik} \quad , \tag{3.10}$$

where $C_{ik}$ is the $i^{th}$-layer component of the eigenvector $\mathbf{C}_k$ of $\mathbf{D}$ associated with the eigenvalue $\lambda_k$ (for the Newtonian relaxation system described by eqs. (3.7, 3.8), the $\lambda_k$ are real and positive):

$$\sum_j D_{ij} C_{jk} = \lambda_k C_{ik} \quad . \tag{3.11}$$

Comparison of the zeroth-layer solution for the case of a $\delta$-impulse forcing ($e(t) = c^\delta\, \delta(t)\,,\ r_k(t) = r_k^\delta\, \delta(t)$ , with constant $c^\delta$ , $r_k^\delta$), with the composite-layer impulse response function (3.4) yields the tuning conditions

$$\lambda_k = \tau_k^{-1} \tag{3.12}$$

$$\frac{r_k^\delta\, C_{0k}}{c^\delta} = a_k \qquad (k = 0, \ldots, n-1) \quad . \tag{3.13}$$

The condition $\lambda_0 = \tau_0^{-1} = 0$ is satisfied through the conservation of carbon by the analogue model, which requires $\sum_j D_{ij} = 0$ and therefore a singular propagator, $|\mathbf{D}| = 0$.

The eigenvectors $\mathbf{C}_k$ and eigenvalues $\lambda_k$, and thereby also the forcing representation in eigenvector coordinates $r_k^\delta$, depend on the layer thicknesses $h_i$ $(i = 0, \ldots, n-1)$ and diffusion coefficients $\eta_i$ $(i = 1, \ldots, n-1)$. These must be determined numerically such that the conditions (3.12) and (3.13) are fulfilled.

With given $\tau_0 = \infty$ and the renormalization condition $\sum_i a_i = 1$, the composite-layer IRF (3.4) has six remaining independent parameters. For $n = 4$, the analogue clearly contains the required four time constants (one of which is infinite). However, it contains seven rather than six free tuning parameters (four layer thicknesses $h_i$ and three diffusion constants $\eta_i$). The additional degree of freedom arises because the analogue model computes only the carbon content of the layers, not their concentrations. Thus the model is determined through $R_c$ only up to an arbitrary scaling factor: the transport matrix $\mathbf{D}$ is homogeneous in the ratios $\eta/h$, and the thicknesses

| | *a) R*01 | GM | *b) R*01 | NA | *c) R*93 | GM |
|---|---|---|---|---|---|---|
| $h_s$ | 64 | m | 73 | m | 56 | m |
| $h_0$ | 672 | m | 768 | m | 664 | m |
| $h_1$ | 419 | m | 479 | m | 262 | m |
| $h_2$ | 1136 | m | 1299 | m | 1641 | m |
| $h_3$ | 2382 | m | 2723 | m | 6119 | m |
| $\eta_1$ | 16.88 | m/y | 19.30 | m/y | 6.83 | m/y |
| $\eta_2$ | 9.04 | m/y | 10.33 | m/y | 6.05 | m/y |
| $\eta_3$ | 6.32 | m/y | 7.23 | m/y | 14.89 | m/y |

Table 3.2: Layer thicknesses and diffusion coefficients tuned to (*a, b*) HAMOCC 1% impulse response *R*01, (*c*) *R*93 from Maier-Reimer [1993] (both IRFs in Fig. 3.1, Table 3.1). For (*a, c*), the model was tuned using global-mean temperature chemistry, for (*b*), using North Atlantic chemistry.

of all layers can be changed by an arbitrary factor, provided the carbon exchange coefficients are changed by the same factor.

The additional degree of freedom can be fixed by the known relation between the carbon content and $CO_2$ concentration of the atmosphere. Applying the known linear-limit ratio of the $CO_2$ concentrations in the two subsystems atmosphere, mixed layer of the composite layer, one obtains for the layer thicknesses of the mixed-layer and composite-layer (expressed in equivalent water units), after some algebra:

$$\begin{aligned} h_s &= \frac{\xi_p w_p}{A_{oc}\, m_C\, \Sigma C_p} \cdot \frac{A_4}{1-A_4} \quad , \\ h_0 &= \frac{\xi_p w_p}{A_{oc}\, m_C\, \Sigma C_p} \cdot \frac{1}{1-A_4} \quad , \end{aligned} \tag{3.14}$$

where $\xi$ is the preindustrial Revelle buffer factor (see below), $m_C$ the molar mass of carbon, and $A_{oc}$ the area of the world ocean.

table: layer thicknesses

## 3.5 Introduction of nonlinear chemistry

The differential cascade analogue to the IRF model has been introduced above primarily as a mathematical tool to reproduce the response of the

more sophisticated carbon-cycle model to anthropogenic forcing via the tuning to an intermediate IRF model, without reference to real physical processes or observations. However, it appears reasonable to ascribe now a specific physical interpretation to the composite layer of the differential analogue by regarding it as composed explicitly of the atmosphere and the mixed layer. Although we have used this terminology already in the above analysis, the physical interpretation has had no mathematical implications so far apart from determining the free scaling parameter of the analogue model (which is irrelevant as long as we consider only the net carbon content of the composite layer, without attaching a physical significance to the layer). By interpreting the composite layer physically, we may now extend the linear IRF model into the nonlinear domain by considering the nonlinear chemical equilibration between the atmosphere and the mixed layer.

While the Newtonian flux $q_1$ from the zeroth (composite) layer into the first oceanic layer is still linear at large partial pressures of $CO_2$, the surface-layer carbon content anomaly $c_s$ becomes a nonlinear function of the composite-layer carbon content anomaly $c_0$. The function $c_s = c_s(c_0)$ can be computed from the nonlinear chemistry of the mixed layer, given the thicknesses of the mixed-layer and the atmosphere and the equilibrium ratios of the partial pressures of $CO_2$ in the atmospheric and ocean. Thus, the expression $c_0/h_0$ in the analogue's dynamical equations (3.7,3.8) is no longer equal to the surface layer concentration. However, the thicknesses of the composite layer and its subsystems are chosen to ensure this is the case in the linear limit:

$$\lim_{c_0 \to 0} \left( \frac{c_s}{h_s} \right) = \frac{c_0}{h_0} \quad . \tag{3.15}$$

The evolution equations (3.8) therefore need to be reformulated for the two uppermost layers in terms of the explicit nonlinear relation $c_s(c_0)$:

$$\begin{aligned} \dot{c}_0 &= e(t) - \frac{\eta_1}{h_s} c_s(c_0) + \frac{\eta_1}{h_1} c_1 \\ \dot{c}_1 &= \frac{\eta_1}{h_s} c_s(c_0) - \frac{\eta_1 + \eta_2}{h_1} c_1 + \frac{\eta_2}{h_2} c_2 \end{aligned} \tag{3.16}$$

The linear equations (3.7) and (3.8) for $\dot{c}_2$ and $\dot{c}_3$ remain unchanged.

For the numerical integration of the nonlinear analogue, the nonlinear relation $c_s(c_0)$ is evaluated at each time step by computing the chemical equilibrium determined by the various chemical processes associated with the dissolution and dissociation of $CO_2$ in seawater.

Solving the system for several slightly perturbed values of $pCO_2$ relative to its preindustrial value $pCO_{2,p}$ yields a finite-difference estimate of the

preindustrial buffer factor $\xi_p$. With consistent values of $pCO_{2,p}$, $\Sigma C_p$, and $\xi_p$, the thickness of the composite layer, $h_0$, (and thereby its volume, given the total surface area $A_{oc}$ of the world ocean) can be computed from eq.(3.14). The carbon content anomaly in the mixed layer, $c_s$, can then be found numerically for any given carbon content anomaly in the composite layer, $c_0$.

## 3.6 Terrestrial carbon allocation

The terrestrial part of the NICCS CARC module is an adapted version of the nonlinear IRF model described by Joos et al. [1996]. It is driven by the logarithmic NPP flux assumed in the original bern model:

$$\Delta f_{\mathrm{NPP}}(t) = f_0 \cdot \ln\left(\frac{w_p + c_a(t)}{w_p}\right) \quad , \tag{3.17}$$

$$\text{where} \quad f_0 = f_{\mathrm{NPP,O}} \cdot \beta_{\mathrm{NPP}} \tag{3.18}$$

For compatibility with the differentially-formulated oceanic part of the NICCS CARC module, the IRF model describing the respirational decay has been translated back into a differential linear box analogue consisting of four independent carbon pools $i$, each with content $c_{Bi}(t)$. The net flux into each pool is the difference between the pool's fraction of the nonlinear NPP and a linear decay term representing respiration, with the rate coefficients from the IRF given by Joos et al. [1996]:

$$c_B(t) = \sum_{i=1}^{4} c_{Bi}(t) \quad , \tag{3.19}$$

$$\dot{c_{Bi}} = b_i \Delta f_{\mathrm{NPP}}(t) - \frac{1}{\tau_{Bi}} c_{Bi}(t) \tag{3.20}$$

As NICCS is designed for repeated long-term scenarios, it should desirably be run at time steps as long as $\Delta t = 5$ years. Two of the decay time constants are shorter than this, which would lead to numerical instability in an explicit forward-integration algorithm. Instead of running the model at shorter time steps, we adopted an approach that is similar to the teatment of the air-sea exchange in the composite atmosphere-plus-ocean-surface layer (Chapter 2.1): the biospheric short-term carbon overturning through the fast reservoirs $c_{B1}$ and $c_{B2}$ is approximated by one reservoir that is in instantaneous equilibrium with the atmospheric $CO_2$ concentration. Its content is the sum of the contributions to the production flux into the fast reservoirs, each multiplied with the corresponding decay time constant, interpreted as the

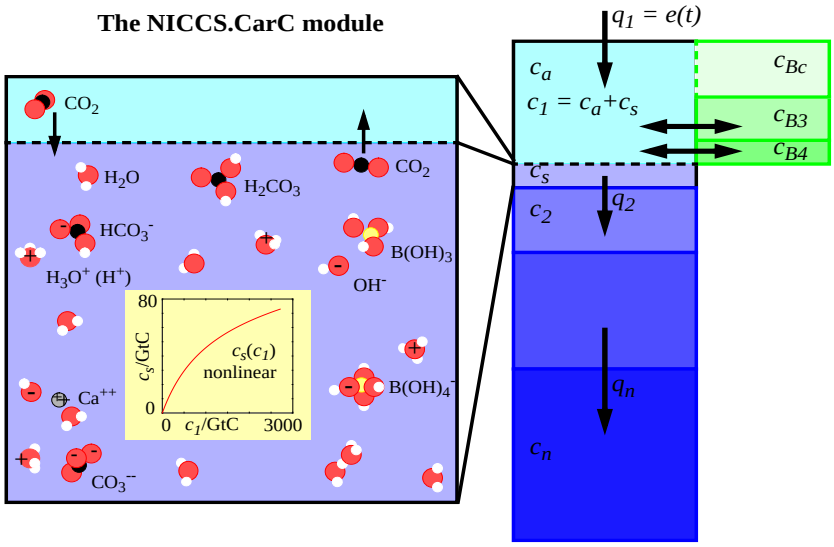


Figure 3.2: Complete carbon cycle model.

reservoir's average throughflux time:

$$\begin{aligned} c_{Bc}(t) &= \tau_c \cdot \Delta f_{\mathrm{NPP}}(t)) \quad , \\ \text{with} \quad \tau_c &= b_1\,\tau_{B1} + b_2\,\tau_{B2} \quad . \end{aligned} \tag{3.21}$$

Thus, description of the global terrestrial carbon cycle reduces to two dynamical reservoirs $c_{B3}$ and $c_{B4}$ (the equations of which still have to be forward-integrated) and a single equilibrium reservoir:

$$c_B(t) = c_{Bc}(t) + c_{B3}(t) + c_{B4}(t) \quad . \tag{3.22}$$

## 3.7 NICCS Ocean-plus-land CARC module

To include the terrestrial biosphere substitute model into the CARC module, the three biosphere pools are coupled to the atmosphere of the ocean-atmosphere CARC box analogue (via NPP and return flux, see Fig. 3.2). Of the ocean CARC box model equations (3.16), only the first one has to be modified, the one which describes the C perturbation in the atmosphere and

mixed layer:

$$\begin{aligned}
\dot{c_1} &= e(t) - \frac{\eta_2}{h_s}\, c_s(c_1) + \frac{\eta_2}{h_2}\, c_2 \; - \; \dot{c_{Bc}}(t) - \dot{c_{B3}}(t) - \dot{c_{B4}}(t) \\
&= e(t) - \frac{\eta_2}{h_s}\, c_s(c_1) + \frac{\eta_2}{h_2}\, c_2 \; - \qquad (3.23) \\
&\quad A(c_1) \cdot \dot{c_1} \; - \; (b_3 + b_4) \cdot B(c_1) \; + \\
&\quad \frac{1}{\tau_{B3}} \cdot c_{B3} \; + \; \frac{1}{\tau_{B4}} \cdot c_{B4}
\end{aligned}$$

$$\text{with} \qquad A(c_1) = \frac{\tau_c \cdot f_0}{c_a(c_1) + w_0} \cdot \frac{dc_a}{dc_1} \qquad (3.24)$$

$$\text{and} \qquad B(c_1) = f_0 \cdot \ln\left(\frac{c_a(c_1) + w_0}{w_0}\right) \quad . \qquad (3.25)$$

The atmosphere-ocean model is then augmented by three equations describing the additionally sequestered biospheric carbon. Together with the unchanged equations for the deep ocean layers, the complete model can then be written:

$$
\begin{aligned}
\dot{c_1} &= D(c_1) \cdot \Big\{ e(t) - \frac{\eta_2}{h_s}\, c_s(c_1) + \frac{\eta_2}{h_2}\, c_2 - \\
&\qquad (b_3 + b_4) \cdot B(c_1) \; + \; \frac{1}{\tau_{B3}} \cdot c_{B3} \; + \; \frac{1}{\tau_{B4}} \cdot c_{B4} \Big\} \\
\dot{c_2} &= \frac{\eta_2}{h_s}\, c_s(c_1) - \frac{\eta_2 + \eta_3}{h_2}\, c_2 + \frac{\eta_3}{h_3}\, c_3 \\
\dot{c_3} &= \frac{\eta_3}{h_2}\, c_2 - \frac{\eta_3 + \eta_4}{h_3}\, c_3 + \frac{\eta_4}{h_4}\, c_4 \\
\dot{c_4} &= \frac{\eta_4}{h_3}\, c_3 - \frac{\eta_4}{h_4}\, c_4 \\
\dot{c}_{Bc} &= A(c_1) \cdot \dot{c_1} \\
\dot{c}_{B3} &= b_3 \cdot B(c_1) \; - \; \frac{1}{\tau_{B3}} \cdot c_{B3} \\
\dot{c}_{B4} &= b_4 \cdot B(c_1) \; - \; \frac{1}{\tau_{B4}} \cdot c_{B4} \qquad (3.26)
\end{aligned}
$$

$$
\begin{aligned}
\text{with} \qquad D(c_1) &= \frac{1}{1 + A(c_1)} \\
&= \left( 1 \; + \; \frac{\tau_c \cdot f_0}{c_a(c_1) + w_0} \cdot \frac{dc_a}{dc_1} \right)^{-1} \qquad (3.27)
\end{aligned}
$$

The system (3.26, 3.27) contains a number of nonlinear functions of the carbon content perturbation $c_1$ in the combined atmosphere-sea-surface layer: $c_s$, $c_a = c_1 - c_s$, $A$, $B$, and $D$. These can be computed in advance and written to look-up tables, in order to speed up the integration. A simple predictor-corrector scheme was implemented; it has been tested in a biosphere-alone version to accurately reproduce the results of the IRF model.

In cases where only the oceanic carbon uptake is of interest, the biospheric uptake can be switched off by setting $\beta_{npp} = 0$.

# Chapter 4

# The climate change (CLIC) module

In addition to the carbon-cycle (CARC) IRF, we require as second component of our IRF model an IRF representation of the physical coupled atmosphere-ocean climate system (CLIC). This was calibrated against the Hamburg AOGCM, as described in Hasselmann et al. [1993], Cubasch et al. [1992]) and Hasselmann et al. [1997]. However, in contrast to these applications, we consider now not only the global mean temperature as climate-change index, but generalize the CLIC-IRF representation to include four representative two-dimensional fields: near-surface temperature ($T_{2m}$), cloud cover ($clo$), precipitation ($pre$), and sea level ($sea$).

Schlesinger et al. [1998] proposed a procedure for combining a number of fixed spatial patterns with time-dependent coefficients in which the spatial patterns were derived from several equilibrium climate change simulations with a coupled atmospheric general-circulation/mixed-layer-ocean model, while the trajectories of the corresponding time-dependent coefficients were computed by an energy-balance-climate/upwelling-diffusion-ocean model. Although this provides a number of spatial patterns and dynamic responses which can be combined to describe the net responses to different forcing mechanisms (greehouse gases and direct sulfate aerosol forcing, for example), the spatial signals and temporal evolutions were derived from different models and were therefore not necessarily consistent. Furthermore, the parent models were strongly simplified in at least one of their components (atmosphere or ocean) and were thus less reliable with respect to the net spatio-temporal response than a fully coupled AOGCM. However, the validity of a separation of variables into spatial patterns of change with associated time-dependent factors has been confirmed by other authors, see Hunting-

ford and Cox [2000] and citations therein.

Huntingford and Cox [2000] reproduced (decade-averaged) global mean changes in a number of impact-relevant surface climate variables (for each month of the year) using a two-box model fit to two 150-year/250-year greenhouse integrations with the Hadley Center AOGCM. The corresponding relative scaling patterns of regional changes were obtained by fitting the AOGCM's (decade-averaged monthly) global mean time series to the individual time series in each land grid cell by variation of one scaling factor per grid cell. Thus the temporal and spatial signals represent one common parent model and calibration experiment.

In the following, we pursue the same basic pattern-projection strategy as Huntingford and Cox [2000], deriving both the spatial and temporal information simultaneously from the same transient AOGCM simulation. We then reproduce the (dimensionally reduced) space-time dependent AOGCM signal with an IRF model. To enhance the signal-to-noise ratio we separated the space-time dependent AOGCM output fields into noise and signal components using an EOF analysis applied to a long transient experiment (850 years) with the parent AOGCM, and restricted the analysis furthermore to annual means.

## 4.1 Purpose and components

The clic module translates time-dependent changes of the atmospheric $CO_2$ concentration into space-time dependent changes in a choice of climatic variables. The variables thus available to-date are the annual means of near-surface temperature ($T_{2m}$), total cloud cover ($clo$), precipitation ($pre$), and sea level ($sea$). This choice accounts for impact relevance on the one hand and signal detectability on the other, and is intended to be extended to diurnal and annual cycles and statistical properties of these variables and possibly other variables that may be found of importance.

The module consists of one IRF module to each of its climatic variables and, to each variable, a two-dimensional global pattern representing the spatial distribution of the signal. The purpose of the IRF modules is to reproduce the time evolution of the global-mean greenhouse signals. As the patterns are constant in time, they are ignored for calibration of the IRF modules. However after calibration, in operation of the NICCS clic module, the patterns are multiplied with the climate response time series generated by the IRF models to yield the composite spatiotemporal signal of climate change.

The spatial patterns have been extracted by Dr.R.Voss from a calibration simulation with the parent model (850 years ECHAM3-LSG with $CO_2$ growing to 4xCO2 in 120 years, then constant) through EOF analysis, together and consistent with the time series used for calibration of the IRF models.

## 4.2 Spatiotemporal, multi-variable climate change signals

To extract the climate change signal from the AOGCM response, consisting of a superposition of the externally forced signal and the natural variability of the AOGCM, we represent the response (forced scenario minus control run) as the superposition

$$f^v(x,t) = \sum_i p_i^v(t) \cdot f_i^v(x) \tag{4.1}$$

of a set of EOFs (*empirical orthogonal functions*) $f_i^v(x)$ with associated time-dependent scalar coefficients, the *principal components* (PCs) $p_i^v(t)$. The EOF decomposition maximizes the fraction of total variance explained at any given expansion order.

The time-evolution of the coefficients $p_i^v(t)$ for which the climate change signal can be clearly distinguished from the background natural climate variability (cf. Cubasch et al. [1992], Santer et al. [1994]) can then be represented by an IRF model in the same way as the mean-temperature in the case of a single-index CLIC-IRF.

The EOF patterns and corresponding PCs used for our IRF model were extracted from an 850-year transient AOGCM simulation with the periodically-synchronously coupled models ECHAM3 and LSG [Voss et al., 1998, Voss and Mikolajewicz, 2001]. The (equivalent) $CO_2$ concentration was prescribed as exponential growth up to the fourfold 'preindustrial' level (330 ppm) at year 120, after which the concentration was kept constant.

The AOGCM's 32 latidue circels are listed in Table 4.1 (from south to north), while the longitudes are integer multiples of 5.625 degrees. An idea of the model's resolution is given by its land-sea mask (Figure 4.1).

The signal analysis was carried out for the annual means of near-surface temperature, precipitation, cloudiness, and sea level. The time series of the first six principal components for each of the four fields are shown in the four left panels of Figure 4.2. The PCs of second and higher order show statistical fluctuations around zero, without a clear signal. However,

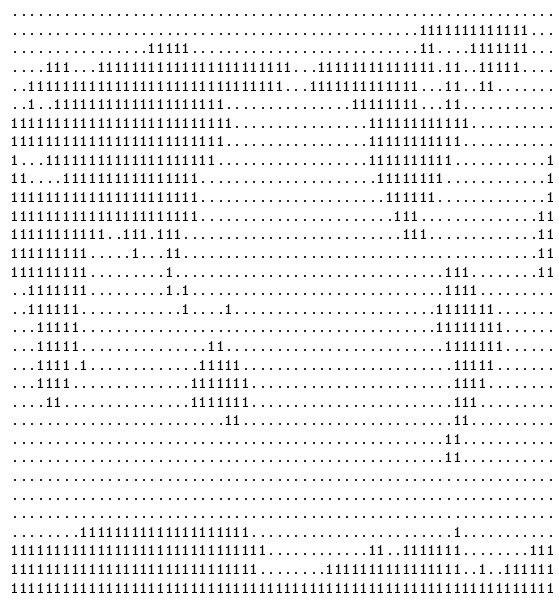

Figure 4.1: Land-sea mask of the ECHAM3 grid.

the first PCs, $p_1^v(t)$, of all four variables start close to zero, but then clearly emerge from the noise during the course of the simulation. The signal growth closely follows the increase in the forcing during the first 120 years, but continues to increase after the forcing is kept constant, although on a slower time scale. The signal is best discernible in the sea level rise, but can be clearly distinguished from the noise also in the three atmospheric variables. Extrapolation of the $p_1^S(t)$ curve for sea level rise suggests that equilibrium would not be reached until well after a thousand years.

| | | |
|---|---|---|
| -85.7605871204 | -80.2687790722 | -74.7445403686 |
| -69.2129761693 | -63.6786355611 | -58.1429540492 |
| -52.6065260343 | -47.0696420596 | -41.5324612466 |
| -35.9950784112 | -30.4575539611 | -24.9199286299 |
| -19.3822313464 | -13.8444837343 | -8.30670285651 |
| -2.76890300773 | 2.76890300773 | 8.30670285651 |
| 13.84448373438 | 19.38223134643 | 24.91992862995 |
| 30.45755396115 | 35.99507841127 | 41.53246124666 |
| 47.06964205969 | 52.60652603435 | 58.14295404920 |
| 63.67863556110 | 69.21297616937 | 74.74454036864 |
| 80.26877907225 | 85.76058712044 | |

Table 4.1: Latitude circles of the ECHAM3 grid.

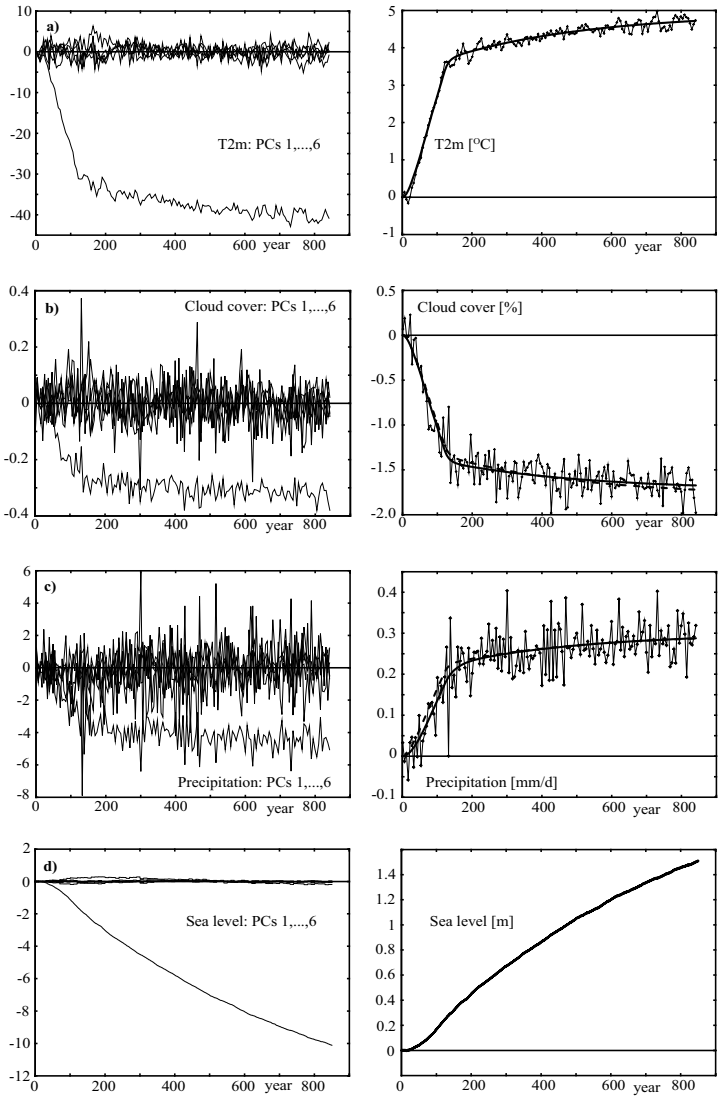


Figure 4.2: *Left, from above:* Principal component analysis of the changes (scenario minus control) in (a) 2m-temperature, (b) cloud coverage, (c) precipitation, and (d) sea level, in the transient 4x$CO_2$, 850-year simulation with the ECHAM3-LSG AOGCM. Shown are time series of the leading six principal components $p_1^v, ..., p_6^v$. *Right:* Fit of IRF models to the $p_1^v$ time series. Sign reversals are due to renormalization, for convenience, to unit global pattern mean and global-mean time series. Also shown for cloud coverage and precipitation changes are the appropriately rescaled temperature response curves (*dashed*).

## 4.3 Impulse-response representation

Since the climate change signals of all four variables considered can be well captured by the first EOFs, while the higher EOFs are indistinguishable from the noise, the regional climate change signals can be reproduced by an IRF representation of just the first term in each of the expansions (4.1),

$$f^v(x,t) \approx p_1^v(t) \cdot f_1^v(x) \tag{4.2}$$

$$p_1^v(t) \approx \frac{1}{\ln 2} \int_{t_0}^{t} R^v(t-t') \cdot \frac{d}{dt'} \ln\left(\frac{w(t')}{w_p}\right) \cdot dt' \quad . \tag{4.3}$$

The assumed logarithmic relation between concentration and radiative forcing corresponds to the standard representation of the near-saturation of the principal $CO_2$ infra-red absorption bands [IPCC, 1990, Myhre et al., 1998]. For concentrations below the reference value of 2x$CO_2$, the logarithmic expression yields a slightly warmer equilibrium than the linear model, while at higher concentrations the warming is significantly weaker. To fit the IRF function $R^v(t)$ to the AOGCM scenario simulation, the function was represented as a sum of exponentials:

$$R^v(t) = S^v \sum_i a_i^v \left(1 - \exp\left(\frac{-t}{\tau_i^v}\right)\right) \quad , \tag{4.4}$$

where $\sum_i a_i = 1$, so that $S^v$ represents the model's asymptotic climate sensitivity to a $CO_2$ doubling.

The climate change signal patterns $f_1^v(x)$ were normalized to have unit global means (Figs.4.3 – 4.6). Thus, the $p_1^v(t)$ time series represent global mean climate change signals, the patterns indicating where the change is larger ($f_1^v(x) > 1$) or smaller ($f_1^v(x) < 1$) than the global mean.

The time constants $\tau_i^v$ and amplitudes $a_i^v$ of $R^v$ were obtained by a least-squares fit of the IRF model to the $p_1^v$ time series (Table 4.2). Low signal-to-noise ratio did not permit determination of more than two time constants of the IRFs. Least-square fit experiments on a coarse 2d $\tau_1^v$-$\tau_2^v$ grid (with the $a_i^v$ optimized at each $\tau_1^v$-$\tau_2^v$ gridpoint) indicated that for the atmospheric variables (temperature, cloud cover, precipitation) the fit quality (rms) is relatively little changed within a range of appropriate combinations of the two time constants (300 - 700 years for $\tau_1^v$ and 12 - 28 years for $\tau_2^v$). Only for sea level the time constants were well determined at $\tau_1^v = 830 \pm 20$ years and $\tau_2^v = 30 \pm 5$ years. Note that the relative weightings of the short and long time scales are very different from those of the atmospheric IRFs, for which the short-time relaxation terms dominate over the long-time terms by factors of 2-4, whereasthe short-term contribution to sea level change is as

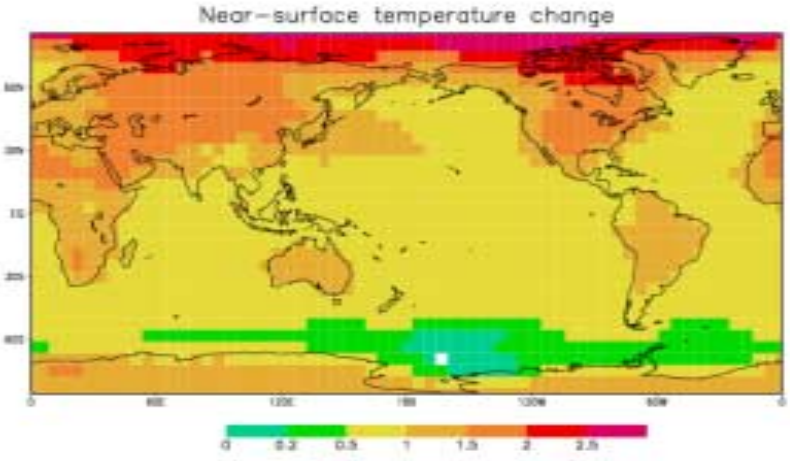


Figure 4.3: Near-surface temperature change pattern (mean= 1).

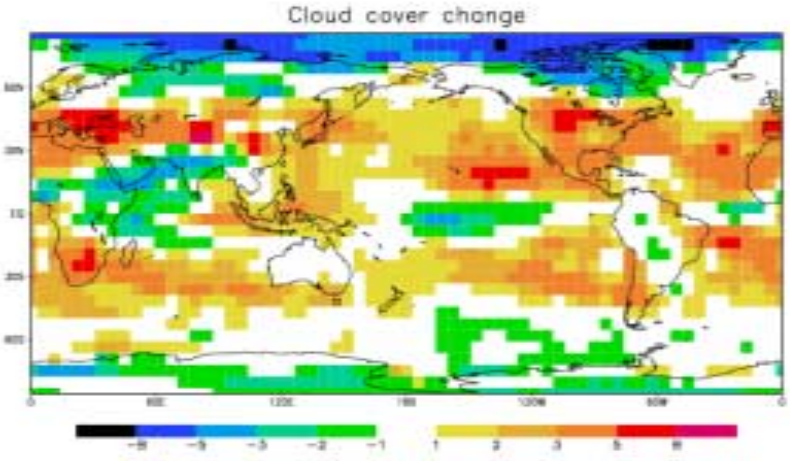


Figure 4.4: Cloud cover change pattern. Note that positive values indicate decreasing coverage.

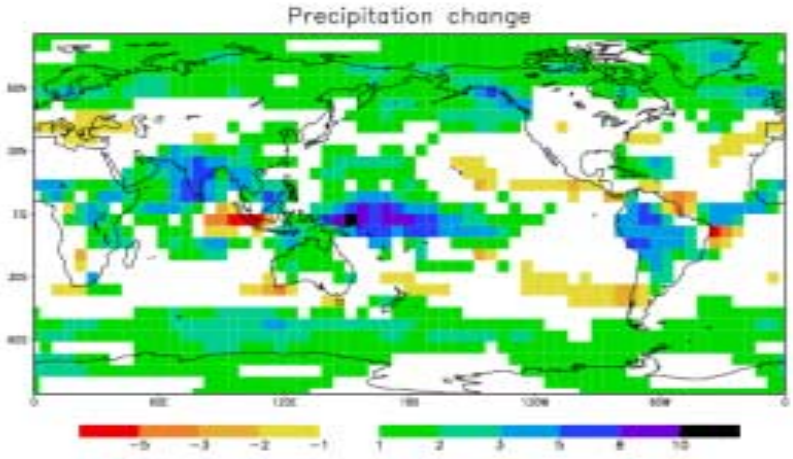


Figure 4.5: Precipitation change pattern.

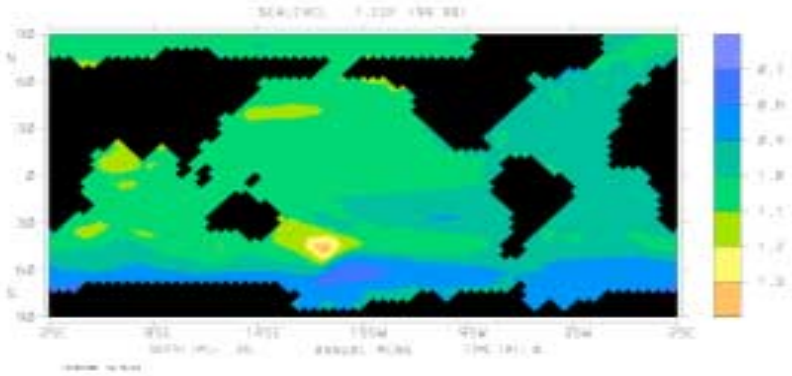

Figure 4.6: Sea level rise pattern.

small as 4 % of the long-term contribution. See below for details of fitting procedures.

Although cloud cover and precipitation are important variables for impact studies, their climate change signals exhibit lower signal-to-noise ratios than the near-surface temperature and are thus less reliably determined (Fig. 4.2, right panels, and calibration method description below). However, all three atmospheric variables represent simultaneous expressions of the total atmospheric response and may therefore be expected to exhibit similar time response characteristics. The responses would be identical, for example, if the atmosphere responds quasi-instanteously to changes in the sea surface temperature, sea-ice cover, and land moisture distribution, and the dynamic response characteristics of these variables with "memory" can be represented by a single joint EOF pattern. We have accordingly tested the fit of a single IRF to all three variables, using the $t_{2m}$ IRF model (which is most closely constrained by the data), appropriately scaled by the individual sensitivities (-0.871 % for *clo* and 0.145 mm/d for *pre*). A good fit was achieved for both cloud coverage and precipitation, with rms errors only 3 % greater than those of the independent best fits.

## 4.4 Calibration method

Finding an appropriate parametrization upon which to base the aggregate model is, in our case, most straightforward, namely a sum of decaying exponentials, which is the natural choice for a simplest-possible aggregate model. Still, fitting an IRF model to AOGCM output is a nontrivial task, as the quality and reliability of the fit crucially depend on (a) the amplitude of the signal as compared with the noise, and (b) the size of the samples (in our case: the length of the simulation).

Mathematically formulated, calibration of the IRF models is a numerical optimization problem, or more specific, the minimization of a *cost function* in the space spanned by the model parameters. An appropriate cost function is the sum of the squared differences between sample data (the AOGCM response time series) and the IRF model prediction. The IRF for each of the climate variables has four parameters, namely two time constants $\tau_i$ and the corresponding two amplitudes $a_i$.

The most straightforward method to determine the paramters of the IRFs is crude-force fitting by simultaneous variation of all four parameters. However, this is unsatisfactory even in cases where a numerically stable minimum is found (e.g. for $T_2m$) as it gives no idea about the shape of the minimum of

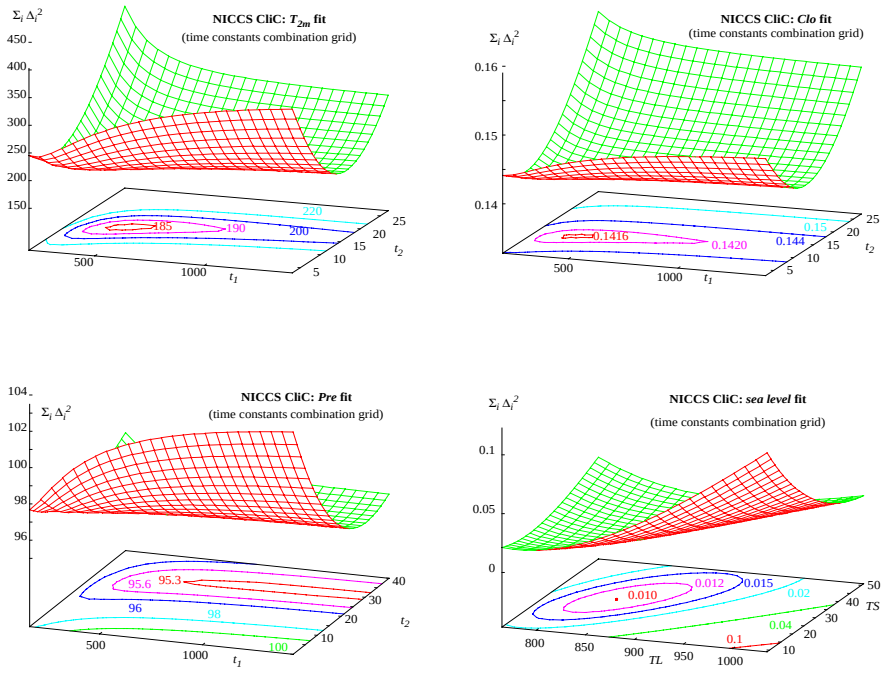


Figure 4.7: NICCS clic calibration: fit IRF models to the $PC_1$ time series from AOGCM simulation. Shown is the fit quality (sum of squared residuals for optimized IRF amplitudes $a_1^v$, $a_2^v$) on arrays of fixed combinations of the IRF time constants $\tau_1^v$, $\tau_2^v$.

the cost function in the 4D sparameter space, and thus about the robustness of the fit.

For closer inspection of the problem, I have developed a special calibration software package that allows for automatic standard numerical optimization of any choice out of the four parameters (henceforth referred to as *automatic variables*) at fixed values of the remaining parameters (the complement choice). The program allows further for scanning a grid of combinations of fixed values of the complement choice of parameters (henceforth referred to as *grid variables*) with optimization of the automatic variables at each gridpoint.

The most appropriate choice of automatic variables was found to be the two amplitudes $a_1, a_2$, leaving the time constants $\tau_1, \tau_2$ as grid variables. Thus the values of the time constants $\tau_i$ were varied through a two-dimensional array of $\tau_1, \tau_2$ combinations, linearly equidistant in each of the time scales. At

| $v$ | $a_1^v$ | $\tau_1^v$ | $a_2^v$ | $\tau_2^v$ | $S^v$ |
|---|---|---|---|---|---|
| $t_{2m}$ | 0.290 | 400. | 0.710 | 12. | 2.39 $^o$C |
| $clo$ | 0.212 | 400. | 0.788 | 12. | -0.837 % |
| $pre$ | 0.305 | 400. | 0.695 | 28. | 0.146 mm/d |
| $sea$ | 0.963 | 830. | 0.037 | 30. | 1.137 m |

Table 4.2: Amplitudes, time constants, and climate sensitivities for the IRFs of global and annual mean near-surface temperature, cloud coverage, precipitation, and sea level, fitted to the transient ECHAM3-LSG 850-year 4x$CO_2$ experiment.

each gridpoint, i.e. at each combination of fixed $\tau_1, \tau_2$ values, the amplitudes $a_1, a_2$ were determined by a standard least-squares optimization procedure to yield the best fit possible at these values of the two decay time constants.

Thus projected onto the two-dimensional $\tau_1$-$\tau_2$ surface, the minimum of the cost function (sum of squared differences between IRF model and parent AOGCM) in the four-dimensional IRF parameter space exhibits the typical banana shape frequently found in higher-than-two-dimensional optimization problems (see Fig.4.7), except in the case of sea level where the minimum is well-defined. Especially in the case of the precipitation model, the minimum is degenerate and essentially parallel to the $\tau_1$ axis, which means that the long time constant of the precipitation IRF cannot be determined at all from the AOGCM data. Consequently, the parameters may be varied through a wide range of values without significant deterioration of the cost function when the system is moved along the valley floor. Still of course the shape and characteristics of the IRF (and of the fit) do vary considerably along this path.

We conclude that even the ECHAM3-LSG, 850 year, transient 4x$CO_2$ experiment allows at most for a very coarse determination of the long time constant and its amplitude to the IRF models of the atmospheric variables (especially of the high-noise variables characterizing the atmospheric hydrological cycle). Also the accuracy to which we can estimate the short time constants is fairly limited. The most reliable fit is obtained for near-surface temperature which is taken to be a good model for the time evolution of the climate sigal in all of the three atmospheric variables. In contrast, the IRF model for sea level is well-determined through the fit.

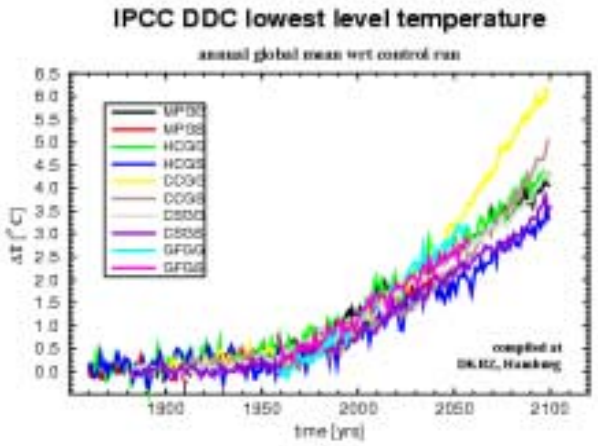


Figure 4.8: global mean temperature change computed by various AOGCMs for common prescribed 100-y scenario (with kind permission by H.Luthard)

## 4.5 IRF representations of current AOGCMs

For estimating the climate-model-related uncertainties in scenario projections of future climate change (and their relative weight in comparison with scenario-related uncertainties), it is clearly desirable to set up an ensemble of systematic IRF representations of currently existing AOGCMs. For this purpose, all AOGCMs should ideally (but not necessarily) be forced by the same common emission time series.

Such an ensemble of transient experiments on different models with common forcing was performed during the Coupled Model Intercomparison Project (CMIP). The prescribed emissions are a combination of historical data from year 1860 until present and scenario projections (exponential growth of 1% / year) for the next century until year 2100. Among the simulation output from the CMIP set of transient experiments, time series of a range of annual-and-global-mean variables, appropriate for calibration of aggregate models, are available in the CERA database (`http://www.dkrz.de/ipcc/ddc/html/dkrzmain.html`) at the German Climate Computing Center (DKRZ, Fig.4.8).

However, despite generous professional help (special thanks to H.Luthard!), two major problems were encountered on the way to meaningful and reliable IRF models for the current AOGCM fleet that made the task almost prohibitively time-consuming in practice and for the time being:

First, while *output* from many AOGCM scenario simulations is both available and well-documented in the data base, the exact common *input*, namely the $CO_2$ concentration time series, was unavailable in the database and could neither be easily obtained from the respective participating institutions. Of course, for fitting aggregate relations, the input forcing is as crucial a necessity as the output response. But AOGCMs differ widely in their formulation of the radiative forcing through $CO_2$ and other greenhouse gases as well as their "preindustrial" start concentration. Thus I have performed a few fit experiments with an assumed 1%/year growth in the *equivalent* $CO_2$ concentration, but cannot claim that this truly represents the forcing that was prescribed the respective parent AOGCMs.

Second, there is the technical problem of limited length of the time series (240 years), aggravated by the fact that the forcing is rather weak (and the response signal hardly discernible) during the first half of the simulations. Thus, for even a coarse determination of the longer of the two IRF time constants, these simulations are definitely too short. Even with an (almost) arbitrary choice of, say, $\tau_1 = 800$ years, the remaining short time scale could only be fit within a rather wide uncertainty due to the low signal-to-noise ratio imposed by the internal AOGCM variability.

To summarize, my attempt to explore the CMIP results for a reliable IRF representation of the current fleet of AOGCMs was at most partly successful and deserves further improvement. Basic requirements would be an ensemble of significantly longer transient greenhouse simulations with clear and sufficient I/O documentation.

# Chapter 5

# Nonlinear Impulse response representation of the coupled Carbon cycle-plus-Climate system (NICCS)

Coupled together, the CARC and CLIC modules form an aggregate model that describes the total net response of the global climate system to the total, globally integrated, combustion of fossil fuels.

The most straightforward application of NICCS is the fast and accurate computation of the response of atmospheric $CO_2$ concentration and climate to given emission scenarios. Examples of such scenarios are presented in this chapter, covering time horizons from a few decades to a millenium. Comparison with an older simplified model [Wigley and Raper, 1993] in Chapter 5.3 yields a mutual gain in confidence. As in the impulse experiments described above, the sensitivity of the projections to different model variants is further checked, and the CARC module is again validated against its parent three-dimensional ocean carbon transport model in Section 5.4. Before these applications, the Chapter is opened with a systematic description of the model characteristics.

## 5.1 Nonlinear response to $CO_2$ emission impulses

To illustrate the main dynamical features of our nonlinear IRF model, we computed the response of three variants of the model to three different $\delta$-function $CO_2$-emission inputs, representing a sudden increase of the pre-industrial atmospheric $CO_2$ concentration by factors of 1.25, 2 and 4, respectively (Fig.5.1). For comparison, we also ran the parent ocean carbon cycle model for these cases. The IRF model variants were:

1. the linear ocean carbon uptake module combined with linear radiative forcing (the linear convolution, or LC variant, as used in the impulse-response climate module of Hasselmann et al. [1997], thick lines in Fig.5.1).

2. the nonlinear ocean IRF analogue together with the logarithmic radiation model (the NO variant, thin lines), and

3. the same as the NO variant, but with the nonlinear ocean carbon cycle augmented by a simple $CO_2$-fertilized terrestrial biosphere carbon pool, adapted from Joos et al. [1996] (the BJ variant, thin dashed lines).

The weakest $CO_2$ input, representing an increase of the initial atmospheric $CO_2$ concentration by 25 %, or $\approx$ 140 GtC, relative to the pre-industrial level, corresponds to the total accumulated anthropogenic emissions from early industrialization until the 1980s. The response of the ocean carbon cycle (NO) is still close to the linear case (LC). Inclusion of the land biosphere pool (BJ) leads to a faster decay initially, which slows down later, however, when the additional sequestered biospheric carbon starts returning to the atmosphere. The small asymptotic biospheric retention is determined by the equilibrium between the slightly increased NPP and the respirative decay of the additional carbon.

The temperature responses of all three model variants exhibit a relatively rapid adjustment to the sudden $CO_2$ increase initially, with time scales governed by the heat uptake of the ocean, mainly in the upper 1 km. This is followed by a slow temperature decrease mirroring the decay of the $CO_2$ concentration. The nonlinear model yields substantially larger temperature changes than the linear model, as the $CO_2$ concentrations remain well below the $2\times$preindustrial level, the break-even point at which the linear and logarithmic greenhouse forcing are the same. The enhanced logarithmic forcing relative to the linear forcing in this low-concentration range overcompensates the concentration drawdown by the land biosphere carbon pool.

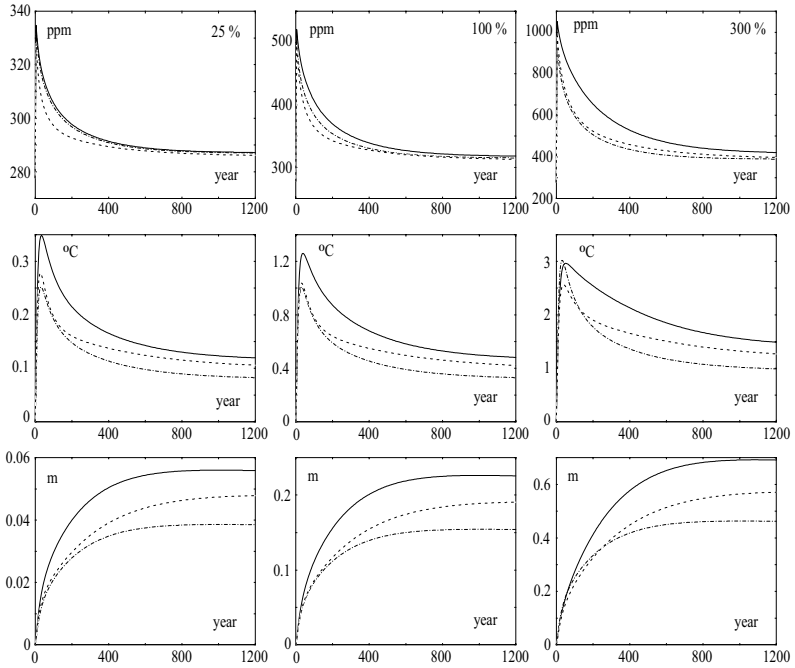


Figure 5.1: Nonlinear response of the coupled carbon cycle-climate model (NICCS) to sudden increases of the preindustrial atmospheric $CO_2$ concentration by 25%, (*left*), 100% (*center*), and 300% (*right*). *Downwards from top*: atmospheric $CO_2$ perturbation, global-mean near-surface air temperature change ($^oC$), and global-mean sea level change (m). Each panel shows the response of three IRF model variants: the nonlinear ocean $CO_2$ model without (NO, *full lines*) and with land biosphere (BJ, *dashed*), in both cases coupled to the logarithmic greenhouse forcing climate module, and the coupled linear convolution models of oceanic $CO_2$ uptake and climate change (LC, *dot-dashed*).

The response in sea level is dominated by the extremely slow warming of the deep ocean. Thus the fast initial temperature response to the sudden $CO_2$ increase, which was governed mainly by the heat uptake in the main thermocline of the ocean, does not appear as a significant signal in the sea level response. This is characterized rather by the long time scales describing the gradual relaxation of the $CO_2$ concentration to its equilibrium asymptotic value, both processes being determined by the rate of penetration of tracers ($CO_2$ and heat) into the deep ocean.

The intermediate impulse, representing an initial doubling of the $CO_2$ concentration relative to the preindustrial state, corresponds to the estimated accumulated emissions (560 GtC) for a typical business-as-usual emissions scenario some time near the middle of this century. Although the oceanic uptake is already somewhat slower than in the first experiment with weaker input, the overall climate response is not drastically changed. The difference between the linear and logarithmic greenhouse modules has become smaller, thereby reducing the greenhouse forcing relative to the linear case and partially compensating the effect of the relatively higher $CO_2$ concentrations resulting from the slower nonlinear carbon uptake.

In contrast, the largest $CO_2$ impulse, corresponding to a sudden $CO_2$ quadrupling (1650 GtC input), is sufficiently large to drive the oceanic carbon uptake well out of its linear regime, although even this input is still substantially smaller than estimates of the total fossil fuel resources – including anticipated but not yet discovered resources – of 4000 to more than 25000 GtC, cf. IPCC [1996] p.40 (Technical Summary) and p.87 (Nakićenović). As the peak temperature response of 3 $^oC$ is now above the break-even point of the logarithmic radiative forcing, the nonlinear variant yields a weaker forcing than the linear variant. The effect is sufficiently strong to overcompensate the higher $CO_2$ concentrations of the nonlinear ocean uptake model, so that the peak warming is slightly lower than in the linear variant. Both the peak warming and the subsequent decay of the $CO_2$ concentration are retarded relative to the linear case. The impact of the nonlinearities is least pronounced in all three model variants in sea level, where the largest impulse produces only a weak retardation relative to the linear case.

For greater numerical efficiency of the NICCS model, in which the CARC-IRF and CLIC-IRF modules were coupled together, we constructed also for the CLIC IRF model an equivalent differential box-model analogue that could be directly coupled to the differential equivalent of the CARC IRF module. Both modules could then be integrated within the same time-integration loop, avoiding also the second nested time-variable loop required for the standard integral formulation of the CLIC IRF model.

We point out in conclusion that the limitation to the one-dimensional representation of annual mean values of four selected variables is not dictated a priori by the model design. The approach may be readily generalized to higher-order EOFs, if these can be reliably distinguished from noise through sufficiently long integrations or Monte Carlo simulations, and it can be applied to any variable that is (directly or indirectly) provided by the parent AOGCM, such as seasonal variability or higher-moment statistics. The system's response to forcing mechanisms other than greenhouse gases, like sulfate or volcanic aerosols, or solar variability, can be similarly treated in terms of further linearly superimposable IRF models.

## 5.2 Global warming scenarios of the next 30 years (Kiel/VW)

As an example of climate impact cost estimation over a typical economic planning time horizon, three scenarios are presented that were studied with an economic general equilibrium model (GEM) developed at the department for environmental resources of the Institute for World economy (IFW) in Kiel, Germany. As the model development project was supported by the Volkswagen Foundation, the model and the respective scenarios may be called, in the context of this thesis, the VW model/scenarios.

**Translating climate change into regional economic costs**

Goal of the study was an estimation of the impact of climate change on various economic sectors in each of eleven economic standard world regions (see Table 5.1).

Monetary quantification of total related damage would clearly be necessary for realistic modelling of economic feedbacks of climate change on the development of the global human civilization. However this fundamental problem is far from resolved by a number of reasons, most notably the principal difficulty of valuing common goods, the complexity of natural ecosystems, and the fact that, even without any climate change, population and infrastructure development exert a strong and increasing pressure upon most ecosystems. This pressure results in considerable changes to their adaptability and vulnerability, upon which now climate change is imposed.

Therefore, only direct impacts on economic sectors (including agriculture and managed ecosystems) were considered in the VW model. Climate damage costs due to changes in atmospheric climate are computed, for each economic region, as two-dimensional linear functions of the regional mean

| Abbr. | Name | Countries |
|---|---|---|
| WEU | Western Europe | European Community EC-15 |
| NAM | North America | USA, CAN |
| PAO | Pacific Oceania | Australia, New Zealand Japan |
| FSU | Former Soviet Union | |
| MEA | North Africa & Middle East | Morocco, Algeria, Tunesia, Libya, Egypt, Lebanon, Syria, Iraq, Iran, Gulf Staates, Saudi Arabia, Yemen, Jordan (*not included:* Turkey, Afghanistan, Pakistan, Israel) |
| CPA | Centrally Planned Asia | China |
| PAS | Pacific Asia | Republic of Korea, Indonesia, Malaysia, Philipinies, Singapore, Thailand, Taiwan |
| IDI | India | India |
| LAM | Latin America | Mexico & South America (*not included:* Central America and Carribean) |
| AFR | Sub Saharan Africa | Africa without Morocco, Algeria, Tunisia, Libya, Egypt |
| ROW | Rest of the World | Rest of South Asia (Myanmar, Vietnam, ...), Central America and Carribean, European Free Trade Area, Central European Assoicates (Norway, Switzerland, Poland, ..., Turkey), Rest of the World (Afghanistan, Pakistan, ..) |

Table 5.1: Economic world regions in the Kiel (VW) model.

changes in temperature and precipitation.

Sea level rise is generally estimated from coupled model results to be in the order of some decimeters during the 21st century. As the desirable full monetarization of the ecological impacts of sea level rise is practically infeasible, the problem was, like in other studies, restricted to estimation of costs of adaptation of managed coastal structures (dikes, harbour construction etc.), "with ... no consideration of coastal dynamics. There is concern that these studies understate nonmarket values" (IPCC [1996], p.292).

Coupling variables for the damage cost modules were annual and regional mean values of the changes in near-surface temperature, precipitation, and sea level. For each of three $CO_2$ emission scenarios, the annual and regional mean changes in the three climate variables were computed, together with the regional spread of the change, in each of the eleven regions at each model time step.

The regional mean changes are computed by multiplication of the time-dependend global mean change from the NICCS CLIC module, $p_1^v(t)$, with the eleven (area-weighted) regional averages $\langle f_1^v \rangle_R$ over the spatial patterns $f_1^v(x)$ of change (Figs.4.3 - 4.6). Likewise, the regional spread of the changes is computed by multiplication of $p_1^v(t)$ with the regional standard deviation $\sigma_R(f_1^v)$ of the pattern values. Thus, both the regional mean changes and the regional spread of the changes scale proportionally with the global mean.

The regional averages and standard deviations of the pattern values are computed using binary region masks (in analogy to the land-sea mask shown in Fig.4.1) and a standard meteorological averaging routine. The resulting region-specific scaling factors for the changes in temperature, precipitation, and sea level are listed in Tables 5.2, 5.3, and 5.4.

As the regions are defined over land only, changes in sea level could not be averaged over the regions themselves but over a belt some grid cells broad (around 2000 km) along the respective coastlines. The resulting regional means are hardly sensitive to the exact choice of this belt as sea level changes fairly homogeneously in the parent AOGCM.

The impact module was driven by absolute changes in temperature and *relative* changes in precipitation. As the regional-averaging operation $\langle . \rangle_R$ does not commute with the division through absolute precipitation, the relative change of the regional mean, $p_1^{pre}(t) \frac{\langle f_1^{pre} \rangle_R}{\langle P \rangle_R}$, is in general not equal to the regional mean of the relative changes in each grid cell, $p_1^{pre}(t) \langle \frac{f_1^{pre}}{P} \rangle_R$. The difference is especially pronounced in regions where the spread of the rela-

| Region | $\langle T_{2m} \rangle_R$ | | $\sigma(T_{2m})_R$ |
|---|---|---|---|
| AFR | 1.19812 | $\pm$ | 0.150656 |
| CPA | 1.44889 | $\pm$ | 0.279139 |
| FSU | 1.64368 | $\pm$ | 0.185673 |
| IDI | 1.13002 | $\pm$ | 0.232731 |
| LAM | 1.15064 | $\pm$ | 0.185937 |
| MEA | 1.57341 | $\pm$ | 0.235240 |
| NAM | 1.65586 | $\pm$ | 0.295361 |
| PAO | 1.18825 | $\pm$ | 0.118900 |
| PAS | 1.03429 | $\pm$ | 0.182620 |
| ROW | 1.29949 | $\pm$ | 0.277487 |
| WEU | 1.34278 | $\pm$ | 0.156593 |
| GLB | 1.00000 | $\pm$ | 0.402235 |

Table 5.2: Regional averages and spreads of the near-surface temperature change pattern (Fig.4.3). These numbers scale with the time-dependent global mean change.

| | $\langle P \rangle_R$ | $\langle f_1^{pre} \rangle_R$ | $\frac{\langle f_1^{pre} \rangle_R}{\langle P \rangle_R}$ | $\langle \frac{f_1^{pre}}{P} \rangle_R$ | $\sigma_R \left( \frac{f_1^{pre}}{P} \right)$ |
|---|---|---|---|---|---|
| AFR | 3.08138 | 1.218680 | 39.5500 | 39.7174 | 62.7685 |
| CPA | 1.94910 | 0.913607 | 46.8733 | 53.2525 | 61.2937 |
| FSU | 1.52276 | 1.002460 | 65.8321 | 56.0314 | 77.5903 |
| IDI | 2.41246 | 4.051000 | 167.9200 | 170.2440 | 96.4515 |
| LAM | 3.94498 | 2.099220 | 53.2124 | 46.8359 | 67.4052 |
| MEA | 0.273316 | 0.757959 | 277.3200 | 643.5140 | 849.3860 |
| NAM | 1.85053 | 0.689100 | 37.2380 | 30.5351 | 55.6320 |
| PAO | 2.09444 | 1.122230 | 53.5814 | 71.8907 | 58.9384 |
| PAS | 4.56631 | 2.261980 | 49.5363 | 59.6154 | 51.4962 |
| ROW | 2.32307 | 1.022370 | 44.0094 | 152.5130 | 354.2590 |
| WEU | 1.97504 | 0.214692 | 10.8701 | -16.3887 | 81.3676 |
| GLB | 2.7343 | 1.000000 | 36.5724 | 61.1596 | 226.4780 |

Table 5.3: Regional mean of absolute precipitation from the ECHAM3-LSG control run (mm/d), regional mean of precipitation pattern, relative change of the regional pattern mean (in % $(\mathrm{mm/d})^{-1}$), regional mean and spread of relative changes (in % $(\mathrm{mm/d})^{-1}$). The four columns to the right, containing pattern-derived quantities, scale with the time-dependent global mean change in mm/d.

| Region | $\langle Sea \rangle_R$ | | $\sigma(Sea)_R$ |
|---|---|---|---|
| AFR | 1.01 | $\pm$ | 0.05 |
| CPA | 1.07 | $\pm$ | 0.05 |
| FSU | 1.06 | $\pm$ | 0.05 |
| IDI | 1.12 | $\pm$ | 0.05 |
| LAM | 0.95 | $\pm$ | 0.05 |
| MEA | 0.98 | $\pm$ | 0.05 |
| NAM | 0.99 | $\pm$ | 0.05 |
| PAO | 1.08 | $\pm$ | 0.05 |
| PAS | 1.08 | $\pm$ | 0.05 |
| ROW | 1.00 | $\pm$ | 0.05 |
| WEU | 0.98 | $\pm$ | 0.05 |

Table 5.4: Regional averages and spreads of the sea level change pattern (Fig.4.6). These numbers scale with the time-dependent global mean change.

tive changes $p_1^{pre}(t)\,\sigma_R\left(\frac{f_1^{pre}}{P}\right)$ is large. For the VW model, the mean of the relative changes, together with their spread, was found more suitable for impact assessment than the relative change of the mean.

Example: for each mm/d increase in global mean precipitation, the relative changes in Middle-East-North-Africa (MEA) change by 644 % on average, the spread of the relative changes is 849 %, but the mean precipitation in mea in will change by 'only' 277 %. Applied to the "BTC" scenario with its global mean precipitation change of 0.052 mm/d (= 19 mm/yr) in year 2030, the regional average of the absolute precipitation in MEA, 0.27 mm/d (= 100 mm/yr), will increase by 0.039 mm/d (= 14 mm/yr). This means a relative increase of the regional mean by 14 %. In contrast, the regional mean of the relative changes in each grid cell is 33.4627 %, consistent with the large regional spread of the relative increases of 44 %.

The result consists, for each emission scenario, in eleven regional climate change scenarios in three variables (and spreads), respectively. Those time series were then used to drive the regional impact cost modules.

**Regionalization problems**

- **Resolution** The coarse spatial resolution of the parent AOGCM does not permit quantitative interpretation of subcontinental-scale structures in the patterns. Climatic change in smaller regions such as PAS or WEU can thus not be reliably estimated. To keep the regions as large as possible for robust averages, some grid cells on the borderlines were

assigned all adjacent regions.

- **Precipitation** The global precipitation change pattern shows both increasing and decreasing precipitation in different climatic zones. Some of the economic regions cover several zones, as e.g. FSU, NAM, or LAM. Thus local changes of different sign tend to cancel in the average, leading to underestimates of the impact costs. This applies especially to ROW which is dispersed over many parts of the globe.

- **Sea level** The largest uncertainty in the prediction of sea level change lies in the parent ocean AOGCM, as thermal expansion is the only modelled cause. Although this is probably the most important contribution, at least two others are expected to be of importance as well. First, melting (or accumulating) land ice may increase or decrease the total mass of water in the ocean, with resulting sea level changes of centimeters (up to meters in the extreme case of destabilization of the West Antarctic ice shield and its release into the ocean). The effect, although potentially of considerable magnitude, has not been modelled reliably until today and is highly uncertain even with respect to the sign. Second, changed wind conditions and surface currents may induce drastic local changes in some coastal regions. This has not been satisfactorily modelled on a global scale either. In summary, we must accept that our model, or any model, could well over- or underestimate the expected changes by about 100 percent. Still we believe that our estimate belongs to the most robust ones available by now.

- **Variability and extreme events statistics** Both nature and economy have adapted to irregular events like storms, floods, and droughts during years to millenia. They are probably more vulnerable to changes in their frequency and intensity than to gradual changes of the annual means. Prediction of changes in the variability is currently subject to considerable scientific effort. The task is difficult, no real consense is reached yet. Thus in spite of the importance of changes in variability, we avoided to make estimations available in a strongly aggregated model for coupling with impact models.

**Comparison of the three scenarios from the climatological perspective.**

All of the three economic scenarios studied with the GEM cover the time horizon from 1990 to 2030 (Fig.5.2). The $CO_2$ emissions start at a common rate of 6 GtC in 1990. The most carbon-intensive scenario is termed "Back-to-coal" in the context of that study (BTC). Its emissions grow linearly to 12 GtC in 2030. In a "Constant Emissions" (COE) scenario, the emissions are constrained to stay constant at the 1990 value of 6 GtC. Between these

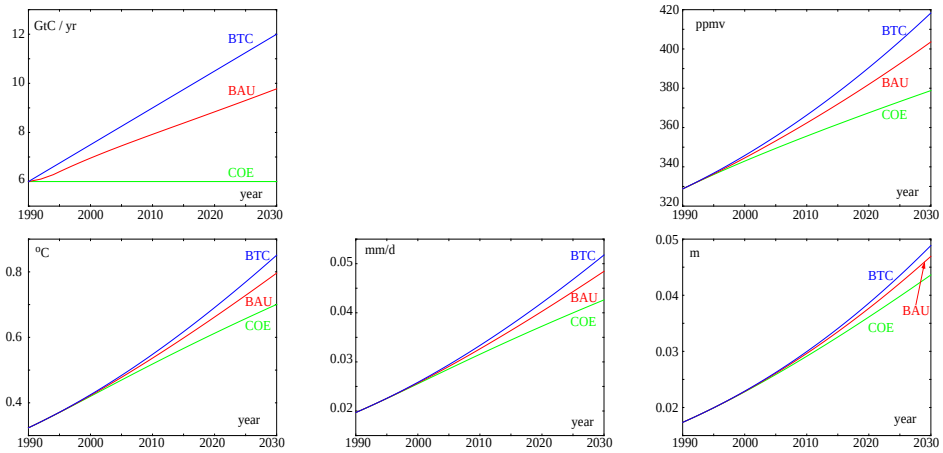


Figure 5.2: $CO_2$ emissions (upper left panel), concentration (upper right panel), near-surface air temperature (lower left panel), precipitation (lower middle panel), and sea level (lower right panel) for the three Volkswagen scenarios "Back to coal" (BTC), "Business as usual" (BAU, not identical with the 1000-year BAU of Chapter 5.4), and "Constant Emissions" (COE).

extremes lies a baseline "Business-as-usual" scenario (BAU) in which the emissions grow approximately linearly to 9.7 GtC in year 2030.

The carbon cycle (CARC) and climate change (CLIC) modules are spun up by a period of historical emissions from 1800 to 1990. This spinup is necessary because of the inertia of both the CARC and CLIC systems, both of which keep reacting to historical emissions throughout the whole 40-year period under investigation. For this purpose, the historical emissions are conveniently approximated by an exponential growth.

The climate response is, within the time frame under investigation, remarkably similar over the whole spectrum of econonomic policy options (expressed in emissions: from staying constant at 6 GtC/y to doubling the rate in only 40 years). The total changes in atmospheric concentration and all climate variables remain small until the end of the simulation period in year 2030. However the trends are virtually unmitigated. Even a freezing of the global $CO_2$ emissions at any, pragmatically chosen, constant rate is not sufficient for stabilization of the atmospheric concentration (see also Chapter 5.4 below). The steepness of the increase suggests larger changes if extrapolated beyond the simulation time window. This holds for all three scenarios, despite the wide range of policies considered. From the similarity of the climate responses to considerably differing emission scenarios it becomes evident that even drastic political measures, however immensely important for

the long-term evolution, cannot be expected to yield a perceptible influence on short-term climate change during, say, the coming half century. The underlying problem of time scale mismatch between the economic and the planetary system is discussed in more detail below in chapter 8.

As in most global economic climate change studies, the damage and adaptation costs were found to be only marginal, in the order of a few percent of gross domestic production. The reasons appear to be common among most existing studies, and seem to be independend of the details of any of the involved models:

- restriction to a climatologically short time horizon of typically not more than a century, and only 40 years in the VW model,
- restriction to changes that can be modelled with some degree of confidence, namely annual means and coarse patterns, but no local climate changes and impacts, and no variability changes,
- no (or poor) cost estimation of common goods, especially biological diversity and productivity of natural ecosystems,
- disregard of potentially fatal synergetic effects of climate change with other human interferences such as pollution and space consumption mostly in those parts of the planet's surface that had previously been most valuable in terms of diversity and productivity, namely coastlines, river deltas and valleys.

Having in mind the response time lag of the planetary system (that is long compared with both individual human time perception and economic or political planning horizons) and thus the planetary changes expected for the coming centuries, it must be concluded that the costs computed by our model and others cannot adequately reflect the historical and geological significance of global change.

## 5.3 Global warming scenarios of the next 100 years (IIASA)

Six energy scenarios of the coming 100 years have been compiled at the International Institute for Applied System Analysis, IIASA, and the World Energy Council, WEC [Nakićenović et al., 1998]. The underlying projections of the development of population, economy, energy intensity, technology, resources and environmental responses in the regions of the globe are reflected

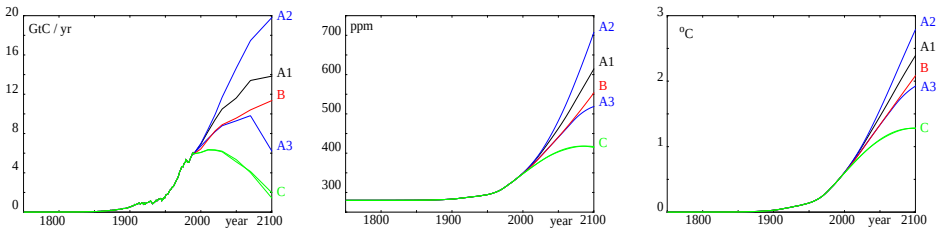


Figure 5.3: $CO_2$ emission scenarios (*right panel*), resulting $CO_2$ concentrations (*middle panel*) and global mean temperature rise (*right panel).* Computations were made with the nonlinear ocean $CO_2$ model with land biosphere (BJ).

in widely different $CO_2$ emission paths (Fig.5.3). In the end of the 21st century, the spectrum ranges from below 2 GtC/yr for a stabilization target (case C) to around 20 GtC/yr in the upper extreme (scenario A2).

For each of the six scenarios, the CO2 emissions were translated into increasing atmospheric concentrations and the corresponding climate change (only global mean temperature change is shown). The results of the NICCS computations fall close to the results of the model of Wigley and Raper [1993], Wigley et al. [1994] originally used for the scenarios, well within the uncertainty range estimated by Nakićenović et al. [1998].

The results clearly illustrate that the concentrations will not soon stop rising as the uptake into the natural reservoirs is too slow to compensate the release of fossil carbon. This holds even for the case that the emissions are reduced drastically during the coming 100 years (case C). However for most scenarios not even the emissions stop increasing, and the largest anthropogenic interference with the climate system is expected outside the time horizon under consideration. Thus it appears adequate from the perspective of natural sciences to consider possible consequences of fossil fuel combustion also beyond the coming century, despite the fact that the future history of human civilization cannot be predicted even in a coarse sense over longer time horizons.

## 5.4 Global warming scenarios of the next 1000 years (Total resources)

Typical scenarios of climate change like those shown above are computed over time horizons of 100 years [IPCC, 1992, Nakićenović et al., 1998, IPCC (Nakićenović & al.), 2000]. It has been pointed out by several authors, in particular Cline [1992] (page 399, see also Hasselmann et al. [1997]) that this time span is too short to cover the full range of the climatic consequences of today's policies, leading to dangerous underestimates of long-term climate change impacts. For many of the scenarios currently under discussion, the emissions have not ceased growing by the end of this century, and even after the emissions begin to fall, the cumulative $CO_2$ input continues to rise. Because of the long residence time of $CO_2$ in the atmosphere, it is the cumulative emissions rather than the instantaneous emissions that govern climate change. The slow uptake of the $CO_2$ input by the oceans and the terrestrial biosphere and the large heat capacity of the ocean together produce an exceedingly long memory of the climate system extending over many centuries (cf. Fig. 5.1).

This is further illustrated in Figs. 5.4 and 5.5, which show the $CO_2$ concentrations and climate change computed with the three IRF model variants described above, together with the $CO_2$ concentrations computed with the ocean carbon cycle parent model, for two representative 1000-year emission scenarios. The first case corresponds to a long-range 'Business as Usual' (BAU) scenario in which essentially all estimated fossil fuel resources are burnt in the course of a few centuries. The scenario corresponds to typical BAU scenarios (cf IPCC [1996]) for the 21st century, while over the entire time horizon, the total cumulated BAU emissions amount to 15000 GtC, which lies in the middle range of estimates of total fossil resources (see above). In the second 'Frozen Emissions' (FRE) scenario, the emissions are kept constant at the 1990 level of 5.5 GtC/yr. The FRE scenario is representative of the cumulative emissions of typical "drastic-reduction scenarios" (cf IPCC [1996]) for the period up to 2100.

In both scenarios, the largest changes in atmospheric $CO_2$ and climate occur well after the year 2100, with a millenium-time-scale decay of the climate signal even after the emissions have faded out. For the BAU scenario, the $CO_2$ concentrations reach extremely high values, between ten and twenty times higher than the preindustrial level, for which direct physiological damages to living organisms must be expected. The associated temperature changes are of the order of $10^oC$. However, even the FRE scenario yields temperature

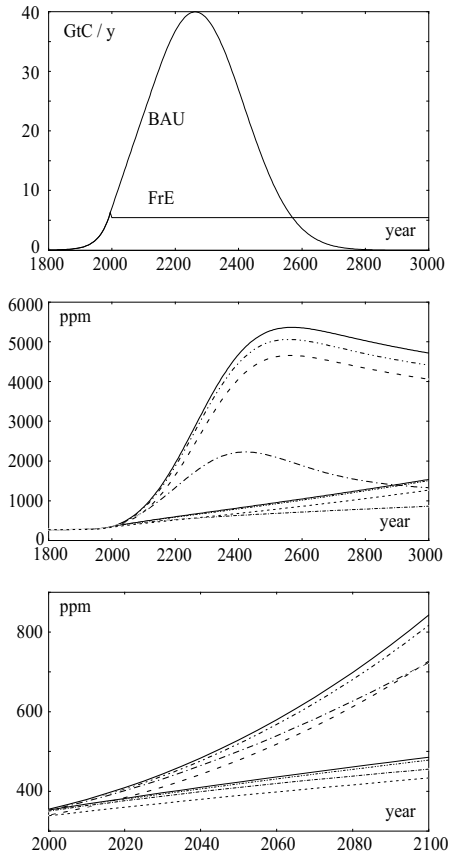


Figure 5.4: 'Business-as-usual' (BAU) and 'Frozen emissions' (FRE) $CO_2$ emission scenarios (*upper panel*) and resulting $CO_2$ concentrations computed over the same 1000-year integration period (*middle panel*) and for the next 100 years (*lower panel).* Computations were made with three IRF model variants: the nonlinear ocean $CO_2$ model without (NO, *full lines*) and with land biosphere (BJ, *dashed*) and with the linear convolution model (LC, *dot-dashed*), and also with the parent 3D ocean carbon cycle model HAMOCC3i (*dot-dot-dashed*).

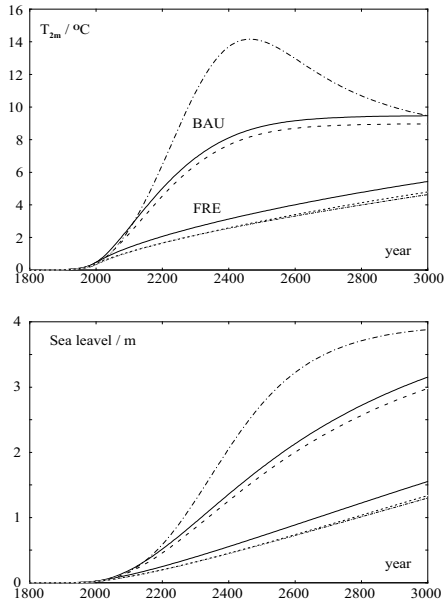


Figure 5.5: Annual-global-mean climate change for scenarios BAU und FRE computed using three IRF model variants: the nonlinear ocean $CO_2$ model without (NO, *full lines*) and with land biosphere (BJ, *dashed*), in both cases coupled to the logarithmic greenhouse forcing climate module, and the coupled linear convolution models of oceanic $CO_2$ uptake and climate change (LC, *dot-dashed*).

changes of the oreder of 5°C in the long term, of the same order as the warming since the last ice-age. Climate changes of this magnitude lie, of course, well outside the linear regime, in a range in which all climate models, including the parent models against which NICCS was calibrated, are no longer reliable. Thus, the computations should be interpreted only as an indication and warning of the major, basically unpredictable climate changes that can be anticipated if business-as-usual or insufficiently restrictive climate policies are pursued over long periods.

The linear ocean carbon cycle IRF model (LC) severely underestimates the $CO_2$ concentrations predicted by the parent model (HAMOCC3i) for the BAU scenario. The concentrations are reduced by 25 % already before the year 2100, while the peak concentration is reached two centuries too early and is too small by a factor of three. In contrast, the atmospheric $CO_2$ concentration computed with the nonlinear ocean carbon IRF module (NO) agrees

with the parent model to within 10 % during the entire 1000-year BAU period, including even the extreme peak value of 5000 ppm. Note that in all runs the initial state was defined as the preindustrial state in the year 1800, so that the different model variants yield different $CO_2$ concentrations and climate states already today. This is most visible in the run with the land biosphere module.

Driving the ocean-chemistry module at a strongly reduced temperature (Northern Atlantic winter instead of global mean temperature) did not modify the results significantly, while inclusion of the land biosphere module (BJ) shifted the concentrations down by about 15 % in both scenarios. However, the terrestrial biosphere could have a stronger impact if the feedbacks through changes in temperature and water availability are included. In the BAU scenario, the impact of the terrestrial biosphere is particularly weak, since the logarithmic radiative forcing is insensitive to relative changes in $CO_2$ concentrations for large background concentrations. In the FRE climate response, the combined nonlinearities of ocean chemistry, land vegetation, and radiation happen to very nearly cancel.

In general, the net climate response of the IRF module was found to be rather robust with respect to details of the carbon cycle module, for example with regard to the direct temperature effect on ocean chemistry, the capacity of the terrestrial pool or the modification of the terrestrial biosphere through changes in climate. Although the $CO_2$ concentrations become more uncertain at higher levels, this is compensated in part by the decreased sensitivity of the climate response to changes in the $CO_2$ concentration as the $CO_2$ infrared absorption bands become more saturated.

A comparison of the changes in global mean temperature, as proxy for the atmospheric variables, with sea level (Fig. 5.5) shows that sea level responds much more slowly than the atmospheric variables, as found already in the impulse experiments. Since the dominant time scale of the sea level response (800 years) is large compared even with the multi-century growth time of the BAU concentrations, the sea level response for this scenario is similar to the response to a step-function increase in $CO_2$ concentration discussed earlier. The sea-level rise for the FRE scenario is approximately linear over the entire period.

# Chapter 6

# Application of NICCS with detailed models of the terrestrial biosphere

The preceding chapter 5 illustrated the straightforward application of the NICCS model to a number of given $CO_2$ emission scenarios. In this chapter, examples are given for its use in combination with sophisticated, spatially resolving models of the terrestrial biosphere. The main interest is in the impact of simultaneous changes in the $CO_2$ concentration and climatic fields on the allocation of fossil-fuel carbon in the land biosphere.

Next to the ocean, the land biosphere is the second biggest carbon reservoir that can act as a relatively fast sink for anthropogenic carbon. IPCC [1995] estimate the total pool size to 2190 GtC, composed of 610 GtC in the vegetation itself and 1580 GtC in soil and detritus. A more recent estimate is 2050 GtC (550 GtC in the vegetation plus 1500 GtC in litter & soil), with an annual exchange with the atmosphere of 100 GtC (both from Knorr [1997]).

## 6.1 The biosphere's response to climatic and other changes

The anthropogenic mean land-use change flux, mainly from forest clearing in the tropics, is estimated by various authors to be in the range from 1 to 2 GtC/a. IPCC [1990], for example, estimated the annual average net flux to the atmosphere from land-use change to $1.6 \pm 1.0$ GtC/y during the decade

of the 1980s.

This is widely believed to be more than compensated by a biospheric carbon uptake elsewhere. The increase in atmospheric $CO_2$ is by almost a factor of two slower than even the fossil-fuel emissions alone, presently 6 GtC/y. Since the oceanic uptake is believed to account for only 0.5 to 2.5 GtC/y, many authors suggest that the carbon budget must be balanced by a net biospheric uptake of around 1 to 3 GtC/y during the 1980s and 1990s, mainly in the northern middle latitudes (see e.g. Tans et al. [1990], Keeling and Shertz [1992], Friedlingstein et al. [1995], Joos and Bruno [1998]). The uptake by the land vegetation is believed to be due to forest regrowth and to a fertilization by elevated $CO_2$ and nutrient concentrations. These hypotheses are supported by trend measurements of both $CO_2$ and $O_2$ concentrations [Keeling et al., 1996] which allow for a distinction between oceanic and land-biospheric uptake.

On the other hand, Schlesinger [1993] argued that a northern $CO_2$ sink of this magnitude should have doubled the size of the boreal forests in only a few decades which would have been clearly distinguishable. And although $CO_2$ fertilization is well documented from laboratory experiments, its future global relevance is questionable. Photosynthesis is in most places limited by regional factors like the availability of water and nutrients, and the biospheric carbon storage is subject not only to climate feedbacks but also to the ever-growing impact of direct human influences. The total magnitudes and the relative importances of the various processes involved are not well known. Even the present-day production and decomposition rates of the land biosphere are quite uncertain, the estimated global net primary production (NPP), based on a combination of vegetation models and satellite data sets [Knorr, 1997], lying in the range $76 \pm 36$ GtC/y.

Thus it is still subject to debate whether at all the land biosphere acts as a net $CO_2$ source or sink, and whether or not it can be expected even in a future warmer climate to substantially counteract anthropogenic emissions by sequestration of additional carbon in the biomass pools (see e.g. Schlesinger [1993] for a review). The following interactions affect the $CO_2$ uptake by the land vegetation (cf. IPCC [1995]):

1. Anthropogenic emissions of nitrogen compounds may provide an additional fertilization that depends on the spatial distribution of both the emissions and the biomes, together with their respective natural nutrient supply. However, the effect (even if well-known) could hardly be described in terms of only a few scalar variables, as is required for an IRF model.

2. The fertilizing effect of anthropogenic nitrogen may be regionally compensated or even reverted by acidified rain and toxines, both of which are often associated with human emissions. A drastic example is the huge region completely cleared of vegetation by mining dust and smoke on the Kola peninsula.

3. Increased temperatures would prolong the growing season in temperate and subpolar latitudes, leading to higher carbon uptake during the year (where permitted by nutrient and water supply).

4. At the same time, increased temperatures could both accelerate or slow down the respirational return of sequestered carbon into the atmosphere, depending on water supply (which in turn could also change with climate).

5. In their simulation experiments, Sellers et al. [1996] found a feedback mechanism by which the water respiration response of the land vegetation to increased $CO_2$ concentrations strongly affects the hydrological cycle, thus giving an additional contribution to atmospheric temperature and circulation change comparable in magnitude to the pure radiative greenhouse effect.

6. Strong synergetic effects between vegetation cover and the climate, especially the water cycle, reported by Gayler and Claussen [1997], Claussen et al. [1999], and Ganopolski et al. [1998], are likely to be responsible for the desertification of the Saharan-Arabian region for some 5000 years b.p., which in their model occurred rather rapidly (about 300 years) compared with the very smooth transition in the orbital forcing during the Holocene. Such feedback mechanisms could strongly amplify weak changes in the radiation budget due to anthropogenic emissions of greenhouse gases and aerosols.

7. The terrestrial source of atmospheric carbon through massive changes in land cover / land use, approximately compensated by the terrestrial regrowth / fertilization sink (see above), cannot be treated as a physical consequence of climate change, but is related rather to socio-economic factors like poverty and population pressure. However, it represents an important contribution to the atmospheric carbon budget.

8. Impacts of these perturbations may be intensified by species composition feedbacks on the regional and global level. Both the ethical questions of responsibility and the political-economic questions of sustainable availability of resources are aggravated by the fact that anthropogenic changes to global biological diversity are in general irre-

versible on the time scales of natural genetical evolution, beyond $10^6$ years (see `http://www.pik-potsdam.de/posters/htm`).

Thus, exact quantification of the global net vegetation response to the different local impacts of climate change is presently not possible, even with respect to the sign, and will require considerable future research. Including the biospheric carbon uptake into attempts to long-term climate change prediction still appears speculative in view of these numerous quantitative and even qualitative uncertainties.

On the other hand, there is a strong scientific and political need for investigations in the terrestrial biosphere. For example, it is currently discussed in the political arena to what extent regionalized terrestrial carbon sinks may be accounted for as potential partial compensation for fossil emissions on the national level. Accordingly, terrestrial biosphere models are required not only for closing the global carbon budget but also for assessing the magnitudes of regional sinks. Other important purposes are the prediction of the impacts of climate (and other) change on diversity, functionality, and productivity of the biosphere, and assessment of regional and global biospheric feedbacks on water cycle, temperature, and circulation patterns.

The scientific community supports a range of different model types that serve these different purposes. First, there have been, for several decades, a number of strongly idealized models, like the bern box model [Siegenthaler and Joos, 1992] and its IRF aggregate representation that has been adapted from Joos et al. [1996] by Hooss et al. [2001] for use in the NICCS CARC module. Second, there are coarse-resolution models of spatial ecosystem distributions (e.g. BIOME, Prentice et al. [1992]) and of biological diversity (e.g.Kleidon and Mooney [2000]). Third, there are plant-scale-process-based terrestrial carbon cycle models calibrated against field observations and validated against satellite data for the regional and global scales:

- the Frankfurt Biosphere Model (FBM) [Janacek et al., 1989, Kindermann, 1993, Lüdecke, 1994, Lüdecke et al., 1995, Kohlmaier, 1997, Kohlmaier et al., 1998, Heimann, 1998, Kicklighter et al., 1999]
- the High-Resolution terrestrial Biosphere Model of the Community Terrestrial Biosphere Model (HRBM/CTBM) [Esser et al., 1994, Wittenberg and Esser, 1997, Heimann, 1998, Kicklighter et al., 1999]
- the Biosphere-Energy-Transfer-Hydrology model (BETHY, Knorr [1997]),
- the Lund-Jena-Potsdam Dynamical Global Vegetation Model (LPJ, sometimes LPJ-DGVM, Sitch et al. [2000]).

## 6.2 Aggregate models of the terrestrial biosphere

It is desirable to make the predictive skill of advanced land biosphere models available to the integrated assessment community in the form of communicable and computationally efficient aggregate models of global terrestrial carbon sequestration, in the same way as was discussed in the preceding Chapters for complex 3D models of the ocean carbon cycle and the climate system.

Again, the concentration range to which aggregate models of the land biosphere may be applied should be extended beyond the linearization limits by explicit sublinear $CO_2$ fertilization. Furthermore, it is desirable to model the dependence of NPP and respirational decay on climate and nutrient availability, wich are both expected to change as a consequence of human activity.

### Response to $CO_2$ only

A simple and elegant method of aggregating the box-type global biosphere of the Bern model for its response to elevated $CO_2$ has been published by Joos et al. [1996]: only the respirational *decay* of additionally allocated carbon is described by a linear IRF model, while the nonlinear relation between global *production* and $CO_2$ concentration is treated in a separate equation. Both this relation and the decay IRF are obtained by fits to globally-integrated carbon fluxes from experiments with the parent biosphere model. This aggregate model has been adapted for the NICCS CARC module, (see Chapters 2.4 and 3.6).

The approach described by Joos et al. [1996], namely to combine a nonlinear NPP formulation that depends instantaneously on the $CO_2$ concentration with a linear IRF model of the respirational decay, has recently been applied by Meyer et al. [1999] to construct impulse-response aggregate models of two spatially resolving (2D-) terrestrial biosphere models, namely the HRBM/CTBM and the FBM. $CO_2$ fertilization of the global NPP is shown in the upper panel of Fig.6.1, and the decay IRFs in Fig.6.2.

### Response to $CO_2$ concentration and climate change

Aggregate modelling of the net terrestrial carbon response to simultaneous changes in both $CO_2$ *and* climate is less straightforward, even if nutrient supply and ecosystem distribution were still assumed to remain unchanged. However, by introducing climate sensitivities into the abovementioned nonlinear aggregate model of the HRBM/CTBM, Meyer et al. [1999] succeeded in providing a global aggregate model that responds to changes in both the $CO_2$ concentration and climate.

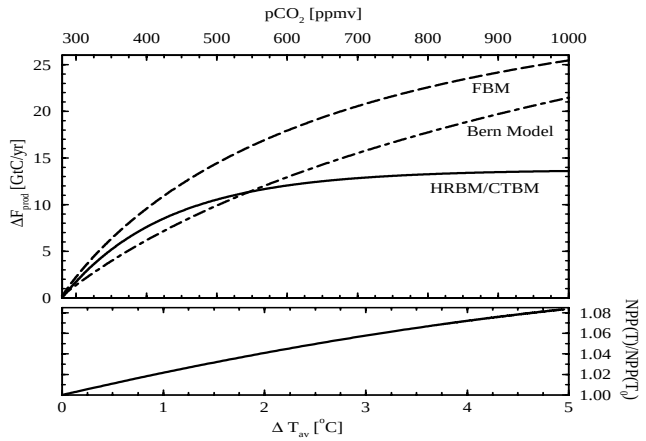


Figure 6.1: *Upper panel:* Global NPP response to increasing $CO_2$ concentrations of three models of the terrestrial carbon cycle. *Lower panel:* Global NPP response to simultaneous changes in the fields of near-surface temperature, total cloud coverage, and precipitation, with all these input signals proportional to global-mean temperature *(Figs.6.1 - 6.4 with kind permission by R.Meyer.).*

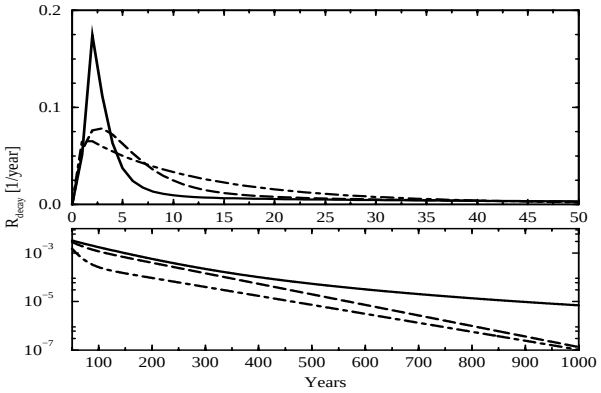


Figure 6.2: Impulse-response functions from three terrestrial carbon cycle models, describing the decay flux of additionally sequestered carbon back into the atmosphere. *Upper panel:* The first 50 years from the impulse with linear axes. *Lower panel:* The rest of the 1000-year simulations with logarithmic vertical axis. The models are: HRBM/CTBM *(solid)*, FBM *(dashed)*, and the bern box biosphere *(dot-dashed)*.

In a first step, the IRF aggregate model is reformulated into a differential analogue consisting of five independent boxes (see Fig.6.3). The total fluxes into and out of this box model are, at fixed climate, equivalent to that of the IRF model. However, as discussed in Sec.2.1 in the context of the NICCS nonlinear ocean carbon cycle IRF model analogue: differential formulations have the advantage that they can be designed such that nonlinear relations can be introduced and treated explicitly. Thus, in a second and third step, the in- and outfluxes to and from the box model's boxes (the nonlinear formulation of the $CO_2$ fertilization of the NPP and the linear decay of the sequestered carbon through heterotrophic respiration) have been made climate-sensitive. The sensitivities were found through fitting the model's productivity to experiments with the HRBM/CTBM in which the prescribed climatology was changed using the NICCS spatial patterns of annual-mean climate change:

- For fitting the productivity, both the $CO_2$ concentration and the first principal component (PC1) time series of $T2m$, $Clo$, and $Pre$ from the same transient ECHAM3-LSG experiment that was also used for calibration of the NICCS CLIC module (see Sec.4.2), were prescribed to the HRBM/CTBM.
- For determination of the decay time constants $1/k_i$, the HRBM/CTBM was forced by the NICCS climate fields of which the amplitudes were changed in 15 steps of 800 years each.

The complexity of the aggregate response of the global biosphere to the changes in three different climate fields is drastically reduced by the fact that the NICCS climate change signals (local $T2m$, $Clo$, and $Pre$ in all grid cells) are all proportional to the global-mean near-surface temperature change $\Delta T$ (see Chapter 4.3):

- The integral influx $f_{NPP}$ can be expressed as a product of only two simple functions of $CO_2$ and global-mean $\Delta T$ (Fig.6.1).
- the in- and outfluxes to and from each box $i$ are governed by the allocation fraction $b_{i,0}$ and the decay rate constants $k_{i,0}$. These are made climate-sensitive by coefficients that are exponential functions of $\Delta T$ with sensitivity constants $\beta_i$ and $\alpha_i$:

$$\frac{dN_i}{dt} = \frac{b_{i,0} \cdot \exp(\beta_i \Delta T_{av})}{\sum_j b_{j,0} \cdot \exp(\beta_j \Delta T_{av})} \cdot f_{NPP} - k_{i,0} \cdot \exp(\alpha_i \Delta T_{av}) \cdot N_i \quad . \qquad (6.1)$$

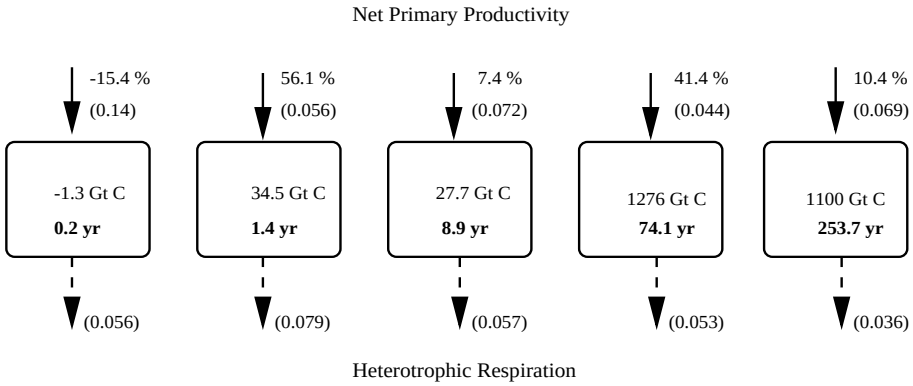


Figure 6.3: Differential IRF-tuned aggregate model of the HRBM/CTBM. The numbers are: *(above the boxes)* zero-climate-change allocation fractions $b_{i,0}$ in percent and their climate sensitivities $\beta_i$ in $\mathrm{K}^{-1}$; *(inside the boxes)* preindustrial carbon stocks $N_i$ in GtC, zero-climate-change decay time constants $1/k_{i,0}$ in years, and *(below the boxes)* their climate sensitivites $\alpha_i$ in $\mathrm{K}^{-1}$.

### Scenarios

To check this climate-sensitive aggregate model of the terrestrial carbon cycle against its parent model (the HRBM/CTBM under $CO_2$ and climate change), and the three $CO_2$-only-dependent IRF models mentioned above against their three parent models (the Bern, FBM, and HRBM/CTBM models under $CO_2$ change only), Meyer et al. [1999] applied all of these models to three concentration stabilization scenarios (S450, S650, WRE1000 from Schimel et al. [1997]). The climate forcing for the HRBM/CTBM under climate change and its climate-sensitive aggregate model was computed for each of the three $CO_2$ concentration scenarios using the NICCS CLIC module.

The diagnostic quantity in which the seven models were compared was their global net carbon allocation, or net ecosystem production (NEP, shown for comparison of all models in Fig.6.4).

In all cases, the NEP increases over time until a scenario-specific maximum is reached between 2030 and 2050, followed by a decrease when the NPP becomes slower than the decay.

For each scenario, the asymptotic net uptake after infinite times, termed by Meyer et al. [1999] the "ultimate capacity", is the time integral over the NEP curves:

$$C_\infty = \int_{-\infty}^{\infty} f_{\mathrm{NEP}}\left(t, pCO_2(t)[, T(t)]\right) dt \quad . \tag{6.2}$$

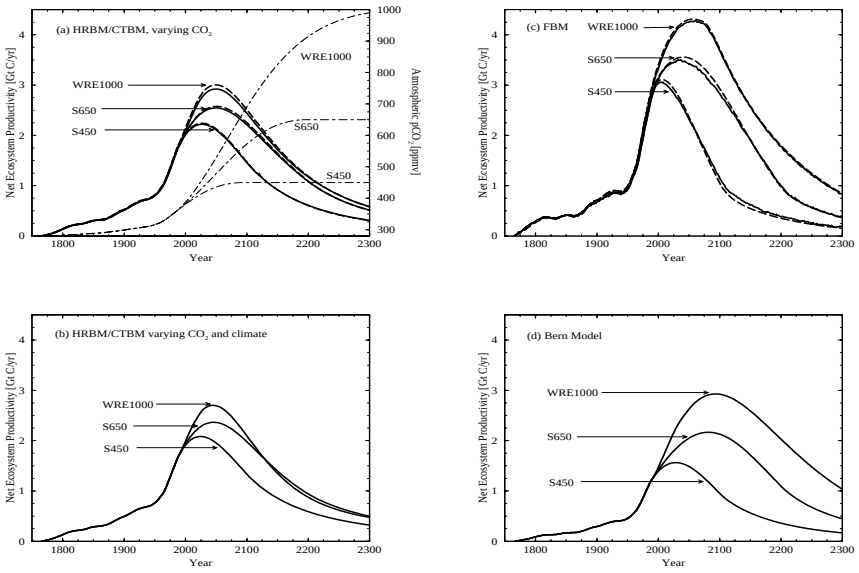


Figure 6.4: 3 scenarios, 7 models. *Dot-dashed curves and right vertical scale in (a):* $CO_2$ concentrations prescribed according to IPCC stabilization scenarios S450, S650, and WRE1000. *All other curves (a-d):* Global NEP response computed by three terrestrial carbon cycle models *(full lines)* and their impulse-response-based aggregate models (dashed). *(a)* HRBM/CTBM and its IRF aggregate model. *(b)* HRBM/CTBM and its climate-sensitive aggregate (box) model, both forced with climate changes from the NICCS CLIC module in addition to the prescribed $CO_2$ concentration changes. *(c)* FBM and its IRF aggregate model. *(d)* Bern model and its IRF aggregate model.

In short, forcing the HRBM/CTBM (or its aggregate model) with climate *and* $CO_2$ leads to a smaller overall net uptake over time than forcing with changing $CO_2$ alone. Correspondingly, the total equilibrium storage is also smaller. This difference between $CO_2$ alone and $CO_2$ with climate change is more pronounced at higher concentrations. The authors conclude that the positive $CO_2$ fertilization effect on productivity tends to be compensated by the accelerating impact of climate change on plant and soil respiration.

## 6.3 Coupled physical-biogeochemical climate model

The NICCS CLIC module has been coupled together with the HIgh-latitude convection, Low-latitude Diffusion-Advection (HILDA) oceanic carbon cycle component developed in Bern and the Lund-Jena-Potsdam (LPJ) dynamic global vegetation model into a multi-aggregate earth model by Joos et al. [2001].

The model treats atmospheric $CO_2$, oceanic and terrestrial carbon sinks, radiative forcing by greenhouse gases and aerosols, spatiotemporal in four climatic variables ($T2m, Clo, Pre, Sea$ computed by NICCS), and vegetation structure.

For assessment of feedbacks between global warming and the terrestrial carbon storage, the model was forced by prescribed $CO_2$ emissions until year 2100 (Fig.6.5, upper panel) according to six non-intervention scenarios recently published by the IPCC (Nakićenović & al.) [2000], labeled A1B, B2, A2, B2, A1FI, and A1T, comparable in scope and spread to those published by Nakićenović et al. [1998] and mentioned above (Chapter 5).

Fig.6.5 (Joos Fig.2) shows the time series of *(A)* fossil-fuel $CO_2$ emissions prescribed to the multi-aggregate Earth model, and the response of its base variant in *(B)* atmospheric $CO_2$ concentration, *(C)* total perturbation in radiative forcing and non-$CO_2$ contributions *(D)* global-mean near-surface temperature, and *(E)* global-mean sea level (the latter due to thermal expansion only).

Fig.6.6 (Joos Fig.4) shows the sensitivity of the time evolution (31-year running average) of the globally integrated terrestrial and oceanic carbon *release*[1] and the atmospheric $CO_2$ concentration to the choice of the model variant. Various such variants have been tested, reflecting the usual wide

[1] Pedantically, we admit that the net carbon release (at least the oceanic) appears to be negative throughout these scenarios. Thus it is actually rather an *uptake*.

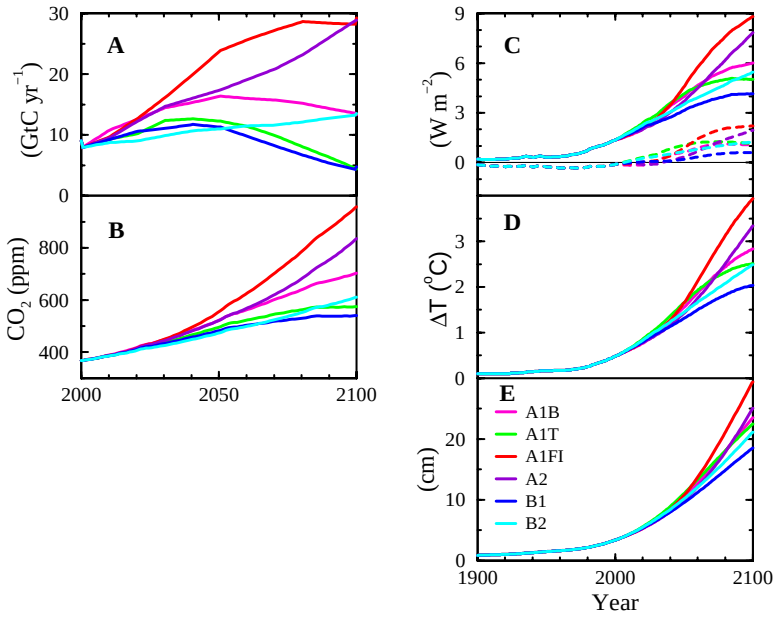


Figure 6.5: (Joos Fig.2) Six scenarios (see text).

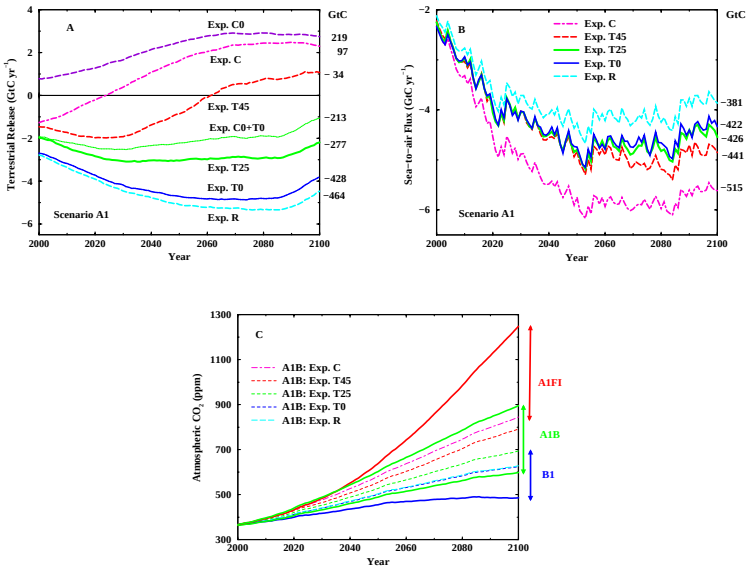


Figure 6.6: (Joos Fig.4) Sensitivity of terrestrial & oceanic $CO_2$ release and atmospheric concentration to the choice of the model variant.

range of uncertainties in any such projections:

- the climate sensitivity factors in NICCS have been changed from 0 through the base variant value 2.5 $^{o}$C to an extreme of 4.5 $^{o}$C,
- the climate impact on soil respiration was switched on and off,
- $CO_2$ fertilization was switched on, or off, or was capped after year 2000, and
- ocean overturning was set to slow or fast.

The spatially resolved terrestrial sources and sinks of two extreme model variants are shown in Fig.6.7 (Joos Fig.6). In one of these extreme variants, the terrestrial biosphere's sensitivity to climate change (or rather, the climate change module) has been switched off, and the $CO_2$-fertilized vegetation is a net sink practically everywhere. In the other extreme variant there is no $CO_2$ fertilization at all, and the vegetation is forced by climate change to release carbon almost everywhere except in the far north and in monsoon regions.

Despite the wide range of uncertainties in any such projections that was illustrated above, it may be worth having a look at the projections made for these six new IPCC scenarios with our best-guess *base model variant* which, of course, lies between the extreme variants. A map of total net carbon release from biological and biogenic pools on land until year 2100 (time integral over base scenario, base model variant) and a graph of zonally averaged expansion and retreat of vegetation types (again, time integral over base scenario, base model variant) are shown in Fig.6.8 (Joos Fig.5).

To investigate the long-term response of terrestrial carbon storage to the emission policy over a longer time period than the 21st century, the model was run for four times 300 years: Two *concentration scenarios* (differring in the rate at which the concentrations grow, and correspondingly in the time point at which they reach the top value of 1000 ppm and from which they remain constant) were prescribed to two model variants (differing in the non-$CO_2$ contribution to the radiative greenhouse forcing, namely zero in one variant and an additional 25% contribution in the other variant).

Fig.6.9 (Joos Fig.7) shows time series of the two 300-year concentration scenarios and of the globally integrated terrestrial carbon release into the atmosphere. The results contribute to the plausibility of the hypothesis that the terrestrial biosphere, although believed to be currently a net sink for fossil-fuel $CO_2$, may well turn into a net source during the 21st century.

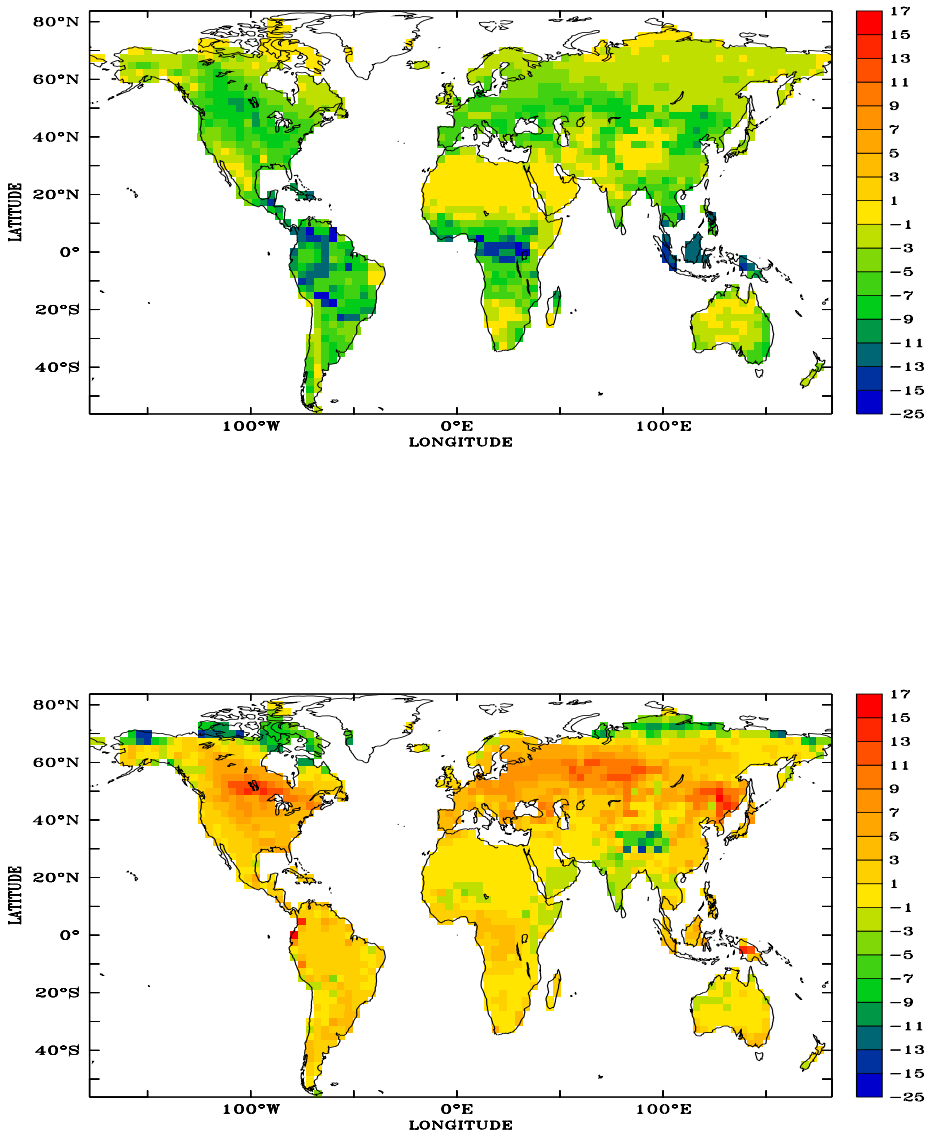


Figure 6.7: (Joos Fig.6) Main contributions to net cumulative terrestrial carbon loss to the atmosphere (in kgC/m$^2$) until year 2100, reference scenario A1B from IPCC SRES 2000, computed through two extreme model variants: (a) $CO_2$ fertilization on, production and respiration insensitive to climate, (b) $CO_2$ fertilization off, production and respiration affected by climate change.

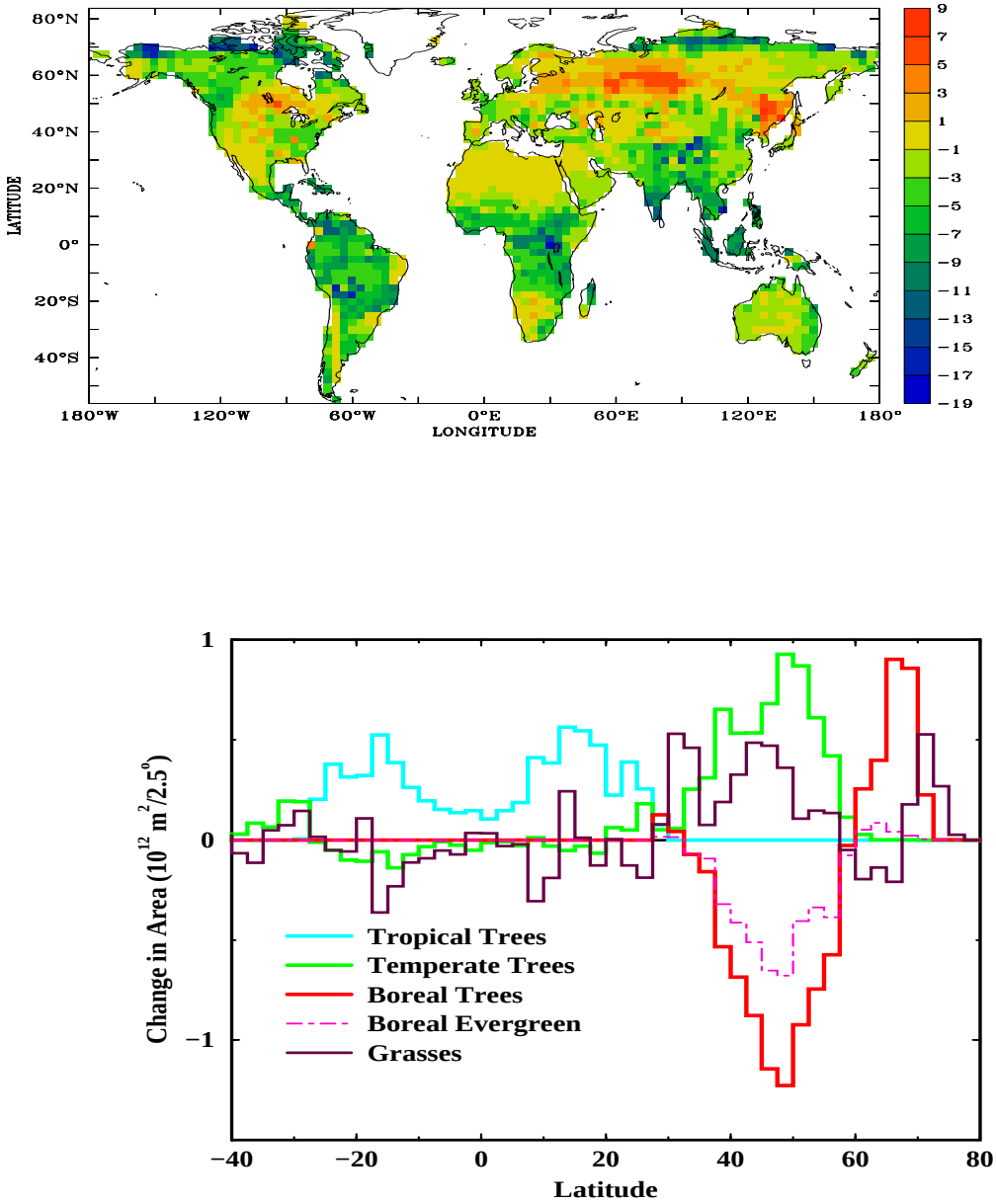


Figure 6.8: (Joos Fig.5) *Upper:* Net cumulative terrestrial carbon release (in kgC/m$^2$), and *Lower:* zonally averaged expansion and retreat of vegetation types, both until year 2100, reference scenario A1B from IPCC SRES 2000, base model variant with both $CO_2$ fertilization and respiration changes through climate.

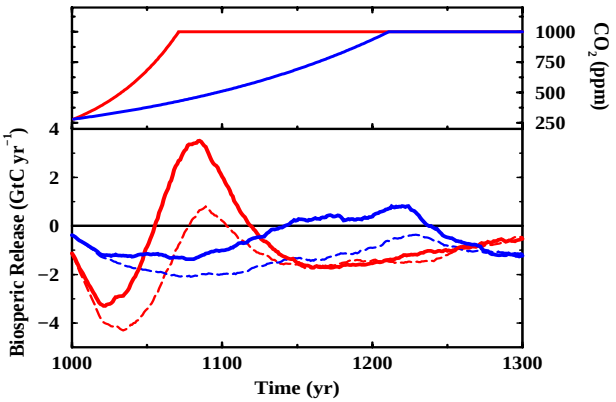


Figure 6.9: (Joos Fig.7) Two *concentration* scenarios, 300-years. Upper: prescribed $CO_2$ concentrations. Lower: terrestrial carbon release into the atmosphere from two model variants (non-$CO_2$ greenhouse contributions set to zero resp. additional 25 %).

(For more detailed discussion, see Joos et al. [2001]).

# Chapter 7

# Applications of NICCS for Integrated Assessment studies

The preceding chapters were concerned with emission scenarios and with the integration of the NICCS modules into a multi-component physical-geobiochemical climate model including a spatially resolving terrestrial biosphere component sequestering fossil-fuel carbon. This chapter describes its incorporation into two basic socio-economic models.

Through its high computational efficiency and its regionally resolved climate change signal prediction, the NICCS model is suitable as component of coupled multi-aggregate world models (see Chapter 1.2) for evaluation of physical-geobiochemical and socio-economic implications of climate change. A typical purpose of such world-model studies is the *integrated assessment* of climate policies, generally including the computation of benefits, risks, and costs resulting from sets of policy options in form of scenarios.

## 7.1 Global change is more than climate change

Central questions about climate change frequently asked by the public in general and by policymakers in particular, and therefore addressed in integrated assessment studies, are the following:

- How will climate change?

- What will be the impacts of climate change?
- Which systems will be impacted?
- Which feedbacks between causes and impacts are to be expected?
- What will be the benefits and costs of climate change (damage costs)?
- What will be the benefits and costs of avoiding or reducing climate damage, and of adapting to a changed planetary environment (abatement/mitigation costs)?
- What can we do to avoid, or at least reduce the risk of, future damage?
- What are the implications, benefits, costs, and side-effects of climate protection policy options?

General problems in answering these questions lie in the complexity of the (natural and civilized) earth system with its multitude of relevant physical-geobiochemical and socio-economic subsystems, and in the pronounced time scale mismatch between the relevant interactions in the different subsystems (see also the discussion of the Volkswagen Model, Chapter 5.2): On the one hand, the political, economic, and public horizons of perception, valuing, and planning, are usually limited to a few decades. In economic theory, the corresponding intertemporal distribution of preference is mathematically reflected in the decay of exponential discount functions. On the other hand, anthropogenic climate change is not, or not yet, perceptible on time scales below several decades to centuries. The relaxation of the system following a hypothetical future fadeout of the perturbation through man and machine will take millenia, even if possible and probable losses of biological diversity (see e.g.Peters and Lovejoy [1992], Simon Levin [2000]) are not taken into account.

The scientific state of the art must therefore be admitted to be far from any comprehensive and complete world model in the sense that it would include all relevant systems, functionalities and feedbacks, and that it could reliably estimate the benefits, threats, damages, and costs resulting from any given policy, or set of policies, on the time scale of the expected changes.

However there is a fleet of sophisticated and well-checked models of many of the involved subsystems being developed for several decades now, both in the natural and the economic sciences. A broad and up-to date overview is regularly given in the Reports of the three Working Groups of the Intergovernmental Panel on Climate Change [IPCC, 2001]. Especially climate models of varying detail and complexity are ordered in a whole hierarchy, with the most detailed, process-oriented, and computationally demanding models on

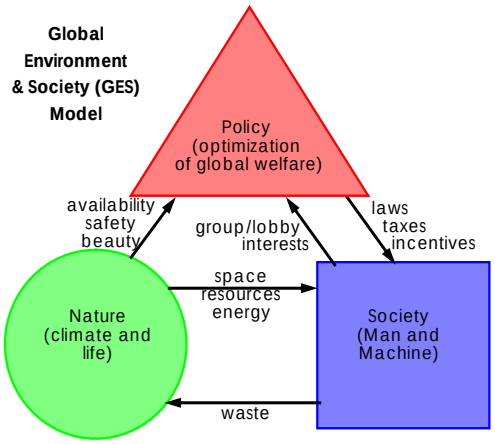


Figure 7.1: General structure of Global Environment and Society (GES) models like SIAM or ICLIPS

the complex end of the spectrum, and with the computationally cheapest and easiest-to-handle on the aggregate end (see Chapter 1.2).

The latter are suitable for coupling into multi-aggregate feedback world models including climate and other geo-bio-chemo-physical as well as macro-economic modules, with the interfaces between climate and economy lying in the energy/fossil fuel consumption and in agriculturure, fishery, forestry, and various other production and health sectors (see Fig.7.1). NICCS with its CARC and CLIC modules are components of two such multiaggregate feedback world models. The different philosophies underlying these two models are coarsely outlined below in the remainder of this Chapter.

## 7.2 Cost-benefit optimization

*Policy optimization* in its most general sense is a mathematical method for finding the best set of social/economic/political measures that lead the world (as it is perceived) into a state in which some appropriately chosen benefit (or cost) index is maximal (or minimal). According to one's preferences, as index may serve

| | |
|---|---|
| (to the optimist) | maximum benefit, |
| (to the economist) | maximum utility, |
| (to the capitalist) | maximum profit, |
| (to the hedonist) | minimum disturbance, |
| or (to the pessimist) | minimum damage. |

These arbitrary examples illustrate the first basic problem encountered when extending the idea of policy optimization to the context of global change: namely finding a world agreement (i.e. an agreement between, at least, the world's policymakers) upon what would be the relevant quantity to maximize or minimize: a communicable consensus definition of a *global welfare (or cost) function* upon which to base the mathematical formulation of the optimization problem. This index should desirably be a function of all quantities that characterize the world's worth to humankind (or, at least, to its policymakers). In the context of Integrated Assessment of climate change, such welfare definitions typically include costs of abatement of and adaptation to climate change, and of the expected damage due to climate change.

However, at a highly aggregate modeling level with idealized cost expressions for abatement and damage, and with a simple global welfare function essentially consisting of an integral over the long-term evolution of these costs, it is possible to perform a rigorous cost-benefit analysis for the intertemporal optimization of global welfare [Hasselmann et al., 1997]. The optimal strategy found is optimal in the mathematical sense that an idealized (and appropriately parameterized) global intertemporal total-cost index is minimal. The solution may be checked for its sensitivity to uncertainties and to basic assumptions about intertemporal equity, climatic and political/economic response time scales, and cooperation between political/economic actors, all unveiled by cumbersome model details.

The Structural Integrated Assessment Model (SIAM) developed by Hasselmann et al. [1997] is technically reduced to the very structure of an IAM, with the simplest-possible parametrizations of the minimum number of climate and cost submodels (see Fig.7.2).

Fig.7.3 shows the base-case optimization result in the five central time-dependent variables of SIAM: $CO_2$ emissions and atmospheric concentrations, global-mean temperature change $T$ as one-dimensional index of anthropogenic climate change, abatement costs (exponentially discounted, $\tau_a = 50$ y), and climate damage costs (not discounted, $\tau_d = \infty$).

After a 200-year spinup period with approximate historical emissions, inertia in the economic system initially delays the implementation of reduction measures so that the emissions continue to grow for some years to decades

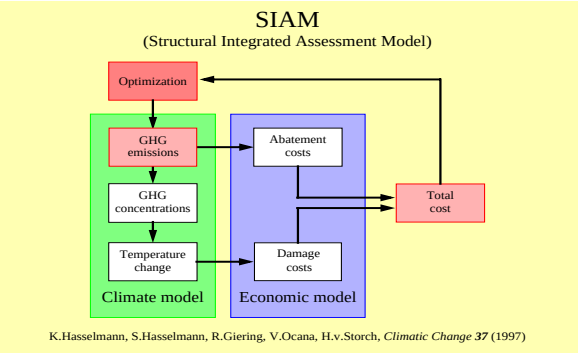


Figure 7.2: SIAM 1997.

from now. After that, they reach a maximum not far above today's rate and decline, first fast, then slower over several centuries, to very small flux rates. Inertia in the carbon cycle and climate system delays the response of concentrations and temperatures to the emission reduction strategy.

Total costs are optimal if the greatest reduction effort is taken immediately, i.e. at the first model time step available for variation through the optimization algorithm. Subsequently, the optimal emissions (and abatement costs) fall back towards what would have been the optimal path if optimized over the whole time period from 1800 to 3000 (instead of being forced to follow the reference scenario A for the first 200 years). The apparent damped oscillations around this hypothetical optimal path are caused by inertia terms in the abatement cost expression. The abatement costs are furthermore damped according to the choice of the discount rate, $\tau_a = 50\,\mathrm{y}$ in the base case shown in Fig.7.3.

In contrast, the damage costs are not discounted in the base case because worth and value of the natural planetary environment is perceived as constant over time. The damage costs therefore closely follow the climate evolution (quadratic in $T$ and $\dot{T}$, with the second term representing damages due to the *rate* of temperature change).

The most prominent sensitivity of the optimal path was found to the choice of the discount rates of the abatement and damage cost expressions. This result has subsequently given rise to most extensive discussions in the growing Integrated Assessment community (see e.g.Nordhaus [1997], Brown [1997], Heal [1997]), because the discount rates reflect very basic assumptions about intertemporal equity, especially about estimation of the worth and value of the natural environment.

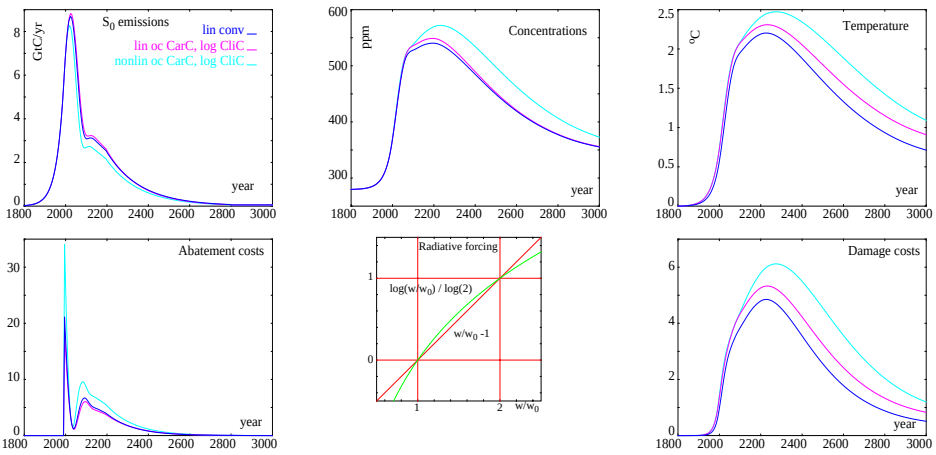


Figure 7.3: Optimal-emission-path scenario $S_0$ from the SIAM study [Hasselmann et al., 1997]. Reoptimized with two nonlinear climate model variants (see text). Also shown is a comparison of the linear and the logarithmic formulation of the radiative forcing in the climate change module.

The sensitivity of the optimal path to uncertainties in all subsystems, as well as to the type and formulation of the economic models, has been continuously under investigation by the Global Environment & Society (GES) group at the Max-Planck institute for Meteorology (MPI Meteo). (K.Hasselmann, S.Hasselmann, H.von Storch, J.S.von Storch, R.Giering, V.Ocaña, U.Kilian, G.Hooss, V.Barth, and M.Weber, pers.comm).

The sensitivity of the optimal path to details of the carbon cycle and climate models, in contrast, was shown to be rather modest already in the original study by Hasselmann et al. [1997]. The study was conducted using linear IRF convolution models of the carbon cycle and global mean temperature. Several IRFs from widely differing parent models were applied in both modules for analysis of the climate sensitivity.

More recently, the optimal emission-path computations of Hasselmann et al. [1997] were repeated using NICCS rather than the original linear IRF model. The optimization results were again confirmed to be rather insensitive to the detailed carbon-cycle and climate submodel formulation (although application of NICCS *did* change the response in $CO_2$ concentration and climate change to the original high-emission scenarios A and B (not shown), in a similar way as discussed in Chapter 5.4 for the 1200-year scenarios BAU und FRE, Figs.5.4 & 5.5).

The optimal paths shown in Fig.7.3 were computed for 5 time-dependent core variables:

1. optimal $CO_2$ emission path
2. the corresponding concentration evolution,
3. global-mean near-surface temperature change ($\Delta T$)
4. abatement costs, and
5. damage costs.

The optimal paths shown were obtained using three climate model variants:

1. Both of the original linear IRF convolution models from SIAM (in the carbon-cycle and the climate module).
2. the same linear IRF model of the ocean carbon cycle, coupled to the nonlinear temperature module with logarithmic formulation of the radiative forcing.
3. NICCS with both nonlinear modules: the ocean-chemistry CARC module (without terrestrial component) and the logarithmic CLIC module.

The differences in the optimal paths between the three variants are explained in the following.

The special panel in the lower row of Fig.7.3 depicts the two forcing formulations as functions of the concentration. The concentrations are normalized to preindustrial. The forcing is calibrated to unity at twice the preindustrial concentration.

The logarithmic forcing is stronger than the linear below the calibration point and significantly weaker above, with a more moderate slope already through the calibration point.

The optimal paths stay below, or close to, the calibration point, which means that climate damages would be more costly if logarithmically computed than if linearily computed (from the same emission path).

However the *marginal* damage costs of a given emission path (i.e. the increase in damage costs through a slight upward shift of the emission path) are smaller in the logarithmic, than in the linear model, because of the weaker slope of the forcing curve near the break-even point.

In contrast, the abatement costs (and the marginal abatement costs) are (trivially) unchanged for unchanged emissions.

As the optimum is found through balancing the *marginal* costs for abatement and damage, it is found not only at higher total costs but also, seemingly paradoxically, at slighly higher emissions. (Intuitively, one could have expected that the higher climate sensitivity would stimulate a stronger motivation for abatement and thus lead to lower emissions rather than to higher.)

Introducing the nonlinear inorganic carbon chemistry into the $CO_2$ module leads to slightly slower oceanic $CO_2$ uptake with correspondingly higher temperatures and costlier damages, which in this case does indeed stimulate a greater effort for abatement.

Although there are visible differences in all variables between the model variants, the three optimal emission paths lie very closely together and were thus found in the NICCS recomputations to be astonishingly robust with respect to the relatively small nonlinear modifications of the climate response in the range of modest climate change (normally less than $3^oC$ warming) occurring in the optimal emission solutions.

## 7.3 Tolerable Windows

In contrast to the rigorous optimization of a single-valued cost or benefit index, *Tolerable Windows* (TW) of climate change impacts and the corresponding *Guard Rails* for TW-compatible policies are searched in an approach to Integrated assessment of CLImate Protection policieS (ICLIPS, Bruckner et al. [1999], Petschel-Held et al. [1999], Füssel and van Minnen [2000]). The formulation is based on the (mathematically weaker and technically more demanding) requirement that a set of impact-relevant quantities stay within appropriate limits.

The goal is formulated more detailed than that of the global-welfare maximization in the SIAM study outlined above, namely to avoid surpassing the limits of maximal tolerable stress to impacted systems (and thus to future populations and their economy), desirably without compromising the structure and functioning of today's world economy.

Critical thresholds defining the tolerable windows for climate impacts are of two distinct kinds:

- Some of the limits to tolerability are given by bifurcations in the non-

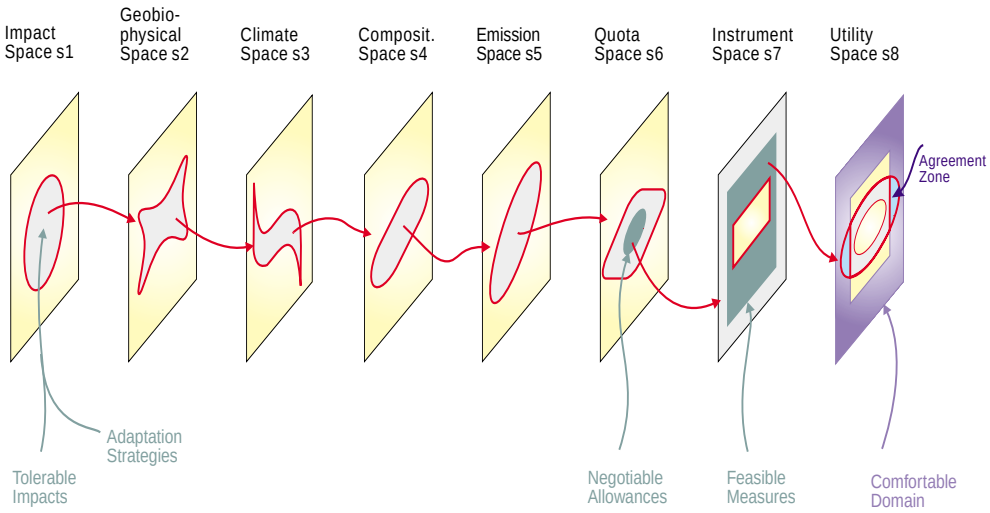


Figure 7.4: Tolerable Windows Approach: tolerable impact windows are translated back through climate and policy windows into the utility space window where the decisions are made.

linear behaviour of the physical planetary system, like a breakdown of the North-Atlantic thermohaline circulation (THC), destabilization of the West-Antarctic ice shield, or disruption of major ecosystems. Transitions of this kind are anticipated to cause impacts of intolerable magnitude.

- Other limits to tolerability are set normatively or based on economic risk assessment.

Once a window of tolerable impact limits is agreed upon, an inverse modelling approach is followed to find all socio-economically feasible policy options that allow the system to stay within that impact window (cf. Fig.7.4). The inverse concept works along the following steps [Petschel-Held et al., 1999]:

- Agree upon a desirable window of tolerable impacts. To this end, the vulnerability of impacted systems must be assessed in terms of critical limits. There are cases where the impacts of climate change, e.g. on crop yield changes in many of the world's regions, can only be estimated by smooth response surfaces that do not exhibit a-priori

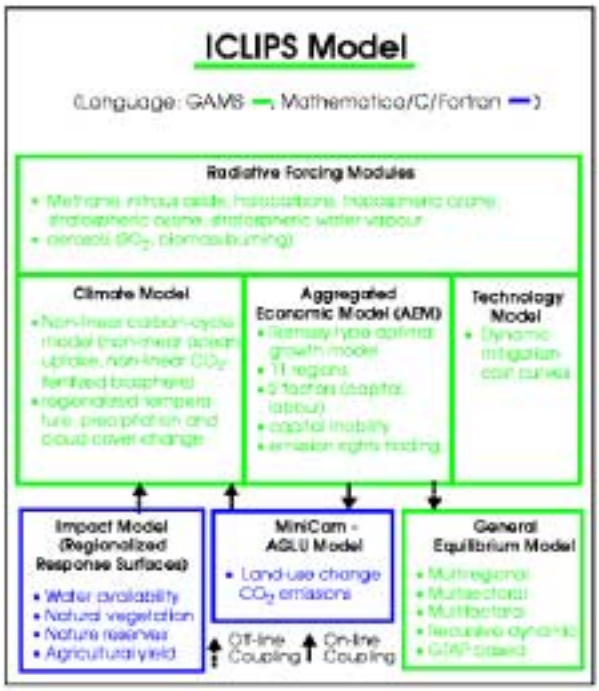


Figure 7.5: The ICLIPS model.

critical thresholds [Rosenzweig and Parry, 1994, Parry et al., 1999]. In such cases, the thresholds of tolerability must be set normatively.

- Translate the impact window back, against the direction of causality, through tolerable windows in the phase subspaces of climate change and emission paths, and finally to a set of policy options ensuring that the system will remain inside the chosen window of tolerable impact.

- Choose from this set of policy options those which are themselves tolerable in terms of political negotiability and economic feasibility. Probably not easy.

The inverse method requires scenario computations for many policy options. The solution thus found is in general not one single optimal trajectory of the socioeconomic-plus-physical earth system but rather a whole corridor of admissible paths, namely the overlap between those policies which are politically feasible and those which lead to tolerable impacts.

The NICCS CARC and CLIC modules are, among others, employed in the

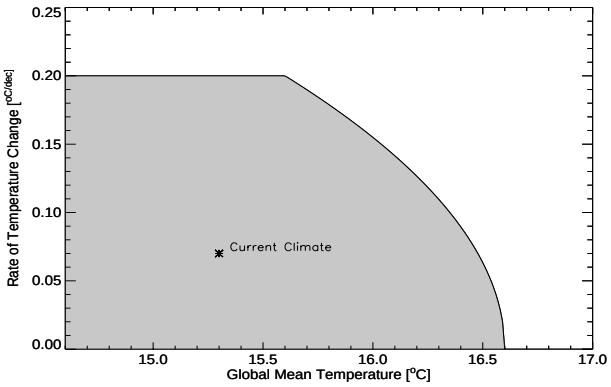


Figure 7.6: Tolerable climate window, limited in temperature and rate of temperature change. The corresponding corridors in $CO_2$ concentrations, emissions, and cumulative emissions are shown in Fig.7.7.

multi-aggregate climate submodel of the ICLIPS model (Bruckner et al. [2001], see Figure 7.5), to our knowledge the most comprehensive intertemporally optimizing integrated-assessment model to-date. The impact on various vulnerable systems is represented as a function of $CO_2$ concentration and either sea level or temperature, cloud coverage, and precipitation. As changes in the atmospheric variables (temperature, cloud cover, and precipitation) are proportional to each other (with the location-dependent proportionality given by the ratio of the pattern values in each grid cell and the climate sensitivities), atmospheric climate change is actually a one-dimensional variable, and the impact is, at any time, a two-dimensional function of the current CO2 concentration and global mean temperature (Füssel and van Minnen [2000]).

The resulting emission corridors for given tolerable impact windows are defined as the set of all points in the system's phase space that can be reached by admissible paths. An example of such corridors is shown in Fig.7.6 as shaded areas in the projections of the phase space unto $CO_2$ concentrations, emissions, and cumulative emissions that keep the system within a given window spanned by maximally tolerable changes in temperature and its rate of change. Note that not every path lying inside the shaded areas in Figs.7.7 and 7.8 is an admissible path. Especially, teh upper boundary of any such corridor is in general *not* an admissible path. However any point on the upper boundary can be reached by, at least, some admissible path that rises to the boundary, touches it in the given point, and falls back into the inner part of the region.

The Tolerable Windwos Approach (TWA) with its critical thresholds and

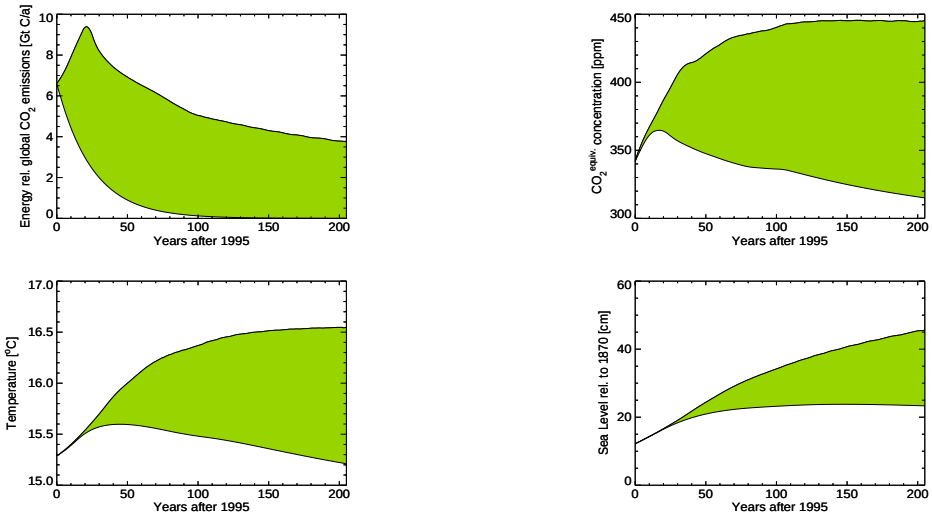


Figure 7.7: The corridors in $CO_2$ emissions, concentrations, temperature, and sea level corresponding to the climate window in Fig.7.6.

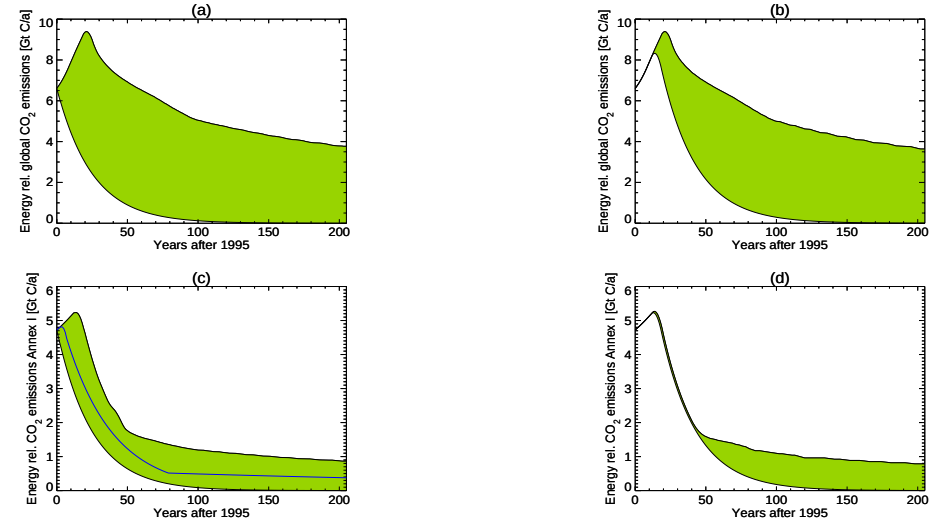


Figure 7.8: Sensitivity of the $CO_2$ emission corridor of Fig.7.7 to policy options leading to delayed reduction: (a, *upper left:*) total corridor spanned by today's options, (b, *upper right:*) delay of emission reduction policies until 2010, (c, *lower left:*) Annex I emissions with equity option, and (d, *lower right:*) as (c) but with reduction delay until 2010.

fixed protection targets appears politically more pragmatic than a Pure optimization exercise in the abstract space of continuous cost functions. However for any guard-rails to be put into effect politically, the normative settings underlying the definition of the target window must be found and agreed upon. If the impact tolerability thresholds are set low and the economic stakes high, the overlap between tolerable and feasible policies may be zero, i.e. the world cannot be saved from undesired future damages at the desired present price. A solution can then only be found through a compromise between raising the tolerance against future environmental damages and lowering today's socio-economic claims to fossil-fuel consumption, until the policy overlap becomes nonzero. In principle, the first admissible path thus found is most naturally an optimal path in the mathematical sense, as any other path would be perceived as more costly in the grand total. However in practice the policy overlap set, once nonzero, immediately expands beyond a single-path solution to yield the general multiple-path, or corridor solution.

# Chapter 8

# Summary and Discussion

## 8.1 The model: capabilibies, limitations, and value

Integrated assessment of anthropogenic climate change requires cost-efficient models of the carbon cycle and the atmosphere-ocean climate system that approach nevertheless the reliability and credibility of complex, state-of-the-art 3D carbon cycle and general circulation models. As a convenient tool for this purpose, we have developed nonlinear impulse-response-function (IRF) representations of the response characteristics of the HAmburg Model of the Ocean Carbon Cycle (HAMMOC3i) and the Hamburg coupled atmosphere-ocean general circulation model ECHAM3-LSG. Coupled together, the net IRF model NICCS (Nonlinear Impulse response model of the coupled Carbon cycle-Climate System) computes the atmospheric $CO_2$ concentration and the resulting changes in selected impact-relevant climate fields (near-surface temperature, cloud cover, precipitation and sea level) for a prescribed 1000 year $CO_2$ emission scenario within less than a second on a workstation. NICCS thus provides a valuable instrument for providing for the integrated assessment community the detailed output information of state-of-the-art climate models without loss of reliability for modest climate change at greatly reduced computational cost.

The limitation of IRF models to modest perturbations (below $CO_2$ doubling and $3^oC$ warming) for which the climate response can be approximately linearized was partially overcome in NICCS by explicit treatment of two dominant nonlinearities: the nonlinear inorganic carbon chemistry governing the $CO_2$ uptake in the ocean, and the logarithmic dependence of the radiative greenhouse forcing on the $CO_2$ concentration. This was augmented by a

land vegetation carbon cycle module with a nonlinear formulation of net primary production. Although inclusion of these nonlinearities removes the more obvious shortcomings of linear response models, it must be stressed that many more nonlinearities arise in the real climate system (and state-of-the-art climate models) at higher climate-change amplitudes, and these can not be adequately reproduced in an IRF model. The lowest-order extension of a linear IRF model to a general quadratic response model, for example, requires already the calibration of a set of three-index response coefficients rather than the set of standard two-index response matrices of a linear IRF model. Thus the introduction of just two dominant nonlinearites into the NICCS model should be regarded only as a stop-gap measure to obtain more realistic order-of-magnitude estimates of amplitudes, without claims to a realistic description of the nonlinear modifications of the climate-change response patterns.

Another shortcoming of NICCS is that it neglects feedbacks of greenhouse warming on the ocean carbon cycle resulting from changes in the ocean circulation, since the ocean carbon cycle IRF was calibrated against a 3D carbon cycle model with a prescribed ocean circulation field. This shortcoming can be overcome by calibrating both modules of a coupled IRF model against a coupled model of the carbon cycle and the general atmosphere-ocean circulation system. However, previous studies with 3D ocean carbon cycle models [Maier-Reimer et al., 1996, Sarmiento et al., 1998] indicate that the feedbacks of global warming on downwelling transport, vertical mixing, solubility and the biological pump partly compensate each other for atmospheric $CO_2$ concentrations up to about 700 ppm, leaving only a small residual effect of global warming on the oceanic $CO_2$ uptake. Maier-Reimer et al. [1996] conclude that 'the currently used modelling strategy of first using a carbon cycle model for the transformation of anthropogenic emissions into $pCO_2$ and subsequently using the output as forcing for a physical climate model, appears justified'. We have accordingly run NICCS in the sequential, decoupled mode, without consideration of global warming feedbacks on the carbon cycle.

At atmospheric $CO_2$ concentrations exceding 700 ppm, 3d ocean carbon cycle models indicate that the reduced ocean circulation and other climate feedbacks tend to slow down the $CO_2$ ocean uptake, so that NICCS probably underestimates the atmospheric $CO_2$ concentration in the high-emission scenarios. Fortunately, however, the uncertainties of high $CO_2$ concentrations map into smaller climate change uncertainties through the logarithmic dependence of the radiative forcing on the $CO_2$ concentration.

Another limitation of present IRF models is that they are unable to simulate an unstable transition of the climate system to a new state, such as a break-

down of the ocean thermohaline circulation, a destabilization of the West Antarctic ice shield, a run-away greenhouse effect triggered by the release of methane trapped in permafrost regions, or a large-scale disruption of terrestrial ecosysems. The various nonlinear, physical-biogeochemical processes involved in surprises of this kind are at not yet well understood. They can not be reliably simulated or predicted today, even with the most sophisticated climate models. Thus, there exist at present no suitable parent models against which an appropriately extended nonlinear IRF model could be calibrated.

Conceptually, many of the above shortcomings can probably be overcome by a suitable generalization of the basic NICCS structure, once the governing processes are understood and the relevant sophisticated parent models needed for calibration have been developed. However, an important generalization of the present NICCS which is feasible already today is the inclusion of further climate change variables provided by the parent model, such as annual and diurnal cycles, the occurrence of extreme events and, generally, changes in the statistics of the internal spatiotemporal variability of the climate system. It is in these properties that the impact of future climate change will probably be felt most strongly.

## 8.2 Applications and combinations

Our examples of the application of NICCS to long-term $CO_2$ emission scenarios demonstrated that the estimated total fossil-fuel resources are more than sufficient to carry the climate system into a range of extreme $CO_2$ concentrations and temperature increases, far in excess of the bounds within which any climate model can presently provide reliable predictions. Even a freezing of $CO_2$ emissions at 1990 levels is unable to stabilize the $CO_2$ concentration and limit global warming to acceptable levels in the long term. However, the long memory of the climate system provides also an opportunity for the gradual transition to carbon-free energy technologies over several decades, without dislocations of the global economy(cf.Hasselmann et al. [1997]). A repeat of the optimal emission path computations of Hasselmann et al. [1997], in which the linear climate module of their coupled climate-socioeconomic model SIAM was replaced by NICCS, confirmed the robustness of the conclusions of these authors with respect to climate model details.

NICCS has been used and is currently being applied in various integrated assessment studies. In the most straightforward approach, an economic model was run on three scenarios for the time between 1990 and 2030, and the

NICCS model was used for translating the resulting emission scenarios into regional climate changes. These in turn were feed back into the economic model to compute climate damage costs [Deke et al., 2001].

The ICLIPS model for computing tolerable windows in climate-related and economic, climate-protection-related stress thresholds [Bruckner et al., 1999, Petschel-Held et al., 1999, Füssel and van Minnen, 2000] contained both the CARC and CLIC modules of NICCS in its multi-aggregate climate submodel. Starting from critical thresholds in the impact variables, an inverse strategy was used to search for a policy regime that allows to avoid crossing the thresholds.

NICCS has furthermore been used for investigations of climate change feedbacks through the terrestrial carbon cycle ([Joos et al., 1999, 2001]), and as an educational tool developed for the EXPO2000 World Exhibition.

The NICCS model is under continuous development. Ongoing activity and future plans and possibilities include further macroecological, paleoclimatic and socio-economic applications and a well-documented, easy-to-use version to be made freely available to the network community.

# Appendix A

# Model variables

## A.1 Carbon cycle

| Symbol | Unit | Entity |
|---|---|---|
| $t$ | year | Simulation time |
| $\Delta t$ | 5 years | Numerical time step |
| $pCO_2$ | ppm | $CO_2$ 'partial pressure' (correctly: airborne fraction) |
| $\Delta pCO_2$ | ppm | $CO_2$ 'partial pressure' perturbation |
| | | |
| $w(t)$ | GtC | Atmospheric carbon load |
| $c_a(t)$ | GtC | Anthropogenic carbon in the atmosphere |
| $c_s(t)$ | GtC | Anthrop. carbon in the oceanic mixed layer |
| $c_0(t)$ | GtC | Anthrop. carbon in the composite layer |
| $c_j(t)$ | GtC | Anthrop. carbon in the $j^{th}$ layer of the analogue |
| $q_j(t)$ | GtC / year | Carbon flux from layer $j-1$ into layer $j$ |
| $e(t)$ | GtC / year | Anthropogenic carbon emissions |
| | | |
| $c_B(t)$ | GtC | Anthrop. carbon allocated by the land vegetation |
| $c_{Bi}(t)$ | GtC | Anthrop. carbon in land biosphere reservoir $i$ |
| $c_{Bc}(t)$ | GtC | Short-term anthr. carbon in land biosphere |
| $\delta f_{npp}(t)$ | GtC / year | Increase in land NPP due to $CO_2$ fertilization |
| $\delta f_{decay}(t)$ | GtC / year | Incr. in respirative C flux (land veg. $\rightarrow$ atm.) |
| $B(c_0)$ | GtC / year | Nonlinear auxiliary function (= additional NPP) |
| $A(c_0)$, $D(c_0)$ | 1 | Nonlinear auxiliary functions |

| | | |
|---|---|---|
| $h_s$ | m | Thickness of the mixed layer |
| $h_0(t)$ | m | Effective thickness of the composite layer |
| $h_j(t)$ | m | Thickness of the $j^{th}$ layer |
| $\eta_j(t)$ | m / year | Newton transfer coefficient (layers $j-1$ and $j$) |
| | | |
| $M_{jk}$, $\mathbf{M}$ | year$^{-1}$ | System matrix of the oceanic $CO_2$ analogue |
| $C_{jk}$ | GtC | $j$th component of $k$th eigenvector of $\mathbf{M}$ |
| $\lambda_k$ | year$^{-1}$ | $k$th eigenvalue of $\mathbf{M}$ |
| $r_k(t)$ | year$^{-1}$ | Forcing in eigenvector coordinates |
| | | |
| $\Sigma C(t)$ | mol / l | Total dissolved inorganic carbon (DIC) |
| $\Delta\Sigma C(t)$ | mol / l | DIC perturbation |
| $CA$ | eq / l | Carbonate alkalinity |
| $\xi$ | 1 | Revelle buffer factor |

## A.2 Climate change

| Symbol | Unit | Entity |
|---|---|---|
| $T(t)$ | $^o$C | Change in global-and-annual mean 2m-temperature |
| $T_i(t)$ | $^o$C | Reservoir in differential temperature analogue |
| | | |
| $f$ | 1 | Radiative forcing |
| $f_n$ | 1 | Normalization factor (forcing at $2x\mathrm{CO}_2$) |
| | | |
| $f_i^v(x)$ | 1 | $i^{th}$ EOF (spatial pattern) of Variable $v$ |
| $p_i^v(t)$ | unit of $v$ | $i^{th}$ PC (time-dependent coefficient) of Variable $v$ |

## A.3 Impulse response functions

| Symbol | Unit | Entity |
|---|---|---|
| $\hat{R}_c(t)$ | 1 | Ocean CARC IRF for atmospheric $CO_2$ |
| $R93(t)$ | 1 | $\hat{R}_c$: 25% IRF of HAMOCC2 [Maier-Reimer, 1993] |
| $R01(t)$ | 1 | $\hat{R}_c$: 1% IRF of HAMOCC3i (recent fit) |
| $R_c(t)$ | 1 | Composite-layer IRF, derived from $\hat{R}_c(t)$ through truncation & rescaling |
| $R_{decay}(t)$ | year$^{-1}$ | Respirative decay IRF for terrestrial carbon |
| $R_B(t)$ | 1 | Terrestrial carbon pool IRF |
| $R_T(t)$ | $^o$C | SIAM IRF for global mean waming |
| $R^v(t)$ | unit of $v$ | NICCS CLIC IRF for global-mean change in variable $v$ (calibrated to signal from PC-EOF analysis) |
| $R^T(t)$ | $^o$C | NICCS CLIC temperature IRF |
| $R^c(t)$ | % | NICCS CLIC cloud cover IRF |
| $R^p(t)$ | mm / day | NICCS CLIC precipitation IRF |
| $R^s(t)$ | m | NICCS CLIC sea level IRF |

## A.4 IRF parameters

| Symbol | Value | Entity |
|---|---|---|
| $A_i$ | (see Table 3.1) | Coefficients in $\hat{R}_c$ |
| $a_i$ | (from $A_i$) | Coefficients in $R_c$ |
| $\tau_i$ | (see Table 3.1) | Absorption time constants in $\hat{R}_c$ and $R_c$ |
| $B_{Ji}$ | (Joos et al. [1996]) | Coefficients in $R_{decay}$ |
| $\tau_{Ji}$ | - " - | Decay time constants in $R_{decay}$ |
| $a_i^v$ | (see Table 4.2) | Coefficients in $R^v$ |
| $\tau_i^v$ | (see Table 4.2) | Warming time constants in $R^v$ |

# Appendix B

# Programs, I and O

```
NICCS & Co software package


------------------------------------------------------------
Note on visualization:

NICCS & Co I/O is compatible
to the free 'gnuplot' software
(load plot.* files supplied with the NICCS package).
------------------------------------------------------------
```

## B.1 CLIC IRF calibration program

```
Name:
-----
IRFFIT

Purpose:
--------
Find optimal IRF representation of parent AOGCM
for CliC module
(fit IRF model output time series
to GCM climate-change scenario
through variation of IRF parameters)


Problem:
--------
Crude-force optimization of two exponentials
is numerically unsatisfactory:
the minimum of the cost function
is a long narrow diagonal (hyper-)valley
(already in two dimensions,
i.e.  fitting a one-exponential-only IRF model).
Problem of fitting the two-or-more-exponential IRF model
seems in practice underdetermined, at least ill-posed.


Solution:
---------
The IRF parameters are divided into two classes, namely


  1. grid variables:
     parameters that are varied in discrete steps
     (or kept fixed if the grid has only point
     in the respective dimension), and

  2. automatic variables:
     parameters that are automatically optimized
     at each gridpoint.


Method:
---------
A 5-digit switch code
```

```
may represent any desired combination
of grid and automatic IRF parameters
(total 4 parameters for 2 exponentials).

grid loop:  at each grid point:  begin

The automatic variables are varied
by the optimization routine E04GEF (NAG)
and passed at each iteration
into IRF model LSFUN2 (self-made)
as argument XC.

The grid point coordinates
(i.e.  the values of the grid variables,
fixed during automatic optimization at grid point)
are passed into LSFUN2
through a COMMON block
containing (formally) all IRF parameters
(used so far:  max 4 parameters in 2 exponential terms).

The 5-digit switch code,
(also in the COMMON block)
tells LSFUN2 how to read
from the COMMON block
only the grid coordinates
(which remain unchanged
during automatic optimization at grid point),
but not the automatic variables
(which were passed as argument XC).
LSFUN2 does not write into the COMMON block.
Thus, until termination of E04GEF,
the common block will hold
both the grid point coordinates
and the first-guess values to the automatic variables.

The final optimized values of the automatic variables
(as returned from E04GEF)
and the grid coordinates (unchanged by E04GEF)
are written to the output
together with the minimal COST function
(sum of squared residuals)
and the IFAIL convergence indicator.

grid loop:  at each grid point:  end
```

Input:
---

1. 5-digit swich code, consisting of:

   (a) first digit:
   number of exponentials in the IRF (NEXP = 1 oder 2)

   (b) the other 4 digits:
   on-off switches
   for automatic optimization (1-0)
   of each of the (max) 4 IRF parameters:

   TL, TS: long and short time constant
   AL, AS: corresponding amplitudes

   Switch should be 0 (not automatically optimized)
   for those parameters that are grid variables.
   A parameter is a grid variable
   if the (2D or 4D) parameter space grid
   is more than one point
   in that parameter's dimension.
   Fig.B.1
   shows combinations.

2. Grid description, including:

   (a) TL,AL,TS,AS,

   (b) number of points in the respective dimension (may be one).

   (c) lower and upper grid boundaries
   (normalized to central point)
   (should be identical if only one point in this dimension)

   Each of TL,AL,TS,AS
   is interpreted according to its switch code (0 or 1)
   either as the coordinates
   of the central (or only) grid point in its dimension,
   or as first-guess automatic variable.

Output:
---

```
  switch    Nexp    Nautom    autom
  10000     1       0         -        both params gridded
one exponential, no optimization,
run (& plot) IRF model at 2D grid point,
compare with GCM

  switch    Nexp    Nautom    autom
  11000     1       1         TL       use only TLAL, AL gridded.
  10100     1       1         AL
  10010     1       1         TS       use only TSAS, AL gridded.
  10001     1       1         AS
  11100     1       2         TL AL    use only TLAL, optimize both.
  10011     1       2         TS AS    use only TSAS, optimize both.
one exponential, optimize one or both parameters

  switch    Nexp    Nautom    autom
  20000     2       0         -        ALl parameters gridded.
two exponentials, no optimization
run (& plot) IRF model at 4D grid point,
compare with GCM

  switch    Nexp    Nautom    autom
  21000     2       1         TL       AL,TSAS gridded.
  20100     2       1         AL
  20010     2       1         TS       TLAL,AS gridded.
  20001     2       1         AS
  21100     2       2         TL AL    TSAS gridded.
  20011     2       2         TS AS    TLAL gridded.
two exponentials,
optimize one or two parameters to one of the exponentials

  switch    Nexp    Nautom    autom
  21010     2       2         TL TS    amplitudes gridded.
  20101     2       2         AL AS    time constants gridded.
  (21001    2       2         TL AS    :  strange but feasible)
  (20110    2       2         TS AL    :  strange but feasible)
two exponentials, optimize two parameters,
one belonging to one exponential,
and the other to the other

  switch    Nexp    Nautom
  21110     2       3
  21101     2       3
  21011     2       3
  20111     2       3
two exponentials, optimize three parameters


  switch    Nexp    Nautom
  21111     2       4
two exponentials, optimize all parameters
(crude-force, so did Reinhard Voss)
```

Figure B.1: table of combinations of N_exp and automatic-optimization switch code for FIT program input

```
On data line per gridpoint:
TL, AL, TS, AS,
COST (sum of squared residuals),
IFAIL (automatic optimization convergence indicator).

Into an additional file,
the IRF model output
(using the optimal fit at the last gridpoint)
is printed together with the GCM time series.
This is particularly useful
if only one fit is performed
(formally, if the optimization has been performed
on a grid containing only one gridpoint) because in that case
the IRF model fit is usually to be plotted
with the GCM scenario output.

I/O file nomenclatura:
----------------------


  1. in or out:
     in.* input file
     g.* output file (grid coords, optimized automatics, cost,
     ifail)

  2. grid variables specification:
     .., one-point grid
     .al.  AL grid (1 grid variable)
     .altl.  AL-TL grid (2 grid variables) .alas.  AL-AS grid
     (2 grid variables)

  3. 5-digit switch (see above):
     number of exponentials (1 or 2)
     and automatic optimization key (0 or 1)

  4. optional further descriptions:
     coarse/medium/fine grid
     automatics optimiziation yes/no
     number of grid lines in each dimension


examples:
 in..10100.opt.01    1-point grid TL, 1-exp IRF, optim AL
 in.TL.10100.opt.05  5-point grid TL, 1-exp IRF, optim AL
 in.AL.11000.opt.05  5-point grid AL, 1-exp IRF, optim TL
```

## B.2 CARC ocean box model calibration program

```
Name:
-----
TUNE

Purpose:
--------
Close preindustrial ocean carbon chemistry,
compute ocean carbon box analogue parameters
(layer thicknesses H_i and diffusion constants ETA_i)
from given 4-exponential ocean CarC IRF
(obtained from HAMOCC response to impulse experiments
using EMR's fit program,
E.Maier-Reimer, pers.comm.).

Method:
-------
Described in thesis.
See also Hooss et al. [2001]

Input:
------
CliC IRF parameters
together with CarC ocean IRF and ocean chemistry parameters
and the NPP / fertilization paramters
are collected in the
input.R????.??  files,
see Fig.B.2.

The input.R????.??  files !must!  be processed
through the tune program (see below)
before first use by NICCS.
( strip off '#'-marked comment lines,
pipe numbers into tune )

Output:
-------
see the tune.R????.??  files
TUNE has been run once for each model variant.
(see the run.* scripts
to see how to use 'tune')

i/o nomenclatura (denote NICCS/LICCS variants):
```

```
#=========================================================================
# Input to tune program. Format is like SIAM input.
# Filter this by "grep -v '#'", pipe through tune into SIAM (MICCS, LICCS)
# SigmaC_0 and xibuf will be computed by the tune program,
# likewise the layer thicknesses (H1,...,H4,Hsurf) and
# diffusion coefficients (ETA2,3,4) of the ocean box model.
#=========================================================================
# 1. Carbon cycle
#=========================================================================
# 1. Ocean-atmosphere IRF: HAMOCC 1% 1999:10
#-------------------------------------------------------------------------
# RW ampl: RWA0           RWA1           RWA2           RWA3           RWA4
      0.131918       0.311146       0.252849       0.209027      0.0950613
# RW time:               RWT1           RWT2           RWT3           RWT4
                  0.2365E+03     0.5952E+02     0.1217E+02     0.1271E+01
#-------------------------------------------------------------------------
# 2. Ocean chemistry (get consistent SigmaC_0 and Xibuf using xibuf.F)
#-------------------------------------------------------------------------
# Chem.:          pCO2_0/ppmv            ALK          Total B            AOC
                0.277715E+03   0.243400E-02   0.409000E-03   0.362000E+15
# Chem.:                K1             K2             KB             KW
                0.995200E-06   0.707600E-09   0.188100E-08   0.646300E-14
# Chem.:             AlphaA         AlphaS       SigmaC_0          Xibuf
                0.471380E+00   0.298800E+08            0.0            0.0
#-------------------------------------------------------------------------
# 1. Land biosphere fertilization paramters
#-------------------------------------------------------------------------
# NPP fertil.          NPP_0        BETANPP
                        60.0          0.287
#-------------------------------------------------------------------------
# 1. Land biospheric decay IRF
#-------------------------------------------------------------------------
# RBJ ampl:              BJ1            BJ2            BJ3            BJ4
                   -0.71846        0.70211       0.013414      0.0029323
# RBJ time:              TJ1            TJ2            TJ3            TJ4
                        2.18           2.86           20.0          100.0
#=========================================================================
# 2. Climate change IRFs
#=========================================================================
# T2m sensitivity to CO2 doubling (global mean in degrees C):
                        2.38742
# RPCT ampl:         RPCTA1         RPCTA2
                  0.290275       0.709724
# RPCT time:         RPCTT1         RPCTT2
                       400.            12.
#-------------------------------------------------------------------------
# Cloud coverage sensitivity to CO2 doubling (global mean in %):
                      -0.0087056
# RPCC ampl:         RPCCA1         RPCCA2
                  0.290275       0.709724
# RPCC time:         RPCCT1         RPCCT2
                       400.            12.
#-------------------------------------------------------------------------
# Precipitation sensitivity to CO2 doubling (global mean in mm/day):
                      0.145257
# RPCP ampl:         RPCPA1         RPCPA2
                  0.290275       0.709724
# RPCP time:         RPCPT1         RPCPT2
                       400.            12.
#-------------------------------------------------------------------------
# Sea level sensitivity to CO2 doubling (global mean in meters):
                      1.13728
# RPCS ampl:         RPCSA1         RPCSA2
                  0.962914      0.0370862
# RPCS time:         RPCST1         RPCST2
                       800.            25.
#=========================================================================
# 3. SIAM econ parameters.
#=========================================================================
# Economy:              TauA           TauD           EbsH
                0.500000E+02   0.100000E+99   0.100000E-03
# Econ.:              Tau_0          Tau_1          Tau_2
                0.100000E+01   0.100000E+03   0.100000E+03
# Econ.:                T_c           Td_c
                0.100000E+01   0.200000E-01
# Econ.:             Nplpar             AN           Beta            Eps
                  1.000000       1.000000       0.000000       0.000100
# Econ.:             Optpar            Ntn
                           0              2
#=========================================================================
# First-guess values only.
# These variables will be changed by the tune program.
#=========================================================================
# 1. Ocean analogue parameters # Layers: H1 H2 H3 H4 Hsurf
         100.0          500.0         1000.0         1000.0           50.0
# Diffus:  ETA1           ETA2           ETA3           ETA4
             0.0            1.0            1.0           10.0
#
#== end ==================================================================
```

Figure B.2: input to tune program (input.R01GM.bJ)

```
-----------------------------------------------
Ocean-carbon IRFs and ocean CO2 chemistry parameter sets:

 R01??  IRF from recent HAMOCC3i 1% impulse experiment
 R93??  HAMOCC IRF from EMR 1993, used in SIAM 1997
 R??GM  global-mean temperature chemistry
 R??NA  northern North-Atlantic winter chemistry

Terrestrial CarC on/off, NICCS/LICCS:

 *.bj, *.nb:  nonlinear boxmodel (NICCS)
              with or without terrestrial component
              in the CarC module,
 *.lc:        linear convolution model (LICCS, CarC is ocean-only)

The following combinations have been compared:

 R01GM.bj  nonlinear standard model
 R01GM.nb  nonlinear model without terrestrial CarC
 R93GM.nb  like R01GM.nb but with different ocean CarC IRF
 R01NA.nb  like R01GM.nb but with cold-water chemistry
 R01GM.lc  LICCS (original SIAM climate model)
```

## B.3 Models

```
SIAM

Name:
-----
Structural Integrated Assessment Model

Purpose:
--------
Optimize CO2 emission scenario

Method:
-------
Minimize 1000-year integrated global costs
through avoiding global change
and through global change
(see Hasselmann et al. [1997])
```

ICLIPS

Name:
-----
Integrated assessment of CLImate Protection Strategies

Purpose:
--------
Agree on protection targets,
find negotiable policy corridors

Method:
-------
Tolerable Windows Approach
(see:
Bruckner et al. [1999],
Petschel-Held et al. [1999],
Füssel and van Minnen [2000],
Bruckner et al. [2001])

NICCS

Name:
-----
Nonlinear Impulse-response representation
of the coupled Carbon-cycle-plus-Climate System

Modules:
--------
Carbon Cycle (CarC) and Climate Change (CliC)

Purpose:
--------

1. CarC:
   compute from a given CO2 emission scenario
   the concentrations

2. CliC:
   compute from a given CO2 concentration scenario
   the climate change

```
Method:
-------
described in thesis see also Hooss et al. [2001]

i/o, short description:
-----------------------
 In:   CarC and CliC parameters
       emission scenario

 Out:  concentration scenario
       global-mean T2m, Clo, Pre, Sea scenarios,
       (can be multiplied with spatial signal patterns)

Input:
------
The output from TUNE
(again to be stripped off
the '#'-marked comment lines)
is piped into NICCS or LICCS
together with an emission scenario data file
(one data point per line:
index, year, emissions in GtC/y) Example of emission scenario
data file:
'run.niccs.ssBF'.

Following upon one such 'tune'-processed parameter file,
NICCS expects further input of
a time-dependent CO2 emission scenario
like one of the following:

 siSIA  SIAM 1997 reference scenario "A"
 siBAU  Business-as-Usual (integral 15000 GtC)
 siFrE  Frozen (=constant) emissions from year 2000.
 sp???  'δ'-impulse emission during the first time interval.
        The '???'  in the filename denote a three-digit number,
        the impulse size
        in percent of preindustrial atmospheric CO2.

For comparison, concentration time series from HAMOCC
(HAmburg Model of the Ocean Carbon Cycle,
Meier-Reimer & Hasselmann 1987, EMR continuously since then)
are provided for the delta-impulse scenarios:

p???.MEAN_ATM.norm

Output:
-------
```

From each scenario simulation, time series of

 co2 emissions,
 co2 concentrations,
 global mean temperature change,
 global mean cloud cover,
 global mean precipitation,
 global mean sea level change, and
 cumulative emissions

are written into one data output file,
named according to the i/o nomenclatura described above
to denote the model, the CarC variant, and the scenario
(see the run.* scripts).

Example of output file:
niccs.R01GM.bJ.BAU
see Fig.B.3

LICCS

Name:
-----
Linear Impulse-response etc. ... System

Purpose & Method:
-----------------
Predecessor to NICCS.
The original linear IRF convolution integral model
of the ocean-carbon-cycle-plus-climate
from SIAM [Hasselmann et al., 1997]
for comparison with NICCS

i/o:
----
see NICCS i/o.

NICAOS

Name:
-----
Nonlinear Impulse-response representation

```
#   year    E /(GtC/y)        W /ppm     T2M /degC        CL0 /%   PRE /(mm/d)        SEA /m    EACCUM/GtC
 1800.00  0.239718E-01  0.277715E+03  0.000000E+00  0.000000E+00  0.000000E+00  0.000000E+00  0.000000E+00
 1805.00  0.276530E-01  0.277762E+03  0.881329E-04 -0.321372E-06  0.536224E-05  0.188432E-05  0.129062E+00
 1810.00  0.318995E-01  0.277811E+03  0.288826E-03 -0.105319E-05  0.175729E-04  0.715960E-05  0.277943E+00
 1815.00  0.367982E-01  0.277862E+03  0.571261E-03 -0.208307E-05  0.347571E-04  0.156381E-04  0.449687E+00
 1820.00  0.424491E-01  0.277917E+03  0.919911E-03 -0.335441E-05  0.559699E-04  0.273061E-04  0.647806E+00
 1825.00  0.489678E-01  0.277977E+03  0.132897E-02 -0.484601E-05  0.808580E-04  0.422886E-04  0.876348E+00
 1830.00  0.564875E-01  0.278046E+03  0.179897E-02 -0.655984E-05  0.109454E-03  0.608277E-04  0.113999E+01
     .
     .
     .
 1970.00  0.308411E+01  0.303516E+03  0.170282E+00 -0.620926E-03  0.103604E-01  0.901723E-02  0.107287E+03
 1975.00  0.355772E+01  0.307584E+03  0.195972E+00 -0.714603E-03  0.119235E-01  0.104025E-01  0.123892E+03
 1980.00  0.410407E+01  0.312299E+03  0.225417E+00 -0.821970E-03  0.137149E-01  0.119933E-01  0.143046E+03
 1985.00  0.473431E+01  0.317784E+03  0.259137E+00 -0.944930E-03  0.157666E-01  0.138188E-01  0.165142E+03
 1990.00  0.546133E+01  0.324161E+03  0.297716E+00 -0.108561E-02  0.181138E-01  0.159122E-01  0.190631E+03
 1995.00  0.630000E+01  0.331581E+03  0.341790E+00 -0.124632E-02  0.207954E-01  0.183103E-01  0.220034E+03
 2000.00  0.708750E+01  0.340044E+03  0.391786E+00 -0.142863E-02  0.238373E-01  0.210484E-01  0.253503E+03
 2005.00  0.787500E+01  0.349472E+03  0.447723E+00 -0.163260E-02  0.272406E-01  0.241534E-01  0.290909E+03
 2010.00  0.866250E+01  0.359853E+03  0.509378E+00 -0.185742E-02  0.309919E-01  0.276444E-01  0.332253E+03
 2015.00  0.945000E+01  0.371182E+03  0.576442E+00 -0.210196E-02  0.350722E-01  0.315360E-01  0.377534E+03
 2020.00  0.102375E+02  0.383465E+03  0.648562E+00 -0.236495E-02  0.394603E-01  0.358392E-01  0.426753E+03
 2025.00  0.110250E+02  0.396714E+03  0.725387E+00 -0.264509E-02  0.441345E-01  0.405622E-01  0.479909E+03
 2030.00  0.118125E+02  0.410943E+03  0.806565E+00 -0.294110E-02  0.490735E-01  0.457110E-01  0.537003E+03
     .
     .
     .
 2255.00  0.399459E+02  0.234830E+04  0.565699E+01 -0.206279E-01  0.344186E+00  0.663500E+00  0.690751E+04
 2260.00  0.399940E+02  0.241567E+04  0.574932E+01 -0.209646E-01  0.349804E+00  0.683197E+00  0.710736E+04
 2265.00  0.400000E+02  0.248321E+04  0.584002E+01 -0.212953E-01  0.355323E+00  0.703017E+00  0.730734E+04
 2270.00  0.399638E+02  0.255082E+04  0.592909E+01 -0.216201E-01  0.360742E+00  0.722951E+00  0.750725E+04
 2275.00  0.398855E+02  0.261840E+04  0.601652E+01 -0.219389E-01  0.366061E+00  0.742991E+00  0.770688E+04
     .
     .
     .
 2555.00  0.663042E+01  0.465711E+04  0.858266E+01 -0.312962E-01  0.522192E+00  0.184930E+01  0.145041E+05
 2560.00  0.623112E+01  0.465790E+04  0.859811E+01 -0.313526E-01  0.523132E+00  0.186667E+01  0.145362E+05
 2565.00  0.584969E+01  0.465797E+04  0.861296E+01 -0.314067E-01  0.524035E+00  0.188393E+01  0.145664E+05
 2570.00  0.548582E+01  0.465736E+04  0.862723E+01 -0.314587E-01  0.524903E+00  0.190106E+01  0.145948E+05
 2575.00  0.513917E+01  0.465610E+04  0.864093E+01 -0.315087E-01  0.525737E+00  0.191808E+01  0.146213E+05
     .
     .
     .
 2985.00  0.672923E-03  0.407975E+04  0.896464E+01 -0.326891E-01  0.545433E+00  0.295258E+01  0.149516E+05
 2990.00  0.577584E-03  0.407373E+04  0.896469E+01 -0.326893E-01  0.545435E+00  0.296156E+01  0.149516E+05
 2995.00  0.495230E-03  0.406775E+04  0.896469E+01 -0.326893E-01  0.545436E+00  0.297047E+01  0.149516E+05
 3000.00  0.424171E-03  0.406181E+04  0.896466E+01 -0.326891E-01  0.545434E+00  0.297930E+01  0.149516E+05
```

Figure B.3: output of scenario simulation (niccs.R01GM.bJ.BAU). the cuts are at: the beginning of the scenario, present time, emission maximum, concentration maximum, and end of the scenario.

```
of the Coupled Atmosphere-Ocean climate System

Purpose & Method:
-----------------
CliC-alone version of NICCS (for concentration scenarios).
 In:   (dummy CarC and) CliC parameters
       concentration scenario

 Out:  global-mean T2m, Clo, Pre, Sea scenarios,
       (can be multiplied with spatial signal patterns)


-end-------------------------------------------------------
```

# Bibliography


R. Bacastow and C. D. Keeling. Atmospheric carbon dioxide and radiocarbon in the natural carbon cycle, II, changes from A.D. 1700 to 2070 as deduced from a geochemical reservoir. In G. M. Woodwell and E. V. Pecan, editors, *Carbon and the Biosphere*, pages 86–135. U.S. Dep. of Comm., Springfield, Va, 1973.

P. Brown. Stewardship of climate, an editorial comment. *Climatic Change*, 37:329–334, 1997.

T. Bruckner, G. Hooss, M. Füssel, and K. Hasselmann. The ICLIPS climate model. *Climate Change*, submitted to special ICLIPS issue, 2001.

T. Bruckner, G. Petschel-Held, F. L. Tóth, H.-M. Füssel, C. Helm, M. Leimbach, and H.-J. Schellnhuber. Climate change decision–support and the tolerable windows approach. *Environmental Modeling and Assessment*, 4: 217–234, 1999.

K. Caldeira and J. Kasting. Insensitivity of Global warming potentials to carbon dioxide emissions scenarios. *Nature*, 366:251–253, 1993.

M. Claussen, C. Kubatzki, V. Brovkin, A. Ganopolski, P. Hoelzmann, and H.-J. Pachur. Simulation of an abrupt change in Saharan vegetation in the mid-Holocene. *Geophysical Research Letters*, 26(14):2037–2040, 1999.

W. Cline. The economics of global warming. *Inst.Internat.Econ, Washington DC*, 1992.

U. Cubasch, K. Hasselmann, H. Höck, E. Maier-Reimer, U. Mikolajewicz, B. Santer, and R. Sausen. Time-dependent greenhouse warming computations with a coupled ocean-atmosphere model. *Climate Dynamics*, 8: 55–69, 1992.

O. Deke, G. Hooss, C. Kasten, G. Klepper, and K. Springer. Economic impact of climate change: simulations with a regionalized climate-economy model. *Kiel Working Paper No.1065, The Kiel Institute for World economics*, 2001.

I. G. Enting, T. M. L. Wigley, and M. Heimann. Future Emissions and Concentrations of Carbon Dioxide: Key Ocean/Atmosphere/Land Analyses. Technical report, 31, CSIRO, Div. of Atmos. Res., Melbourne, Victoria, Australia, 1994.

G. Esser, J. Hoffstadt, F. Mack, and U. Wittenberg. High resolution biosphere model, documentation, model version 3.00.00. *Mitteilungen aus dem Institut für Pflanzenökologie der Justus-Liebig-Universität Giessen*, 2, 1994.

P. Friedlingstein, L. Bopp, P. Ciais, J. Dufresne, L. Fairhead, H. LeTreut, P. Monfray, and J. Orr. Positive feedback between future cliamte change and the carbon cycle. *Geophys.Res.Lett.*, 28(8):1543–1546, 2001.

P. Friedlingstein, I. Fung, E. Holland, J. John, G. Brasseur, D. Erickson, and D. Schimel. On the contribution of $CO_2$ fertilization to the missing biospheric sink. *Global biogeochemical cycles*, 9(4):541–556, 1995.

H.-M. Füssel and J. G. van Minnen. Deriving climate protection targets from guard–rails for the preservation of terrestrial ecosystems. *Integrated Assessment*, 2000. accepted.

A. Ganopolski, C. Kubatzki, M. Claussen, V. Brovkin, and V. Petukhov. The influence of vegetation-atmosphere-ocean interaction on climate during the mid-Holocene. *Science*, 280:1916–1919, 1998.

V. Gayler and M. Claussen. The greening of the Sahara during the mid-Holocene: Results of an interactive atmosphere-biome model. *Global Ecology and Biogeography Letters*, 6:369–377, 1997.

L. Harvey. Managing Atmospheric $CO_2$. *Clim.Change*, 15:343–381, 1989.

K. Hasselmann, S. Hasselmann, R. Giering, V. Ocaña, and H. v.Storch. Sensitivity study of optimal $CO_2$ emission paths using a simplified structural integrated assessment model (SIAM). *Climatic Change*, 37:345–386, 1997.

K. Hasselmann, R. Sausen, E. Maier-Reimer, and R. Voss. On the Cold Start Problem in Transient Simulations with Coupled Atmosphere-Ocean Models. *Clim.Dynam.*, 9:53–61, 1993.

G. Heal. Discounting and climate change, an editorial comment. *Climatic Change*, 37:335–343, 1997.

M. Heimann. Evaluation of terrestrial carbon cycle models through simulations of the seasonal cycle of atmospheric $CO_2$: First results of a model intercomparison study. *Global Biogeochemical Cycles*, 12:1–24, 1998.

G. Hooss, R. Voss, K. Hasselmann, E. Maier-Reimer, and F. Joos. A Nonlinear Impulse-response model of the coupled Carbon cycle-Climate System (NICCS). *Climate Dynamics*, in press, 2001.

C. Huntingford and P. Cox. An analogue model to derive additional climate change scenarios from existing GCM simulations. *Climate Dynamics*, 16: 575–586, 2000.

IPCC. Climate Change, The IPCC Scientific Assessment. IPCC / WMO / UNEP *Cambridge University Press, Cambridge (UK)*, 1990.

IPCC. Climate Change 1992, The Supplementary Report to The IPCC Scientific Assessment Combined with Supporting Scientific Material. IPCC / WMO / UNEP *Cambridge University Press, Cambridge (UK)*, 1992.

IPCC. Climate Change 1994, Radiative Forcing of Climate Change and An Evaluation of the IPCC IS92 Emission Scenarios. IPCC / WMO / UNEP / *Cambridge University Press, Cambridge (UK)*, 1995.

IPCC. Climate Change 1995, Impacts, Adaptations and Mitigation of Climate Change: Scientific-Technical Analyses. Contribution of Working Group II to the Second Assessment Report of the IPCC. IPCC / *Cambridge University Press, Cambridge (UK)*, 1996.

IPCC. Reports. '`http://www.ipcc.ch/`', 2001.

A. Janacek, G. Benderoth, M. Lüdecke, J. Kindermann, and G. Kohlmaier. Model of the seasonal and perennial carbon dynamics in deciduous-type forests controlled by climatic variables. *Ecol.Modelling*, 49:101–124, 1989.

F. Joos and M. Bruno. Long-term variability of the terrestrial and oceanic carbon sinks and the budgets of the carbon isotopes $^{13}C$ and $^{14}C$. *Global Biogeochemical Cycles*, 12:277–295, 1998.

F. Joos, M. Bruno, R. Fink, U. Siegenthaler, T. Stocker, C. LeQuéré, and J. Sarmiento. An efficient and accurate representation of complex oceanic and biospheric models of anthropogenic carbon uptake. *Tellus*, 48B:397–417, 1996.

F. Joos, G.-K. Plattner, T. Stocker, O. Marchal, and A. Schmittner. Global warming and marine carbon cycle feedbacks on future atmospheric $CO_2$. *Science*, 284:464–467, 1999.

F. Joos, C. Prentice, S. Sitch, R. Meyer, G. Hooss, G.-K. Plattner, and K.Hasselmann. Global warming feedbacks on terrestrial carbon uptake under the IPCC emission scenarios. *Global Biogeochemical Cycles*, accepted, 2001.

R. Keeling, S. Piper, and M. Heimann. Global and hemispheric $CO_2$ sinks deduced from changes in atmospheric $O_2$. *Nature*, 381:218–221, 1996.

R. Keeling and S. Shertz. Seasonal and interannual variations in atmospheric oxygen and implications for the global carbon cycle. *Nature*, 358:723–727, 1992.

D. Kicklighter, M. Bruno, S. Dönges, G. Esser, M. Heimann, J. Helfrich, F. Ift, F. Joos, J. Kaduk, G. Kohlmaier, D. McGuire, J. Melillo, R. Meyer, B. Moore, A. Nadler, I. Prentice, W. Sauf, A. Schloss, S. Sitch, U. Wittenberg, and G. Würth. A first-order analysis of the potential role of $CO_2$ fertilization to affect the global carbon budget: a comparison of four terrestrial biosphere models. *Tellus*, 51B:343–366, 1999.

J. Kindermann. Structure of a global and seasonal carbon exchange model for the terrestrial biosphere. The Frankfurt Biosphere Model (FBM). *Water Air Soil Pollution*, 70:684–684, 1993.

A. Kleidon and H. Mooney. A global distribution of biodiversity inferred from climatic constraints: results from a process-based modelling study. *Global Change Biology*, 6:507–523, 2000.

W. Knorr. *Satellitengestützte Fernerkundung und Modellierung des globalen $CO_2$-Austauschs der Landvegetation: Eine Synthese.* PhD thesis, Universität Hamburg, 1997. Max-Planck-Institut für Meteorologie, Examensarbeit Nr.49.

G. Kohlmaier. The Frankfurt Biosphere Model: A global process-oriented model for the seasonal and long-term $CO_2$ exchange between terrestrial ecosystems and the atmosphere, II, global results for potential vegetation in an assumed equilibrium state. *Clim.Res.*, 8, 1997.

G. Kohlmaier, C. Häger, F. Ift, F. Würth, F. Joos, and M. Bruno. Future development of the carbon cycle: the role of the biota/forests within the IPCC stabilization scenarios. In *Carbon dioxide mitigation in forestry and wood industry*. Springer, New York, 1998.

M. Lüdecke. The Frankfurt Biosphere Model: A global process-oriented model of seasonal and long-term $CO_2$ exchange between terrestrial ecosystems and the atmosphere, I, Model description and illustrative results for cold deciduous and boreal forests. *Clim.Res.*, 4:143–166, 1994.

M. Lüdecke, S. Dönges, R. Otto, F. Kindermann, W. Badeck, P. Ramge, U. Jäkel, and G. Kohlmaier. Response in NPP and carbon stores of the northern biomes to a $CO_2$-induced climatic change, as evaluated by the Frankfurt Biosphere Model (FBM). *Tellus B*, 47:191–205, 1995.

E. Maier-Reimer. The Biological Pump in the Greenhouse. *Global Planetary Climate Change*, 8:13–15, 1993.

E. Maier-Reimer and K. Hasselmann. Transport and Storage of $CO_2$ in the Ocean - An Inorganic Ocean-Circulation Carbon Cycle Model. *Clim.Dynam.*, 2:63–90, 1987.

E. Maier-Reimer, U. Mikolajewicz, and A. Winguth. Future ocean uptake of $CO_2$: interaction between ocean circulation and biology. *Climate Dynamics*, 12:711–721, 1996.

R. Matear and A. Hirst. Climate Change feedback on the future oceanic $CO_2$ uptake. *Tellus*, 51B:722–733, 1999.

R. Meyer, F. Joos, G. Esser, M. Heimann, G. Hooss, G. Kohlmaier, W. Sauf, R. Voss, and U. Wittenberg. The substitution of high-resolution terrestrial biosphere models and carbon sequestration in response to changing $CO_2$ and climate. *Global Biogeochemical Cycles*, 13:785–802, 1999.

G. Myhre, E. J. Highwood, K. P. Shine, and F. Stordal. New estimates of radiative forcing due to well mixed greenhouse gases. *Geophys. Res. Lett.*, 25:2715–1718, 1998.

N. Nakićenović, A. Grübler, and A. McDonald, editors. *Global Energy Perspectives*. International Institute for Applied System Analysis / World Energy Council, Cambridge University Press, Cambridge (UK), 1998.

W. Nordhaus. Discounting in economics and climate change, an editorial comment. *Climatic Change*, 37:315–328, 1997.

H. Oeschger and M. Heimann. Uncertainties of predictions of future atmospheric $CO_2$ concentrations. *J.Geophys.Res.*, 88:1258–1262, 1983.

M. Parry, C. Rosenzweig, A. Iglesias, Fischer.G, and M. Livermore. Climate change and world food security: a new assessment. *Global environmental change*, 9 (supplemental issue):52–67, 1999.

R. Peters and T. Lovejoy, editors. *Global warming and biological diversity*. Yale University, 1992.

G. Petschel-Held, H.-J. Schellnhuber, T. Bruckner, F. L. Tóth, and K. Hasselmann. The Tolerable Windows Approach: Theoretical and Methodological Foundations. *Climatic Change*, 41:303–331, 1999.

G.-K. Plattner, F. Joos, T. Stocker, and O. Marchal. Feedback mechanisms and sensitivities of ocean carbon uptake under global warming. *Tellus B, in press*, 2001.

I. Prentice, S. Harrison, R. Leemans, R. Monserud, and A. Solomon. A global biome model based on plant physiology and dominance, soil properties and climate. *Journal of Biogeography*, 19:117–134, 1992.

R. Revelle and H. Suess. Carbon Dioxide Exchange Between Atmosphere and Ocean and the Question of an Increase of Atmospheric $CO_2$ during the Past Decades. *Tellus*, 9:18–27, 1957.

C. Rosenzweig and M. Parry. Potential impact of climate change on the world food supply. *Nature*, 367:133–138, 1994.

B. Santer, W. Brüggemann, U. Cubasch, K. Hasselmann, H. Höck, E. Maier-Reimer, and U. Mikolajewicz. Signal-to-noise analysis of time-dependent greenhouse warming experiments. Part 1: Pattern analysis. *Climate Dynamics*, 9:267–285, 1994.

J. Sarmiento, T. Hughes, R. Stouffer, and S. Manabe. Simulated response of the ocean carbon cycle to anthropogenic climate warming. *Nature*, 393: 245–252, 1998.

J. Sarmiento, J. Orr, and U. Siegenthaler. A perturbation simulation of $CO_2$ uptake in an ocean general circulation model. *J.Geophys.Res.*, 97 C3:3621–3645, 1992.

J. Sarmiento and E. Sundquist. Revised budget for the oceanic uptake of anthropogenic carbon dioxide. *Nature*, 356:589–593, 1992.

IPCC (Nakićenović & al.). Special Report on Emission Scenarios. IPCC, *in press*, 2000.

D. Schimel, M. Grubb, F. Joos, R. Kaufmann, R. Moos, W. Ogana, R. Richels, and T. Wigley. Stabilization of atmospheric greenhouse gases: physical, biological, and socio-economic implications. IPCC *Tech.Pap.III*, Geneva, 1997.

M. Schlesinger, N. Andronova, A. Ghanem, S. Malyshev, E. Rozanov, W. Wang, and F. Yang. Geographical Scenarios of Greenhouse-Gas and Anthropogenic-Sulfate-Aerosol Induced Climate Changes. `http://crga.atmos.uiuc.edu/publications/geoscen_abs.html`, 1998.

W. Schlesinger. Response of the terrestrial biosphere to global climate change and human perturbation. In J. Rozema, H. Lambers, S. van de Geijn, and M. Cambridge, editors, *$CO_2$ and Biosphere, reprinted from Vegetatio, volume 104/105*, pages 295–305. Kluwer Academic Publishers, 1993.

P. Sellers, L. Bounoua, G. Collatz, D. Randall, D. Dazlich, S. Los, J. Berry, I. Fung, C. Tucker, C. Field, and T. Jensen. Comparison of radiative and physiological effects of doubled atmospheric $CO_2$ on climate. *Science*, 271: 1402–1406, 1996.

U. Siegenthaler. Uptake of excess $CO_2$ by an outcrop-diffusion model of the ocean. *J.Geophys.Res.*, 88:3599–3608, 1983.

U. Siegenthaler and F. Joos. Use of a simple model for studying oceanic tracer distributions and the global carbon cycle. *Tellus*, 44B:186–207, 1992.

U. Siegenthaler and H. Oeschger. Predicting future atmospheric carbon dioxide levels. *Science*, 199:388–395, 1978.

U. Siegenthaler and H. Oeschger. Biospheric $CO_2$ emissions during the past 200 years reconstructed by deconvolution of ice core data. *Tellus*, 39B: 140–154, 1987.

U. Siegenthaler and J. Sarmiento. Atmospheric carbon dioxide and the ocean. *Nature*, 365:119–125, 1993.

P. U. Simon Levin, editor. *Encyclopedia of Biodiversity.* Academic Press, 2000.

S. Sitch, I. Prentice, and B. Smith. LPJ- A coupled model of vegetation dynamics and the terrestrial carbon cycle, in: Stephen Sitch, The role of vegetation dynamics in the control of atmospheric $CO_2$ content. *Ph.D.Thesis, Lund university, Sweden*, 2000.

P. Tans, I. Fung, and T. Takahashi. Observational constraints on the global atmospheric $CO_2$ budget. *Science*, 247:1431–1438, 1990.

M. Thompson and J. Randerson. Impulse response functions of terrestrial carbon cycle models: Method and application. *Global Change Biology*, 5: 371–394, 1999.

R. Voss and U. Mikolajewicz. Long-term climate changes due to increased $CO_2$ concentration in the coupled atmosphere-ocean general circulation model ECHAM3/LSG. *Climate Dynamics*, 17:45–60, 2001.

R. Voss, R. Sausen, and U. Cubasch. Periodically synchronously coupled integrations with the atmosphere-ocean general circulation model ECHAM3/LSG. *Climate Dynamics*, 14:249–266, 1998.

T. Wigley and S. Raper. Future changes in global mean temperature and sea level. In R. Warwick, E. Barrow, and T. Wigley, editors, *Climate and sea level change: Observations, Projections and Implementation*, pages 111–133. Cambridge University Press, Cambridge, UK, 1993.

T. Wigley, M. Salmon, and S. Raper. *Model for the Assessment of Greenhouse-Gas-induced climate change, Version 1.2.* Climate Research Unit, University of East Anglia, UK, 1994.

U. Wittenberg and G. Esser. Evaluation of the isotopic disequilibrium in the terrestrial biosphere by a global carbon isotope model. *Tellus B*, 49: 263–269, 1997.

# Acronyms

**Institutions:**

| | |
|---|---|
| IPCC | Intergovernmental Panel on Climate Change |
| WEC | World Energy Council |
| MPIMET | Max-Planck-Institut für Meteorologie |
| DKRZ | Deutsches Klima-Rechenzentrum |
| PIK | Potsdam-Institut für Klimafolgenforschung |
| IFW | Institut für Weltwirtschaft (Univ.Kiel) |
| IIASA | International Institute for Applied System Analysis |
| VW | Volkswagen foundation |

**Scenarios:**

| | |
|---|---|
| BAU | Business As Ususal (scenario) |
| FRE | FRozen Emssions |
| BTC | Back To Coal |
| COE | Constant Emssions |

**Models & data:**

| | |
|---|---|
| GCM | General Circulation Model |
| AOGCM | Atmosphere-Ocean GCM |
| GEM | General Equilibrium Model (of the world economy) |
| CMIP | Coupled atmosphere-ocean Model Intercomparison Project |
| CERA | Climate and Environmental data Retrieval and Archive |
| ECHAM | European Center-and-Hamburg Atmosphere GCM |
| LSG | Large-Scale Geostrophic (ocean GCM) |
| HAMOCC | HAmburg Model of the Ocean Carbon Cycle |
| HILDA | HIgh-latitude convection, Low-latitude Diffustion-Advection (conceptual ocean carbon cycle model) |
| FBM | Frankfurt Biosphere Model |
| HRBM | High-Resolution Biospere Model |
| CTBM | Community Terrestrial Biospere Model |
| BETHY | Biosphere Energy Transfer Hydrology Model |
| LPJ | Lund-Jena-Potsdam (terrestrial biosphere model) |
| DGVM | Dynamic Global Vegetation Model |
| SIAM | Structural Integrated Assessment Model |
| ICLIPS | Integraged CLImate Protection Strategies (project & model) |
| NICCS | Nonlinear Impulse-response representation of the coupled Carbon cycle-Climate System |

NICCS **modules & variants:**

| | |
|---|---|
| CLIC | NICCS CLImate Change module |
| CARC | NICCS CARbon Cycle module |
| LC | Linear Convolution |
| NO | Nonlinear Ocean, logarithmic greenhouse |
| BJ | as NO, but with Biosphere pools (adapted from F.Joos) |

**Technique:**

| | |
|---|---|
| DIC | Dissolved Inorganic Carbon (in sea water) |
| NPP | Net Primary Production (of terrestrial life) |
| NEP | Net Ecosystem Production |
| IRF | Impulse Response Function |
| EOF | Empirical Orthogonal Function |
| PC | Principal Component |
| CPU | Central Processing Unit |
| WWW | World Wide Web |

# Acknowledgements

To Klaus Hasselmann and Ernst Maier-Reimer, for their motivating personal examples of scientific creativity and social integrity.

To our sponsors, to my parents, wife, and daughter, to my whole family and all my friends for their very generous support, again and again, on all levels and in all situations.

To all the many colleagues who contributed, for advice and help and data.

To all involved institutions, and among them very specially to the Max-Planck-Institute for Meteorology, including its administration staff, for exceptional scientific, social, and material support and for the stimulating international atmosphere:

Thanks. We had a time both hard and pleasurable.

# Dank

An Klaus Hasselmann und Ernst Maier-Reimer, für ihre bewegenden persönlichen Beispiele wissenschaftlicher Schaffenskraft und menschlicher Verbindlichkeit.

An unsere Geldgeber, an meine Eltern, Frau und Tochter, an meine ganze Familie und alle meine Freunde für ihre wieder und wieder großzügige Unterstützung auf allen Ebenen und in allen Situationen.

An alle die vielen mitwirkenden Kollegen, für Rat und Tat und Daten.

An alle beteiligten Institutionen, und unter diesen ganz besonders an das Max-Planck-Institut für Meteorologie, einschliesslich Verwaltung, für hervorragende wissenschaftliche, menschliche und materielle Unterstützung und für die anregende internationale Atmosphäre:

Danke. Unsere Zeit war schwer und auch erfreulich.

S · D · G

MPI-Examensarbeit-Referenz:

Examensarbeit Nr. 1-58 Bitte Anfragen bei MPI für Meteorologie in Hamburg

---

**EXAMENSARBEIT Nr. 59**
August 1998
**Variability on decadal scales in Pacific sea surface temperatures and atmosphere ocean interaction in the coupled general circulation model ECHAM4/OPYC3**
Andreas Bacher

**EXAMENSARBEIT Nr. 60**
August 1998
**Development of a Process-Based Model to Derive Methane Emissions from Natural Wetlands for Climate Studies**
Bernadette Walter

**EXAMENSARBEIT Nr. 61**
Dezember 1998
**On the benefit of the adjoint technique for inversion of the atmospheric transport employing carbon dioxide as an example of a passive tracer**
Thomas Kaminski

**EXAMENSARBEIT Nr. 62**
Januar 1999
**Modellierung der Chemie der globalen Strato- und Troposphäre mit einem drei-dimensionalen Zikulationsmodell**
Benedikt Steil

**EXAMENSARBEIT Nr. 63**
Januar 1999
**Ocean-atmosphere interactions on decadal timescales**
Stephan Venzke

**EXAMENSARBEIT Nr. 64**
März 1999
**Modes of Variability as Simulated by a Global Climate Model**
Axel Timmermann

**EXAMENSARBEIT Nr. 65**
Juli 1999
**Numerical Simulation of Scavenging Processes in Explosive Volcanic Eruption Clouds**
Christiane Textor

**EXAMENSARBEIT Nr. 66**
Juli 1999
**Grobstruktursimulation - eine Methode zur Berechnung turbulenter atmosphärischer Strömungen**
Andreas Chlond

**EXAMENSARBEIT Nr. 67**
Dezember 1999
**Satellitengestüzte Abschätzung der Einflüsse von kühler Haut und Schaumbedeckung des Ozeans auf den globalen $CO_2$-Fluß zwischen Ozean und Atmosphäre**
Stefan Ewald

**EXAMENSARBEIT Nr. 68**
Februar 2000
**Die direkte Strahlungswirkung von Aerosolteilchen auf ein Klimamodell**
Anke Maria Allner

**EXAMENSARBEIT Nr. 69**
Februar 2000
**Räumliche und zeitliche Variabilität von Wasserisotopen im polaren Niederschlag**
(Spatial and Temporal Variability of Water Isotopes in Polar Precipitation)
Martin Werner

**EXAMENSARBEIT Nr. 70**
März 2000
**Bestimmung des turbulenten Impulsflusses mit Hilfe von Doppler- und Interferometriemessungen eines Radar-RASS-Systems**
Lutz Hirsch

**EXAMENSARBEIT Nr. 71**
Mai 2000
**Entwicklung und Test eines massenerhaltenden semi-Lagrangschen Transportverfahrens auf einer Kugel**
Markus Peter Olk

**EXAMENSARBEIT Nr. 72**
Mai 2000
**Quantification of Natural Climate Variability in Paleoclimatic Proxy Data Using General Circulation Models: Application to Glacier Systems**
Bernhard K. Reichert

| | |
|---|---|
| **EXAMENSARBEIT Nr. 73**<br>Mai 2000 | **Validation of Clouds in the ECHAM4 Model Using a Dynamical Adjustment Technique**<br>Hans-Stefan Bauer |
| **EXAMENSARBEIT Nr. 74**<br>Juni 2000 | **The Dynamical Link Between the Troposphere and Stratosphere and its Potential to Affect Climate**<br>Judith Perlwitz |
| **EXAMENSARBEIT Nr. 75**<br>Juli 2000 | **Fernerkundung von Eis- und Mehrschichtbewölkung über Meeresuntergrund aus Messungen rückgestreuter Solarstrahlung**<br>Claudio Costanzo |
| **EXAMENSARBEIT Nr. 76**<br>Juli 2000 | **Large-scale SST variability in the midlatitudes and in the tropical Atlantic**<br>Dietmar Dommenget |
| **EXAMENSARBEIT Nr. 77**<br>Juli 2000 | **HOAPS: Eine neue Klimatologie des Süßwasserflusses an der Meeresoberfläche abgeleitet aus Satellitendaten**<br>Volker Jost |
| **EXAMENSARBEIT Nr. 78**<br>September 2000 | **The potential influence of natural climate variability and uncertainty in the design of optimal greenhouse gas emission policies**<br>Victor Ocaña |
| **EXAMENSARBEIT Nr. 79**<br>Oktober 2000 | **Messungen des Reflexionsvermögen der Meeresoberfläche im infraroten Spektralbereich mit dem "Ocean Atmosphere Sounding Interferometer System" (OASIS)**<br>Lars Fiedler |
| **EXAMENSARBEIT Nr. 80**<br>November 2000 | **Vertikalmessungen der Aerosolextinktion und des Ozons mit einem UV-Raman-Lidar**<br>Volker Matthias |
| **EXAMENSARBEIT Nr. 81**<br>Dezember 2000 | **Photochemical Smog in Berlin-Brandenburg: An Investigation with the Atmosphere-Chemistry Model GESIMA**<br>Susanne E. Bauer |
| **EXAMENSARBEIT Nr. 82**<br>Juli 2001 | **Komponenten des Wasserkreislaufs in Zyklonen aus Satellitendaten –Niederschlagsfallstudien-**<br>Christian-Philipp Klepp |
| **EXAMENSARBEIT Nr. 83**<br>Juli 2001 | **Aggregate models of climate change: development and applications**<br>Kurt Georg Hooss |

ISSN 0938-5177